PREDICTION OF THE PERFORMANCE OF RAPID HEATING FURNACES USING PHYSICAL AND MATHEMATICAL MODELLING TECHNIQUES

David Michael Lucas

Thesis submitted to the University of Aston in Birmingham for the degree of Doctor of Philosophy

June 1971

SUMMARY

This thesis shows how a combination of physical and mathematical modelling can be used to predict the thermal performance of tangentially fired rapid billet heating furnaces. The experimental work involves the measurement of mass transfer coefficients in an isothermal scale model of the furnace using a technique based on the measurement of the limiting diffusion controlled current during the electrolysis of an alkaline solution of potassium ferri- and ferrocyanide. Convective heat transfer coefficients are obtained from the mass transfer measurements via the Chilton-Colburn analogy. These coefficients are then combined with a suitable mathematical model of the heat transfer processes in the furnace and the thermal performance predicted.

The procedure has first been checked by calculating the heating times to forging temperature of cylindrical copper and aluminium billets and comparing these with results obtained in an actual prototype furnace. Mathematical models are then used to show that the performance of the prototype furnace can be improved by modifications to its design and to demonstrate the significant improvement in transient response of these furnaces compared with traditional design. Finally both the mass transfer measurements and the mathematical analysis are extended to deal with situations in which the heat flux to the load surface is not uniform.

Acknowledgements

The work described in this thesis was carried out at the Gas Council Midlands Research Station whilst the Author was registered as an external student at the University of Aston in Birmingham. The work of the Author represents only a part of the total integrated effort put into developing and applying physical and mathematical modelling techniques at the Midlands Research Station. In order that the thesis should be continuous and coherent it is therefore inevitable that it contains many experimental and theoretical results which were obtained by other members of the Research Station staff. I would therefore like to acknowledge the contribution of all those involved and in particular the following:

Mrs. R. A. Calsworthy and Mrs. B. E. Moppett who were responsible for the naphthalene and flow visualisation experiments described in sections 2.3 and 3.2 respectively.

Mrs. H. E. Toth and Mr. J. Masters for their help in developing the mathematical model of Chapter 6.

Mr. A. J. Barber for writing the computer programme for the mathematical model of Chapter 7.

Mr. W. A. Davis for his help with the measurement of local mass transfer coefficients and for writing the two dimensional heat conduction programme.

I should also like to thank Mr. W. E. Francis for his guidance and supervision of the work at the Research Station, Dr. B. Gay for his supervision on behalf of the University of Aston and Dr. R. M. Davies for many useful discussions. Finally I am grateful to Dr. W. A. Simmonds, Director of the Gas Council Midlands Research Station, for permission to prepare and submit the thesis.

CONTENTS

INTRODUCTION

This thesis deals with the use of a mass transfer modelling technique for the evaluation of convective heat transfer coefficients in a furnace and the prediction of furnace performance from these results. In the context of the thesis the furnace is taken as being a device for transferring enthalpy from the products of combustion of a hydrocarbon fuel to a load. The techniques described have application to most types of furnaces and also to other heat transfer equipment. However the thesis is concerned only with furnaces for reheating metallic stock before rolling, extrusion or forging and with only one particular design of this type of furnace. This furnace is a gas fired 'single cell' rapid heating furnace designed for reheating cylindrical billets.

The main requirements of any reheating furnace are that it shall produce stock with acceptable temperature distribution and metallurgical properties at a cost as low as possible. The performance of such furnaces are normally assessed in terms of thermal efficiency and in the time taken to heat a billet under working conditions since this has a direct effect on metallurgical properties. The task of the furnace designer is to optimise the design so that the relative importance of these criteria are taken into account.

In order that the optimum design of a furnace shall be made it is essential that the distribution of heat flux and temperature within the furnace can be predicted. The interaction of heat transfer with combustion and flow within the furnace chamber and their dependence on burner and furnace design is complex and as yet no entirely theoretical solution which is universally applicable is available. Furnaces have therefore been designed by means of heat balance and simple radiation calculations together with empirical information and experience. This procedure is reasonably successful for scaling up

existing systems in which radiation is the principal mode of heat transfer. However, it does not stimulate improvements in furnace design, nor can it be used to design furnaces, such as rapid heating furnaces, in which convection plays an important role. In these circumstances it is essential that the effect of furnace design on convective heat transfer coefficients be known and to this end model techniques have been developed at the Midlands Research Station.

In conventional furnaces, the processes of combustion and heat transfer occur simultaneously within the furnace chamber and the heat transfer is principally by radiation. For these processes to occur efficiently, it is essential that a chamber of large volume is provided and this requirement leads to certain disadvantages. The large physical size results in high capital cost and high thermal inertia. The latter in turn leads to long start up periods and difficulties in control of output rate to meet fluctuating demand. In addition the metallurgical benefits to be gained from short heating cycles cannot be achieved without the use of high temperature heads, with the consequent risk of overheating the stock in the event of a shutdown. However, these disadvantages can be largely overcome by the use of a class of gas fired furnaces of much smaller size which have become known as 'rapid heating furnaces'. In this type of furnace the gaseous fuel is burnt in high intensity tunnel burners and the combustion is essentially completed within the burner tunnel. The products of combustion issue at high velocity from the burner and their momentum is used to provide high convective heat transfer within a small aerodynamically designed furnace chamber. It is for the design of this type of furnace that the work described in this thesis is most applicable. The particular furnace considered is a single cell rapid heating furnace designed for

heating cylindrical billets. Combustion products are forced round the circumference of the billet in a furnace chamber which is roughly cylindrical and coaxial with the billet. The design and performance of the furnace has been described by Lawrence and Spittle[1] and also by Francis and Oeppen[2].

In any furnace, heat is transferred to the load by direct radiation and convection from the flame and hot combustion products and by indirect radiation via. reflection and reradiation from the refractory roof and walls. When burning gaseous fuels in conventional furnaces the predominant heat transfer mechanism is non-luminous gas radiation whereas the flames from heavier fuel oils contain incandescent soot particles and contribute luminous radiation. Consequently these modes of heat transfer have received the greatest attention from those concerned with furnace heat transfer. The non-luminous radiation is due almost exclusively to the presence of water vapour and carbon dioxide and each of these gases absorbs and radiates in certain regions of the infra-red spectrum. In this case radiation is dependent mainly on the temperature and partial pressures of the radiating components and on the effective thickness of the gas layer. This process has been studied chiefly by Hottel and his co-workers at the Massachusetts Institute of Technology and the results of their researches are best summarised by Hottel and Sarofim in a recently published text book[3]. Luminous flame radiation is less completely understoood and is dependent mainly on the mixing of air and fuel and consequently on burner design. Work in this field has been carried out at the University of Sheffield and also at the International Flame Research Foundation at Ijmuiden in Holland and again a recently published text book provides the best source of reference to this work[4]. In rapid heating furnaces the combustion of the fuel is

complete and no carbon is formed so that radiation from the combustion products is by non-luminous radiation only. This process is only significant in chambers of large volume and in the type of rapid heating furnace considered in this thesis contributes only up to 10-20% to the total heat lost by the combustion products.

Convective heat transfer in conventional furnaces is, or at least is generally considered to be, negligible and consequently has received little attention in the past. However, it should be emphasised that in any furnace where re-radiation from the furnace walls is a significant factor the controlling step may well be that of convective heat transfer to the walls. Convective heat transfer coefficients have been measured by Sinnott and Siebert[5] for flat plates in a recirculating furnace and by Genna, Nolan and Furczyk[6] for a cylinder in a rectangular box type furnace. In these investigations the convective heat transfer was obtained from the difference between the measured total heat transfer and a calculated value for the radiation. Consequently all the errors of experiments and calculations are included with the convection. Hulse[7] measured convection to the walls of a cyclone type furnace directly by replacing the combustion products by air heated externally. The well known linear equation given by Trinks[8] for convection to plane surfaces in furnaces is in fact not based on measurements made in furnace systems but on data for heat transfer from a heated plate to air flowing parallel to the surface. Hulse and Sargent[9] have shown that the Trinks equation agrees well with data for this case collected by Fishenden and Saunders[10], but there appears to be no report in the literature of a comparison between the Trinks equation and an actual furnace investigation.

In many rapid heating furnaces the design of the chamber is such

that convective data obtained from systems other than furnaces may be directly applied. These include such cases as flow over flat plates, between parallel planes, through and over tubes and ducts of circular and other cross section. In other cases, however, the design will be such that no existing system is sufficiently close to allow data from it to be used. Such a case is illustrated by the single cell furnace considered in this thesis. The use of pilot plant to obtain the required data may be extremely expensive especially if considerable modifications are subsequently needed to achieve a specified performance. In addition the acquisition of convective data in this way may prove difficult and of limited accuracy, particularly if radiative heat transfer is also significant. As a consequence it is often best both from an economic and a technical point of view to obtain the information from mass transfer experiments in small scale isothermal aerodynamic models. The mass transfer techniques also have the advantage that local convective heat transfer coefficients can be evaluated and these would be particularly difficult to obtained from pilot plant measurements.

In the mass transfer modelling techniques the heat transfer surfaces of the furnace are replaced by mass transfer surfacesin the model. The heat transfer coefficients are then derived from mass transfer measurements under conditions of dynamic similarity using the Chilton-Colburn analogy between heat and mass transfer. Two mass transfer techniques have been developed at the Midlands Research Station for this purpose. These are the sublimation of naphthalene into air and an electrolytic technique based on the measurement of the diffusion controlled limiting current to a nickel electrode in an alkaline potassium ferri--ferrocyanide solution. Both methods may be used to obtain coefficients to the entire load or wall

surface and also to small areas on these surfaces. The electrolytic technique is particularly suited to the measurement of local coefficients to the billet in the single cell furnace and the use of the technique to obtain both average and local coefficients in this case is described in detail in this thesis. Although the heat and mass transfer analogy can be deduced theoretically for simple systems there is sufficient uncertainty as to the precise formulation to have made it necessary to confirm the validity in the case of the single cell furnace. To this end small scale convective heat transfer experiments have also been carried out in the furnace models and these are described in the thesis.

The final process of heat transfer from the combustion products to the load is conduction from the load surface to the interior. This process is described by the transient heat conduction equation and many analytical and numerical methods are available for its solution. For furnace heat transfer calculations finite difference methods must normally be used since the boundary conditions are complex and the thermal conductivity and diffusivity of the load change with temperature.

The combined effects of radiation, convection and conduction and their dependence on furnace design is complex. Fortunately in the case of rapid heating furnaces several simplifications can be made. Firstly, combustion is completed within the burner tunnel so that it can be ignored in the heat transfer calculations. Secondly, assumptions concerning the flow of combustion products can generally be made. In the case of the billet heating furnace considered here the furnace is sufficiently well stirred by the momentum of the burner jets that the assumption can be made that at any time the temperature of the combustion products everywhere within the furnace chamber is the same. This is the basis of the 'well stirred furnace' assumption presented by Hottel in his Melchett Lecture of 1960[11]. Hottel's work allows the radiative interchange between the

combustion products, the load and the refractory walls to be calculated for this case. The analysis presented in this thesis is a refinement of Hottel's in that a more realistic assessment is made of convection, also transient conditions in the furnace system are taken into account by coupling the well stirred furnace equations with the transient heat conduction equation for the load.

The thesis firstly reviews briefly the principles of furnace modelling and their application to rapid heating furnaces. The heat and mass transfer analogy and its limitations are discussed and this is followed by practical details of the experimental techniques. The experimental measurements are then presented and discussed. The mass transfer results are incorporated into a mathematical model from which heating times to extrusion temperature of cylindrical aluminium and copper billets are predicted and compared with results previously obtained in an actual prototype furnace. Mathematical models are then used to investigate certain aspects of furnace performance and finally a method is outlined by which the local mass transfer coefficients can be used to predict the detailed temperature distribution within a billet.

NOMENCLATURE

A	=	surface area	(m^2)
b	=	annular gap ($r_w - r_b$)	(m)
C	=	concentration	(kg/m^3)
C_g	=	gross calorific value of fuel	(mJ/m^3)
C_n	=	net calorific value of fuel	($J/m^3(st)$)
C_p	=	specific heat at constant pressure	(J/kg)
c	=	recirculation ratio	-
D_v	=	diffusivity	(m^2/s)
d	=	diameter	(m)
E	=	electrode potential	(V)
e	=	fraction of top burner flow which passes out of flue	-
F	=	radiative interchange factor	-
F_a	=	Faraday Constant	(C/kg-equiv)
f	=	valency change in reaction	
G	=	total fuel used	(J)
H	=	overall heat transfer coefficient	(W/m^2K)
h	=	convective heat transfer coefficient	(W/m^2K)
h_D	=	convective mass transfer coefficent	(m/s)
I	=	heat content	($J/m^3(st)$)
i	=	current	(A)
j	=	j factor for heat and mass transfer	-
L	=	characteristic length	(m)
L_N	=	latent heat of naphthalene	(J/kg mole)
l	=	length	(m)
M	=	mass input rate	(kg/s)
N	=	molecular weight of naphthalene	

$\dot{N}$	=	mass flux	(kg/m^2s)
Nu	=	Nusselt number = hL/λ	-
n	=	number of burners in furnace	-
P	=	volume of combustion products per volume of gas burnt	
Pr	=	Prandtl number = $\frac{C_p\mu}{\lambda}$	-
p	=	vapour pressure	(N/m^2)
Q	=	volume flow rate of combustion products	($m^3(st)/s$)
Q_g	=	volume flow rate of fuel	($m^3(st)/s$)
$\dot{q}$	=	heat flux	(W/m^2)
R	=	gas constant	(J/kg mol K)
R_a	=	volume of air per volume of gas burnt	
Re	=	Reynolds number = $\frac{LU\rho}{\mu}$	-
r	=	radius	(m)
S	=	scale factor	-
Sc	=	Schmidt number = $\frac{\mu}{\rho D_v}$	-
Sh	=	Sherwood number = $\frac{h_D L}{D_v}$	-
s	=	specific gravity of fuel	-
T	=	temperature	(K)
T'	=	temperature after time interval $\delta\tau$	(K)
t	=	number of circumferential elements in cylinder	
U	=	velocity	(m/s)
UA	=	heat exchanger effectiveness	(W/K)
V	=	volume	(m^3)
v	=	tangential velocity	(m/s)
v*	=	velocity ratio	-

w	=	naphthalene weight loss	(kg/s)
x,y,z	=	cortesian co-ordinates	(m)
α	=	thermal diffusivity = $\frac{\lambda}{\rho C_p}$	(m^2/s)
δ	=	time or position increment	
δ_c	=	concentration boundary layer thickness	(m)
δ_h	=	temperature boundary layer thickness	(m)
ε	=	emissivity	-
λ	=	thermal conductivity	(W/mK)
μ	=	viscosity	(Ns/m^2)
ρ	=	density	(kg/m^3)
σ	=	Stefan-Boltzmann constant	(W/m^2K^4)
τ	=	time	(s)
θ	=	angular position	(-)
ω	=	thickness of refractory wall	(m)
ϕ	=	heat transfer rate	(W)

subscripts

a	=	air
B	=	burner
b	=	billet surface
F	=	furnace
f	=	combustion products at flame temperature
final	=	end of soak period
fluc	=	flue gases
g	=	combustion products in furnace chamber
M	=	model
m	=	mean
o	=	bulk
s	=	surface

$_{soak}$ = beginning of soak period

$_{w}$ = wall surface

superscript

* = dimensionless quantity

^{0} = reference conditions

1. FURNACE MODELLING

The purpose of modelling is to permit conditions inside existing or projected equipment to be predicted by carrying out experiments under more controlled and favourable conditions. Such models are not limited to small scale systems geometrically similar to the prototype but also include analogues in which the physical and chemical processes are quite different from those in the prototype. The success of modelling depends on ensuring that there is similarity between the process investigated in the model and in the prototype.

The application of models to the design and improvement of furnace and combustion systems is well established and requires no extensive discussion here. Similarity criteria on which furnace modelling is based are therefore only briefly reviewed with reference to the single cell billet heating furnace. The main part of the section will be concerned with the less usual application of the heat and mass transfer analogy.

1.1 Similarity Criteria

The physical and chemical processes occuring within a system can be described by a set of differential equations. These will usually be balance equations expressing conservation of mass, energy or momentum or the balance of forces. Such equations are dimensionally uniform and by dividing by a characteristic mass, energy or force they can be transformed into relationships between dimensionless groups. The boundary conditions of the equations can also be expressed in dimensionless form by a similar procedure. If all the dimensionless groups containing only independent variables are the same in both prototype and model then the other groups containing the dependent variables which define performance will be the same in both systems. In most cases it is not possible, or even desirable to ensure that every dimensionless group is the same in both systems. The most important features of the prototype may frequently be adequately modelled if only one or two of the groups

are kept constant. These aspects have been reviewed by Beer.[15]

In furnace modelling the most important dimensionless groups are those which define geometric, kinematic, dynamic and thermal similarity.

1.1.1 Geometric Similarity

This implies that every linear dimension of the model bears the same ratio to the corresponding dimension of the prototype. Although geometric similarity can be maintained for studies of non compressible fluid dynamics in isothermal systems, it has to be abandoned when the system is non-isothermal or when chemical reaction is significant. For the single cell rapid heating furnace it will be shown below that geometric similarity cannot be maintained when modelling the burner tunnel.

1.1.2 Kinematic Similarity

This implies that fluid particles follow geometrically similar paths in corresponding intervals of time. In the single-cell furnace the velocity distribution is controlled by the momentum exchange between the burner jet and the cooler recirculating combustion products. The momentum exchange must therefore be adequately modelled if kinematic similarity is to be maintained. The furnace is fitted with high intensity tunnel burners and the combustion is completed within the burner tunnel. Under these conditions the discharge area of the burner in the model must be reduced according to the equation.

$$A_{BM} = A_{BF} \; S^2 \; \frac{T_{gF}}{T_{BF}} \qquad (1.1)$$

The burner exits take the form of rectangular slots running the width of the furnace. The height of the directly scaled burners in the model have therefore been reduced by the ratio T_{gF}/T_{BF}.

1.1.3 Dynamic Similarity

Dynamic similarity requires that the force ratios causing acceleration of masses in the corresponding systems are maintained constant. These forces are inertial, viscous and buoyancy. In the single cell

furnace the last of these is negligible due to the high velocity of the burner. Dynamic similarity then requires only that the ratio of the inertia to viscous forces, i.e. the Reynolds number, be the same in furnace and model.

1.1.4 Thermal Similarity

Thermal similarity requires that the ratio of temperature differences between any two points in the prototype and corresponding points in the model are maintained constant. In a furnace containing radiation absorbing combustion products the combined processes of radiation, convection and conduction cannot be modelled correctly and thermal similarity cannot be obtained. This is one of the reasons why the combination of mathematical and mass transfer modelling which is described later is important.

1.2 The Heat and Mass Transfer Analogy

1.2.1 Derivation from Differential Equations

The basic differential equations governing the convective diffusion of heat and mass are similar. In steady flow and in the absence of chemical reaction and internal generation of heat these simplify to the following:

for heat transfer : $C_p \rho \vec{U} . \nabla T = \lambda \nabla^2 T$ ..... (1.2)

for mass transfer : $\vec{U} \cdot \nabla C = D_v \nabla^2 C$ ..... (1.3)

These equations may be made dimensionless by first defining arbitrary reference quantities U° T° L and C° and dimensionless variables $\vec{U}^* = \vec{U}/U^\circ_\circ$, $T^* = T/T^\circ$, $y^* = y/L$ and $C^* = C/C^\circ$. Then for heat transfer :

$$\frac{C_p \rho U^\circ \vec{U}^*}{L} . \nabla T^* = \frac{\lambda \nabla^2}{L^2} T^* \qquad \text{..... (1.4)}$$

and for mass transfer :

$$\frac{U^\circ \vec{U}^*}{L} . \nabla C^* = \frac{D_v}{L^2} \nabla^2 C^* \qquad \text{..... (1.5)}$$

Dividing (1.4) by $\frac{C_p \rho U^\circ}{L}$ and (1.5) by $\frac{U^\circ}{L}$ we obtain :

$$\vec{U}^* \cdot \nabla T^* = \frac{1}{Re\ Pr} \nabla^2 T^* \qquad \ldots\ldots (1.6)$$

and

$$\vec{U}^* \cdot \nabla C^* = \frac{1}{Re\ Sc} \nabla^2 C^* \qquad \ldots\ldots (1.7)$$

where $\frac{1}{Re\ Pr} = \frac{\lambda}{C_p \rho U^\circ L}$

and

$$\frac{1}{Re\ Sc} = \frac{D_v}{U^\circ L}$$

The solution of equations (1.6) and (1.7) will be identical providing the dimensionless velocity distributions, the boundary conditions and the Re Pr and Re Sc groups are the same in both cases. That is the concentration and temperature profiles will be identical under conditions of geometric, kinematic and dynamic similarity providing the boundary conditions are similar and the Schmidt and Prandtl numbers are equal. In practice we are normally concerned with mass and heat transfer rates to surfaces under conditions in which temperature and concentration gradients at the surface are only significant in the normal direction. The transfer rates are then usually defined through transfer coefficients and a temperature or concentration difference evaluated between the surface and some reference point, i.e.,

$$\overset{\circ}{q} = -\lambda \left(\frac{\partial T}{\partial y}\right)_s = h\,(T_o - T_s) \qquad \ldots\ldots (1.8)$$

and

$$\overset{\circ}{N} = -D_v \left(\frac{\partial C}{\partial y}\right)_s = h_D\,(C_o - C_s) \qquad \ldots\ldots (1.9)$$

or in dimensionless form:

$$\frac{-\lambda}{hL} \left(\frac{\partial T^*}{\partial y^*}\right)_s = (1 - T_s^*) \qquad \ldots\ldots (1.10)$$

and

$$\frac{-D_v}{h_D L}\left(\frac{\partial C^*}{\partial y^*}\right)_s = (1 - C_s^*) \qquad \ldots\ldots (1.11)$$

Then under conditions of similarity :

$$\frac{hL}{\lambda} = \frac{h_D L}{D_v} \qquad \ldots\ldots (1.12)$$

i.e. $Nu = Sh$ $\qquad \ldots\ldots (1.13)$

Equation (1.13) is the basis of the Reynolds analogy and is only applicable in the case of equal Prandtl and Schmidt numbers. In turbulent flow the transport properties in these groups are of course those for turbulent exchange which are, moreover, approximately the same and therefore the analogy is valid.. However in any system there is always a layer close to the wall which is in laminar flow and in this region the equality of Schmidt and Prandtl numbers is not generally realised. In this case whilst the solution of the differential equations are not identical it is reasonable to assume that they will be similar and may be given by the general polynomials :

$$\frac{T^* - T_s^*}{1 - T_s^*} = a\left(\frac{y^*}{\delta_h^*}\right) + b\left(\frac{y^*}{\delta_h^*}\right)^2 + c\left(\frac{y^*}{\delta_h^*}\right)^3 + \ldots\ldots (1.14)$$

and

$$\frac{C^* - C_s^*}{1 - C_s^*} = a\left(\frac{y^*}{\delta_c^*}\right) + b\left(\frac{y^*}{\delta_c^*}\right)^2 + c\left(\frac{y^*}{\delta_c^*}\right)^3 + \ldots\ldots (1.15)$$

where δ_h^* is the dimensionless temperature boundary layer thickness which is a function of Pr, Re and perhaps x^* and z^*, and δ_c^* is the dimensionless concentration boundary layer thickness which is similarily a function of Sc, Re and perhaps x^* and Z^*. Differentiating (1.14) and (1.15) we obtain

$$\left(\frac{\partial T^*}{\partial y^*}\right) = \frac{a(1 - T_s^*)}{\delta_h^*} \text{ and } \left(\frac{\partial C^*}{\partial y^*}\right)_s = \frac{a(1 - C_s^*)}{\delta_c^*} \qquad \ldots\ldots (1.16)$$

substituting into (1.10) and (1.11) and eliminating a,

$$\frac{Lh\ \delta_h^*}{\lambda} = \frac{Lh_d\ \delta_o^*}{D_v} \qquad \ldots\ldots (1.17)$$

dividing by the Reynolds number $\rho U^o L/\mu$

$$\frac{h}{\rho U^o C_p} \cdot Pr.\ \delta_h^* = \frac{h_D}{U^o} \cdot Sc.\ \delta_o^* \qquad \ldots\ldots (1.18)$$

or

$$\frac{h}{\rho U^o C_p} Pr.f(Pr, Re, x^*, z^*) = \frac{h_D}{U^o} Sc.f(Sc, Re, x^*, z^*) \qquad \ldots\ldots (1.19)$$

and under geometric and dynamic similarity

$$\frac{h}{\rho U^o C_p} Pr.f(Pr) = \frac{h_D}{U^o} Sc.f(Sc) \qquad \ldots\ldots (1.20)$$

It will be shown in the next section that we may write $f(Pr) = Pr^{-\frac{1}{3}}$ and $f(Sc) = Sc^{-\frac{1}{3}}$ then

$$\frac{h}{\rho U^o C_p} Pr^{\frac{2}{3}} = \frac{h_D}{U^o} Sc^{\frac{2}{3}} = j \qquad \ldots\ldots (1.21)$$

Equation (1.21) is also a statement of the empirical Chilton-Colburn analogy between heat and mass transfer and is the basis of the mass transfer model work described in this thesis. It is perhaps worth summarising the conditions under which it is valid which have just been deduced from theoretical considerations. These conditions are :

(1) geometric similarity

(2) kinematic similarity

(3) dynamic similarity

(4) similarity of boundary conditions

(5) a minus one third power dependence of δ_h^* and δ_o^* on Pr and Sc.

The first three of these conditions have already been discussed in the previous section. The fourth condition implies that the type of boundary condition, such as constant flux or concentration, is the same in both cases and also that, in the case of mass transfer, the mass transfer rates at the surface are small. The fifth condition is

discussed in the next section.

1.2.2 The Schmidt and Prandtl Number Functions in the j Factors

The correct function of Schmidt and Prandtl numbers to be included in the j factors can only be determined by solution of the relevant differential equations. However analytical solution of these equations is generally impossible and therefore other procedures must be used. These procedures include both differential and integral methods and also the application of analogies based on some physical insight into the transfer mechanisms.

In laminar boundary layer flow similarity solutions to the differential equations can be obtained in some simple cases. The procedure is based on recognising that profiles of velocity, and also temperature and concentration, are geometrically similar at all positions in the system. The partial differential equations of the boundary layer can then be reduced to ordinary differential equations which can be solved numerically. Details of the methods are given by Kays[15] and Schlichting[17] amongst others. As an example Kays gives the following equation for laminar flow over a flat plate.

$$St\ Pr^{\frac{2}{3}} = f(Re) \qquad \ldots\ldots (1.22)$$

An alternative procedure which can be adopted for either laminar or turbulent flow is the application of the boundary layer integral equation together with an assumption concerning either the form of the velocity and temperature profiles or relationships between various integral properties of the boundary layer. For example for laminar flow over a flat plate the assumption of parabolic velocity and temperature profiles leads to:

$$St\ Pr^{\frac{2}{3}} = 0.332\ Re^{-\frac{1}{2}} \qquad \ldots\ldots (1.23)$$

In the case of turbulent flow Deissler[18] applies the boundary layer integral method together with an assumption concerning the magnitude of the

eddy viscosity. The equations were solved numerically and Deissler presents a graph of St versus Pr or Sc for a range of Reynolds numbers. Plotted on a log-log basis the slope of the curve continually steepens from -0.5 to-0.75 as Pr or Sc increases. However the average slope over a wide range of Reynolds numbers is $-\frac{2}{3}$ so that we may write once again

$$St\ Pr^{\frac{2}{3}} = f(Re) \qquad \ldots\ldots (1.24)$$

Turbulent boundary layers have also been analysed by application of analogies based on some physical insight into the transfer mechanisms. The simplest of these is the Reynolds analogy which has already been deduced theoretically. However this method assumes a turbulent boundary layer right up to the wall which is not the case in practice. Prandtl[19] and Taylor[20] modified the analysis by taking into account a laminar sublayer in which turbulent transfer is negligible. Von Kármán[21] recognised that there would be no sharp transition between these zones in practice and therefore introduced a third, or buffer, zone in which molecular and turbulent exchanges are of the same order. These analogies have been applied to both flow over flat plates and fully developed pipe flow and the details can be found in Kays and Schlichting amongst other text books. For example for heat transfer to a flat plate the Von Kármán analogy leads to

$$Nu = \frac{\frac{1}{2}\,Re\,Pr\,C_f'}{1 + 5\sqrt{\frac{1}{2}\,C_f'}\ \{(Pr-1) + \ln\left[1 + \frac{5}{6}(Pr-1)\right]\}} \qquad \ldots\ldots (1.25)$$

This equation together with similar ones derived from other analogies have been plotted as $Nu/\frac{1}{2}\,Re\,Pr\,C_f'$ against Pr by Schlichting. The curves can be approximated with good accuracy near Pr = 1 by

$$\frac{Nu}{\frac{1}{2}\,C_f'\,RePr} = Pr^{-\frac{2}{3}} \qquad \ldots\ldots (1.26)$$

$$\text{or } StPr^{\frac{2}{3}} = \frac{1}{2}\,C_f' \qquad \ldots\ldots (1.27)$$

At higher Prandtl numbers the slope of the curves becomes greater.

The correct form of the Prandtl and Schmidt functions can not easily be deduced from experimental data given in the literature since experiments on any one system have generally been confined to a fairly narrow range of Schmidt and Prandtl numbers. Nevertheless by analysing the existing data in 1934 Chilton and Colburn[22] suggested that

$$St\ Pr^{\frac{2}{3}} = \frac{h_D}{U^\circ}\ Sc^{\frac{2}{3}} \qquad \ldots\ldots (1.28)$$

For this reason the heat and mass transfer analogy expressed in this form is often referred to as the Chilton-Colburn analogy. Experimental data since 1934 has mostly confirmed Chilton and Colburn's suggestion and equation (1.28) appears to be generally accepted.

To summarise, the balance of experimental and theoretical information suggests that the Prandtl and Schmidt number functions in the mathematical statement of the heat and mass transfer analogy (equation 1.20) are complex but over a wide range of conditions the analogy can be expressed by equation (1.28). There is, however, enough uncertainty to make it worthwhile to confirm the analogy experimentally in the case of the single cell furnace. To this end small scale heat transfer experiments have been carried out in the same model as that used for the mass transfer measurements. These experiments will be described fully in a following section but it is worth noting at this stage that they confirm that the correct exponent on the Schmidt and Prandtl numbers is $\frac{2}{3}$.

1.2.3 The Effect of Varying Fluid Properties

The derivation of the heat and mass transfer analogy from the differential equations given in section 1.2.1 was based on the assumption that the physical properties of the fluid are constant everywhere in the system. If this assumption is not made then additional dimensionless groups involving ratios of actual properties to properties at some reference point are introduced. Similar solutions to the differential

equations for heat and mass transfer would then require that these new dimensionless groups are the same in corresponding positions in both systems. Since mass transfer systems are generally isothermal and of course heat transfer systems involve large temperature differences this requirement is never fulfilled. However many empirical schemes have been suggested in the literature to take account of varying physical properties. Some of these schemes are based on more or less logical considerations but the only real test of them is their ability to correlate the experimental data. The calculations which are described later in this thesis use viscosities and Prandtl numbers evaluated at the mean film temperature $\frac{T_g + T_s}{2}$ and the fluid specific heat evaluated from

$$C_p\ (T_g - T_s) = (I_g - I_s)/\rho_g \qquad \ldots\ldots (1.29)$$

1.2.4 Application of the Heat and Mass Transfer Analogy to Furnace Modelling

The heat and mass transfer analogy can be used to obtain convective heat transfer coefficients in furnaces from cold isothermal model techniques. In these techniques the heat transfer surfaces of the furnace are replaced by mass transfer surfaces in the model and heat transfer coefficients obtained from mass transfer measurements under conditions of kinematic and dynamic similarity. Dynamic similarity demands equal Reynolds numbers in the furnace chamber and model. However the Reynolds number for a furnace, or any other complex heat transfer equipment is generally difficult to define since the correct velocity and length terms are uncertain. Nevertheless, if kinematic similarity exists then these quantities are eliminated when Reynolds numbers are equated to give a relationship between the mass input rates of the form:

$$M_F = \frac{M_M\ \mu_F}{S\mu_M} \qquad \ldots\ldots (1.30)$$

similarily equating j factors in furnace and model gives

$$h = S\ \frac{\mu_F}{\mu_M}\ \left(\frac{Sc}{Pr}\right)^{\frac{2}{3}}\ \rho_M\ C_p\ h_D \qquad \ldots\ldots (1.31)$$

In some cases the furnace and model are such that the correct velocity and length are known and therefore Reynolds numbers and j factors can be evaluated. These results may then be correlated over a range of variables and used to predict conditions not actually covered by model tests. In the case of the single cell furnace such a procedure was found to be possible and the method of correlation is described later.

There are many mass transfer systems that could be used for this work and these may be divided into those in which the fluid is basically water and those in which the fluid is air. Water systems are characterised by high Schmidt numbers whilst the air systems have low Schmidt numbers. The water flow systems can be further subdivided into those involving solid dissolution and those involving an electrolytic reaction.

The main requirements of a solid dissolution system are that the dissolution is sufficiently large so that the mass transfer rate can be measured by weight loss or profilometric techniques or by measuring solid concentration in the exit stream. At the same time the rate must not be so large as to cause a significant change in the dimensions of the model. Solids which meet these requirements are benzoic, cinnamic and salicyclic acid amongst others.

The electrolytic techniques are based on the measurement of the diffusion controlled limiting current at an electrode surface. Examples of electrode reactions which have been used in this way are the reduction of copper ions at a copper electrode, the reduction of ferricyanide ions or the oxidation of ferrocyanide ions at a nickel electrode.

The systems in which air is used are all solid sublimation techniques. The requirements of these systems are similar to those for the dissolution systems. The solids most suitable for furnace model work would appear to be naphthalene and paradichlorobenzene.

At the Gas Council Midlands Research Station two mass transfer techniques have been adopted for furnace model work. These are the

sublimation of naphthalene into air and the reduction of the ferricyanide ion at a nickel electrode. This thesis is concerned with the second of these methods. For the sake of completeness, however, the naphthalene technique is described briefly in the following section since the discussion of the work must inevitably include results from both techniques.

2. EXPERIMENTAL TECHNIQUES

2.1 Description of Models

A cross-section of the prototype single cell rapid billet heating furnace is shown in Figure 2.1 The furnace chamber is 76.2 cm long and 25.4 cm in diameter with refractory walls about 12.5 cm average thickness. It is fired tangentially along the whole of its length with high intensity tunnel burners, the tunnels of which are supported every 12.5 cm. The combustion products leave by four 5 cm x 11.4 cm flues along the top of the furnace.

Models of the furnace were constructed from 0.64 cm thick perspex, all dimensions being scaled by 0.35 except the burner slot height which was further reduced to maintain kinematic similarity as described in Section 1.1.2. The majority of the work described in this thesis concerns experiments done using models of a section of the furnace since this was more convenient experimentally. This was considered to be valid since the flow along the length of the furnace was expected to be uniform. Later, this procedure was confirmed using the naphthalene technique in models of the complete furnace. Dimensions of the furnace and of the models used are shown in Table 2.1.

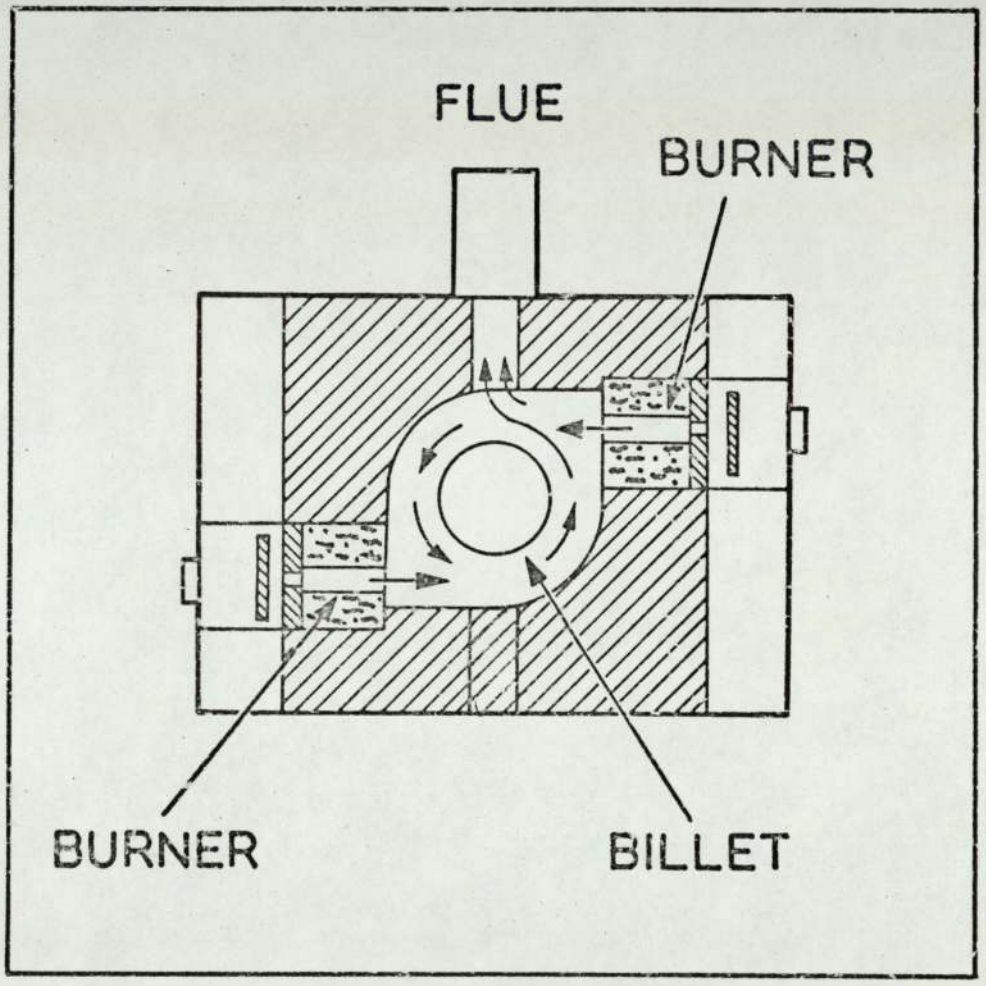

FIG. 2.1. SINGLE CELL BILLET HEATING FURNACE

Table 2.1

Dimensions of Models and Furnace

Dimension	Electrolytic	Naphthalene		Heated Billet	Furnace
	Section Model	Section Model	Full Model	Section Model	
diameter, cm	8.9	8.9	8.9	8.9	25.4
length, cm	7.6	7.6	26.7	7.6	76.2
burner slot height, cm	0.47	0.47	0.47	0.47	1.59
burner length, cm	6.35	6.35	22.0	6.35	62.9
total flue area, cm^2	8.1	8.1	28.3	8.1	232.3
billet diameter cm	-	-	-	2.9	8.3
	3.5	-	-	-	10.0
	3.8	3.8	3.8	3.8	10.9
	-	4.45	-	4.45	12.6
	5.1	5.1	5.1	5.1	14.5
	5.7	5.7	-	-	16.3
	6.35	6.35	6.35	-	18.1

2.2 Mass Transfer Measurements using the Electrolytic Technique

The measurement of mass transfer coefficients using an electrolytic technique has been used extensively. The method consists of measuring the current flowing through the external circuit between a test electrode and a second electrode under conditions in which the current is controlled by the rate at which reacting ions can diffuse to the surface of the test electrode.

2.2.1 Theory of the Electrolytic Technique

In an aqueous solution ions move towards an electrode surface by convective diffusion and as a result of the imposed electric field. However in the presence of a large concentration of an indifferent strong electrolyte the electrical potential in the bulk of the fluid is practically constant and therefore ion movement is due solely to convective diffusion. Under these conditions the convective mass transfer coefficient can be related to the current flowing by the equation:

$$i = AfF_a h_D (C_o - C_s) \qquad \ldots\ldots (2.1)$$

The surface concentration, C_s, of reacting ion depends on the potential applied to the electrode. If this potential is made sufficiently large the surface concentration can be reduced to a negligible value compared with the bulk concentration. The current which can flow therefore reaches a limiting value which is given by

$$i = AfF_a h_D C_o \qquad \ldots\ldots (2.2)$$

and the mass transfer coefficient is therefore.

$$h_D = \frac{i}{AfF_a C_o} \qquad \ldots\ldots (2.3)$$

The several ionic species present in an aqueous solution compete for reaction at the electrode surface. The electrode reaction chosen for the mass transfer measurements must therefore reach limiting diffusion controlled conditions at an electrode potential distinct from that at

which any other reactions can occur. Several reactions fulfill these conditions and have been applied to mass transfer measurements. The most widely used of these are the reduction of the ferricyanide ion[24] and the oxidation of the ferrocyanide ion[25] both in alkaline solution and the deposition of copper from acidic copper sulphate[26], amongst others[27].

For the present work the reduction of the ferricyanide ion from a solution of potassium ferri- and ferrocyanide in sodium hydroxide has been used. The standard electrode potentials for the likely cathode reactions of this solution are

$$Fe(CN_6)^{3-} + e \rightarrow Fe(CN_6)^{4-} \qquad E_1^0 = 0.356 \text{ V} \quad \ldots\ldots (2.4)$$

$$H^+ + e \rightarrow \tfrac{1}{2} H_2 \qquad E_H^0 = 0.000 \text{ V} \quad \ldots\ldots (2.5)$$

The concentrations of the solutions used has been 0.01N potassium ferricyanide and 0.02N potassium ferrocyanide in 1N sodium hydroxide. The reversible electrode potentials at the cathode are then

$$E_1 = 0.356 - 0.059 \log\left(\frac{2 \times 10^{-2}}{10^{-2}}\right) = 0.338 \text{ V} \quad \ldots\ldots (2.6)$$

$$E_H = 0 - 0.059 \log\left(\frac{1}{10^{-14}}\right) = -0.83 \text{ V} \quad \ldots\ldots (2.7)$$

The favoured electrode reaction is therefore the reduction of the ferricyanide ion rather than the evolution of hydrogen.

Once a current begins to flow the electrode potential will alter due to the changed ion concentration at the surface and also due to the irreversibility of the chemical reaction (chemical or activation polarisation). The effect of change in surface concentration can be demonstrated by calculating the polarisation when the concentration of reacting ion has fallen to 1% of the bulk value. The electrode potential is then:

$$E_1 = 0.356 - 0.059 \log\left(\frac{2.99 \times 10^{-2}}{0.01 \times 10^{-2}}\right) = 0.2\text{V} \text{ V} \quad \ldots\ldots (2.8)$$

The chemical polarisation depends upon the reaction concerned, the current flowing and the purity of the electrodes and the electrolyte. In the case of hydrogen evolution the chemical polarisation has been found to be about 0.21 V and therefore the electrode potential must be $-(0.83 + 0.21)\ V = -1.04\ V$ before the reaction supports a significant current. However in the case of ferricyanide reduction, experience has shown that providing sufficient care is taken over electrode cleanliness the chemical polarisation can be kept acceptably small. The current therefore becomes controlled by the rate of diffusion of ferricyanide ions well before hydrogen can be evolved.

The electrical circuit is completed by a nickel anode at which the likely reactions are the oxidation of the ferrocyanide ion and the evolution of oxygen. In this case the oxidation of ferrocyanide is favoured. The net effect of the cathode and anode reactions is therefore that the concentration of ferri- and ferrocyanide ions in the cell remain unchanged.

It is essential to ensure that the polarisation at the anode is small so that the current in the circuit is controlled only by diffusion to the cathode. This is usually achieved by using an anode having a much larger surface area than the cathode. However in the case of the furnace model this is not possible and, therefore, cathode control has been obtained by using twice the concentration of ferrocyanide ions than that of ferricyanide ions. The validity of this can be demonstrated as follows:

Equating the cathodic and anodic currents to each other and to the diffusion of the reacting ions

$$i = fF_a A_c h_{Dc1} (C_{01} - C_{sc1}) = fF_a h_{Da^2} (C_{02} - C_{sa^2}) \quad \ldots\ldots (2.9)$$

where the subscripts 1 and 2 refer to the ferri- and ferrocyanide ions respectively.

Under the experimental conditions concerned

$$h_{Dc1} \simeq h_{Da^2} \ , \ A_c \simeq A_a \ , \ C_{02} = 2\,C_{01}$$

then $$C_{01} - C_{sc1} = 2\,C_{01} - C_{sa^2} \quad \ldots\ldots (2.10)$$

When the current is controlled by diffusion to the cathode $C_{sc1} \simeq 0$

and $C_{sa^2} = C_{02}$

Thus there is always a large concentration of reacting ions at the surface of the anode and therefore the current is only cathodically controlled.

In order to confirm this theoretical analysis, electrode potentials at both anode and cathode have been measured for a typical case using a null balance potentiometer. The solution used was 0.01N in ferricyanide ion, 0.02N in ferrocyanide ion and 1N in sodium hydroxide. The polarisation curves are shown in Figure 2.2 and it is clear that the system is cathodically controlled.

It is interesting to calculate the concentration of the ions at the electrode surfaces under these conditions. Rearranging equation (2.9)

$$C_{sc1} = C_{01} - \frac{i}{A_c f F_a h_{Dc1}} \quad \ldots\ldots (2.11)$$

and $$C_{sA2} = C_{02} - \frac{i}{A_a f F_a h_{Da^2}} \quad \ldots\ldots (2.12)$$

similarly for the product ions:

$$C_{sc2} = C_{02} + \frac{i}{A_c f F_a h_{Dc2}} \quad \ldots\ldots (2.13)$$

and $$C_{sa1} = C_{01} + \frac{i}{A_a f F_a h_{Da1}} \quad \ldots\ldots (2.14)$$

The limiting diffusion controlled currents at the cathode and anode were

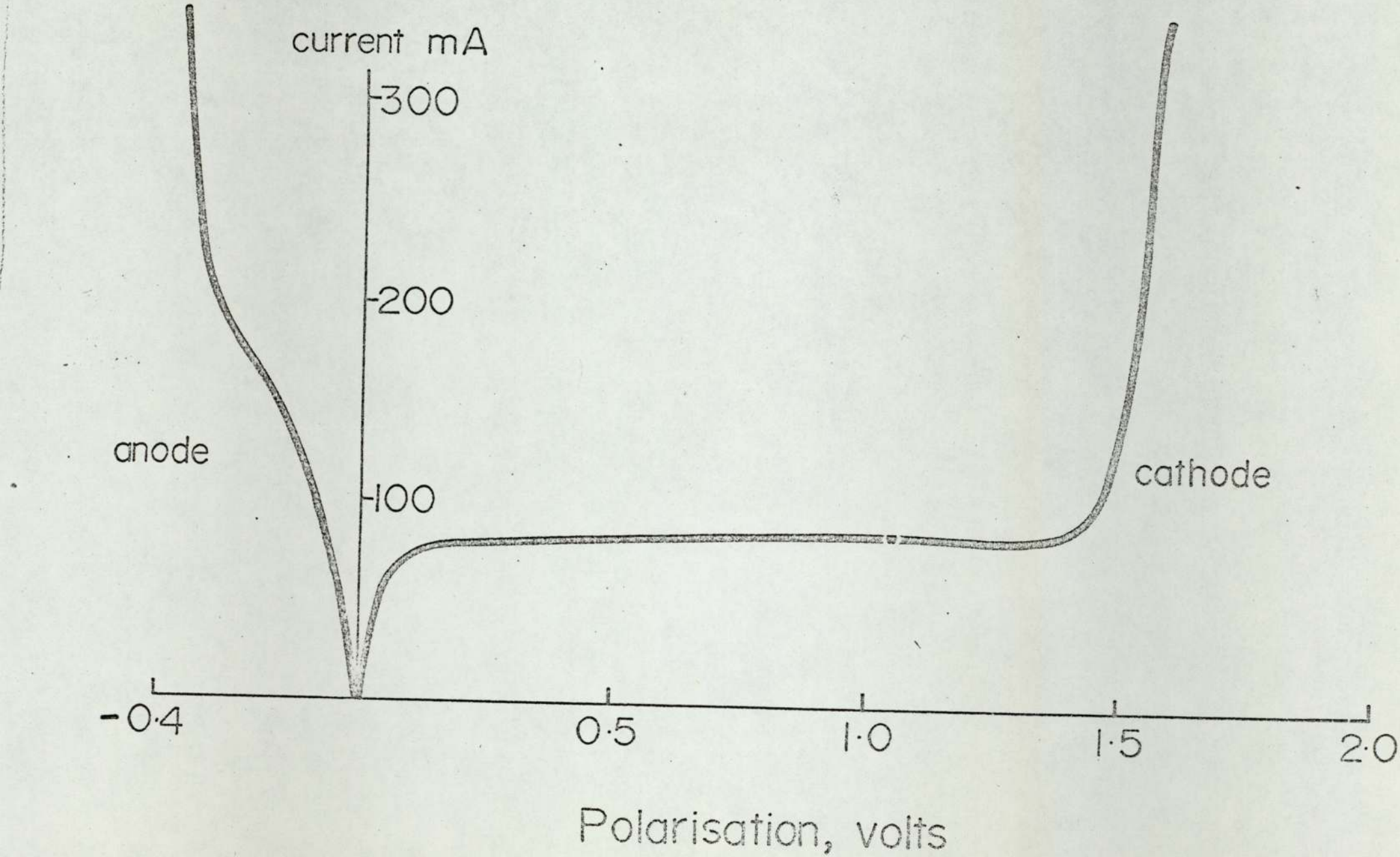

Fig. 2.2 Anode and cathode polarisation curves

first measured and it was thus found that:

$$A_c f F_a h_{Dc1} = 8.0 \text{ A m}^3/\text{kg-ion} \quad \ldots\ldots (2.15)$$

and $$A_a f F_a h_{Da1} = 19.0 \text{ A m}^3/\text{kg-ion} \quad \ldots\ldots (2.16)$$

The mass transfer coefficients for the ferrocyanide ion will not be equal to these values because diffusivities of the two ions are different. But it is assumed that the mass transfer j factors are the same, then for the cathode:

$$h_{Dc1} (Sc_1)^{2/3} = h_{Dc2} (Sc_2)^{2/3} \quad \ldots\ldots (2.17)$$

$$\therefore h_{Dc2} = h_{Dc1} \left(\frac{D_{v2}}{D_{v1}}\right)^{2/3} \quad \ldots\ldots (2.18)$$

From the Nernst equation[28]

$$\frac{D_{v2}}{D_{v1}} = \frac{\lambda_2}{\lambda_1} = \frac{110}{101} \quad \ldots\ldots (2.19)$$

$$\therefore h_{Dc2} = 1.06\, h_{Dc1} \quad \ldots\ldots (2.20)$$

and similarly $$h_{Da2} = 1.06\, h_{Dc}^{\,2} \quad \ldots\ldots (2.21)$$

Then substituting into equations (2.11) to (2.15)

$$C_{sc1} = 10^{-2} \left(1 - \frac{i}{8.0}\right) \text{ kg-ion/m}^3 \quad \ldots\ldots (2.22)$$

$$C_{sA2} = 10^{-2} \left(2 - \frac{i}{20.1}\right) \text{ kg-ions/m}^3 \quad \ldots\ldots (2.23)$$

$$C_{sc2} = 10^{-2} \left(2 + \frac{i}{8.5}\right) \text{ kg-ions/m}^3 \quad \ldots\ldots (2.24)$$

$$C_{sa1} = 10^{-2} \left(1 + \frac{i}{19.0}\right) \text{ kg-ions/m}^3 \quad \ldots\ldots (2.25)$$

Equations (2.22) - (2.25) thus allow the concentration of the ions at the electrode surfaces to be calculated from the measured current. Calculated values for different applied potentials are shown in Figure (2.3). This shows that as soon as the potential is applied the concentration of the ferricyanide ion at the cathode rapidly drops, and is accompanied by a corresponding rise in the ferrocyanide concentration. At the anode the corresponding changes in ion concentrations are much less,

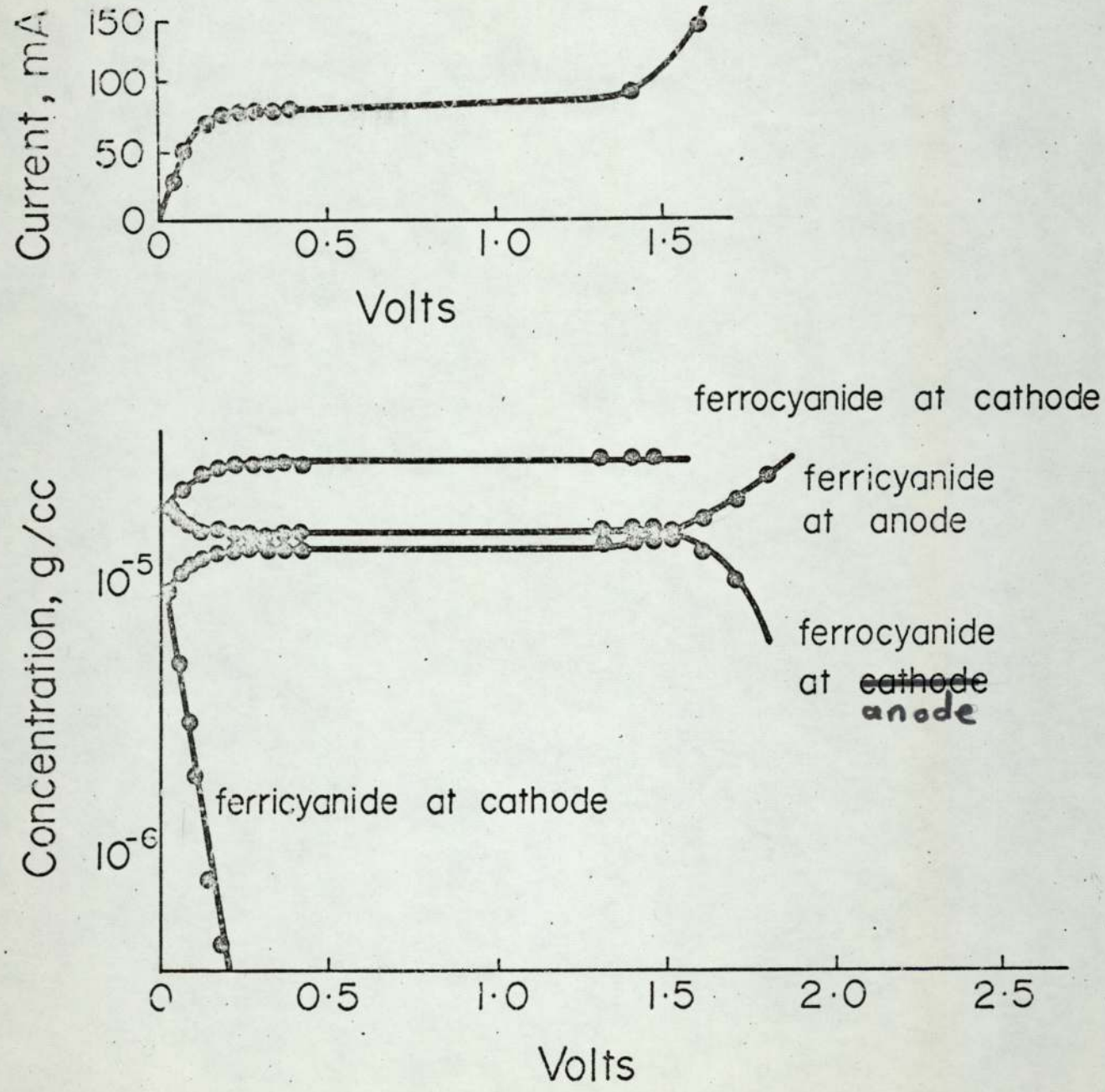

Fig. 2.3 Total polarisation curve and calculated surface concentrations.

once again clearly showing the controlling effect of the cathode.

2.2.2 Physical Properties of the Electrolyte

In order to obtain convective heat transfer coefficients from electrolytic mass transfer measurements it is essential to know the density, viscosity and Schmidt number of the electrolyte.

(a) Density

Providing there is no volume change on mixing the density can be obtained from the known weights of sodium hydroxide and potassium ferricyanide and potassium ferrocyanide used to make up the solution. At 25°C the density was calculated to be 1.04×10^3 kg/m^3 and this value was checked using an hydrometer.

(b) Viscosity

A Cannon-Fenske viscometer was used to determine the relative viscosity of the solution which was found to be 1.24 at 25°C. It was assumed that the relative viscosity would be constant over the small range of temperatures and concentrations used in the experiments.

(c) Schmidt Number

The Schmidt number is obtained from the density, viscosity and diffusivity of the solution. The diffusion coefficient of the ferricyanide ion in a large concentration of indifferent electrolyte has been measured or calculated by various means by several authors and their results are shown in Table (2.2). The value of the function $D\mu/T$ should be a constant according to Eyring's theory[31] and values of this function are shown in the last column of the table. For the work described in this paper it has been assumed that

$$\frac{D_v \mu}{T} = 2.52 \times 10^{-15} \quad N/K$$

Table 2.2 - Comparison of values for D_H/T for ferricyanide ion

Ref.	Tem. (°C)	Viscosity (cP)	Na OH conc (kg-mols/m^3)	$k_3Fe(CN)_6$ conc (kg-mols/m^3	Diffusivity of $Fe(CN)_6^{3-}$ - ion (10^{-10} m^2/s)	D_H/T (10^{-15} n/°K)	Method of calculating diffusivity
24 (k)	28.7	0.915	0.5	0.01	8.80	2.67	Nernst Equation (Ref 28)
24 (a)	25	1.537	2.04	0.01891-0.0199	4.54	2.34	" (Ref 29)
24 (a)	25.7	1.517	2.04	0.0196	4.61	2.33	" (Ref 29)
15	25	1.419	2.03	0.0192	5.24	2.50	Anderson and Saddington (capillary method)
24 (d)	25	1.36	2.0	0.0525	5.80	2.65	Stackelberg and Cottrell (redox method)
24 (t)	25	1.33	1.9	-	5.15	2.30	-
24 (t)	25	1.33	1.9	-	5.65	2.52	(Ref. 24 (a))
24 (q)	25	1.418	2.14	0.0111	5.11	2.43	-
24 (q)	25	1.448	2.23	0.0122	5.22	2.59	-
24 (c)	18-25.7	1.522-1.7859	1.964-2.058	0.0102-.1930	4.19-5.381	2.55	(Ref. 29)
30	25-41.8	0.717-1.140	0.5	0.0009-0.0254	6.7 - 10.57	2.50 ± 0.17	Levich Equation
30	25-25.5	1.109-1.195	1.0	0.0012-0.0486	6.3 - 6.84	2.52 ± 0.1	Levich Equation
30	25-40.7	1.045-1.502	2.0	0.0004-0.1005	5.03-7.63	2.54 ± 0.13	Levich Equations
24 (m)	25	0.9785	0.5	0.025	7.0	2.30	(Ref. 24(m))

2.2.3 Experimental

(a) Measurement of Average Mass Transfer Coefficients

The surfaces of the model corresponding to the heat transfer surfaces of the furnace were first coated with nickel. This was done by either electroplating or by bonding pure nickel sheet onto the perspex surfaces. In the electroplating process tinned copper leads were inserted through holes in the perspex and smoothed flush with the surface. The perspex surface was then softened with solvent and sprayed with silver paste. When the solvents had avaporated off a thin layer of silver remained which acted as a base for subsequent copper and nickel plating. More details of this method are given in the Appendix. The final nickel surface was polished with 'wet and dry' emery paper when either electroplating or pure nickel sheet were used. Once the model had been assembled each surface was activated by using it as a cathode during electrolysis of sodium hydroxide. To facilitate this an additional electrode was plated on the side wall of the model and used as the anode. Hydrogen was evolved briskly from each cathode surface for a period of a few minutes. After activation the anode on the side wall was not used again during the rest of the experiment.

The electrolyte was contained in a thermostatically controlled stainless steel tank. The solution was made up using a known volume of sodium hydroxide and potassium ferri- and ferrocyanide. The ferricyanide concentration of the final solution was checked by measuring the light absorption through a standard cell at a wave length of 450μm using a colorimeter. This instrument was first calibrated using carefully prepared standard solutions. The electrolyte is decomposed by oxygen catalysed by light and therefore nitrogen was bubbled through the solution and a positive nitrogen pressure maintained in the tank. Light

was excluded from the rest of the flow circuit as far as was possible. However, decomposition of the electrolyte still occurred over a period and a fresh solution was prepared each time the model had to be dismantled to change, for example, the size of the billet.

The electrolyte was pumped from the tank through a bank of 'Rotameters' to the model and returned to the tank. A diagram of the flow and electrical circuits is shown in Figure 2.4, the current and voltage being measured with 'Avometers'. When mass transfer to the billet was being measured the billet was made the cathode and the walls the anode of the circuit, the polarity being reversed when mass transfer to the walls was investigated. The voltage applied across the cell was gradually increased and the corresponding current noted until the distinct plateau region of the polarisation curve was reached. A typical set of polarisation curves obtained for a range of flow rates through the model are shown in Figure 2.5. For each of the models the limiting current to the billet and the walls was obtained for a range of billet sizes and volume flow rates.

(b) Measurement of Local Mass Transfer Coefficients

Local mass transfer coefficients have been measured for the billets for three billet sizes. A 2mm wide strip of nickel, the test electrode, was plated along the length of the billet. This strip was separated by about 1mm on each side from the nickel plating covering the remaining billet surface which formed a guard electrode. The test and guard electrodes were each provided with their own electrical contacts and it was checked that the two parts were insulated from each other. Separate electrical circuits as shown in Figure 2.6 were used for the two billet electrodes and these were joined at the model walls which thus formed a common anode. Provision was made to allow the billet to be rotated in the model so that the test electrode could be set in any

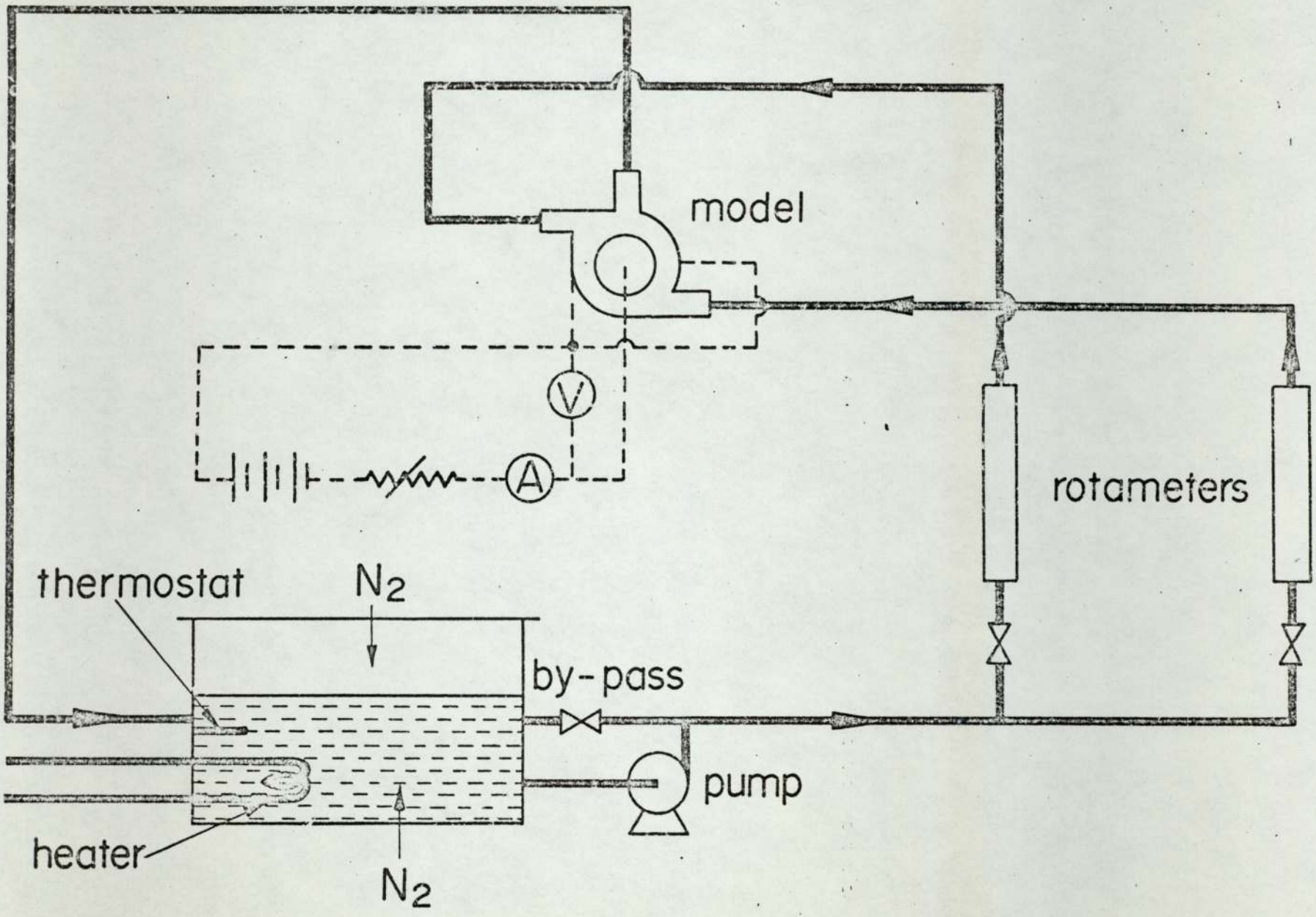
model
V
A
rotameters
thermostat
N_2
by-pass
pump
heater
N_2

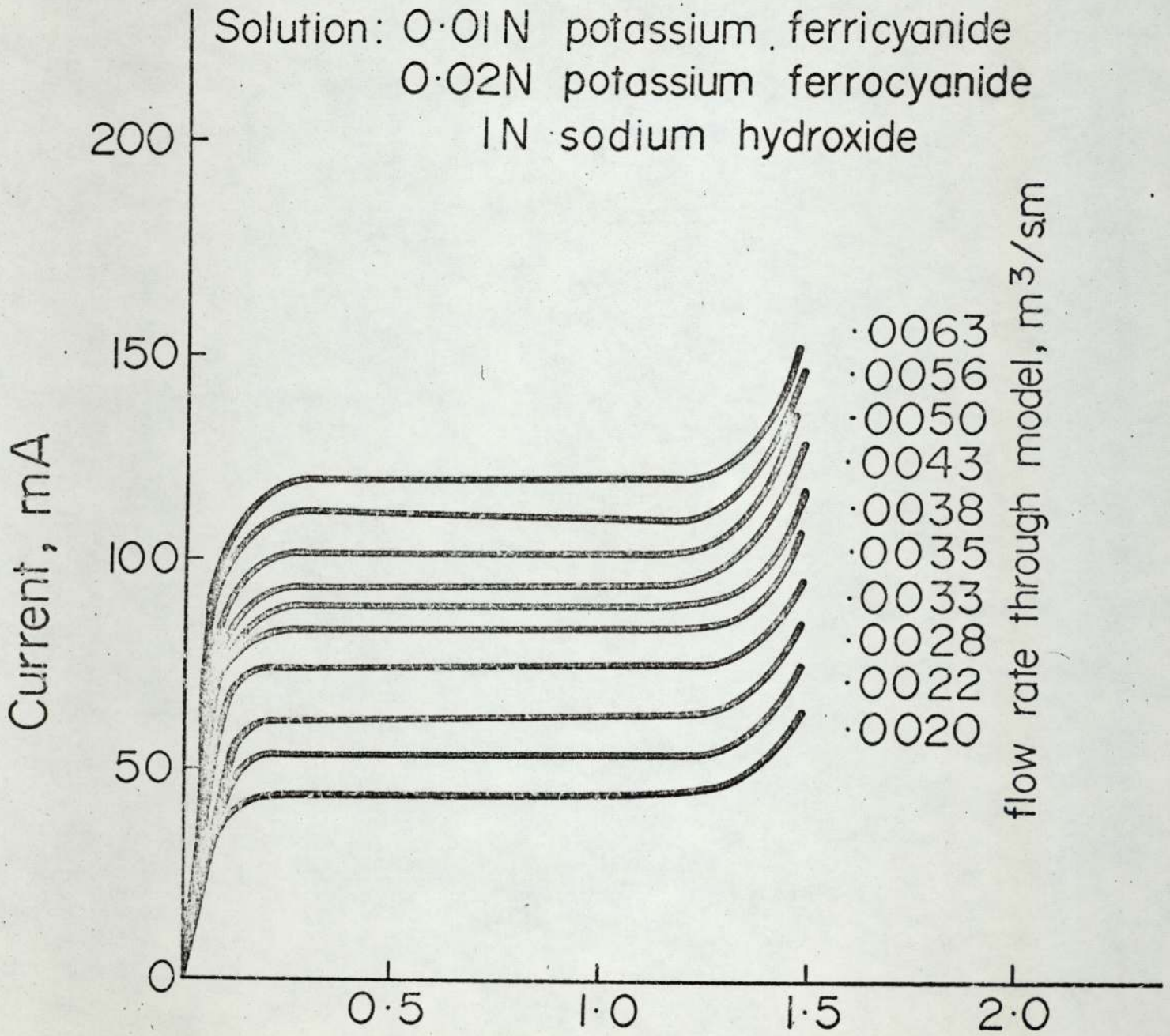

Fig. 2.5 A typical set of polarisation curves for various flow rates.

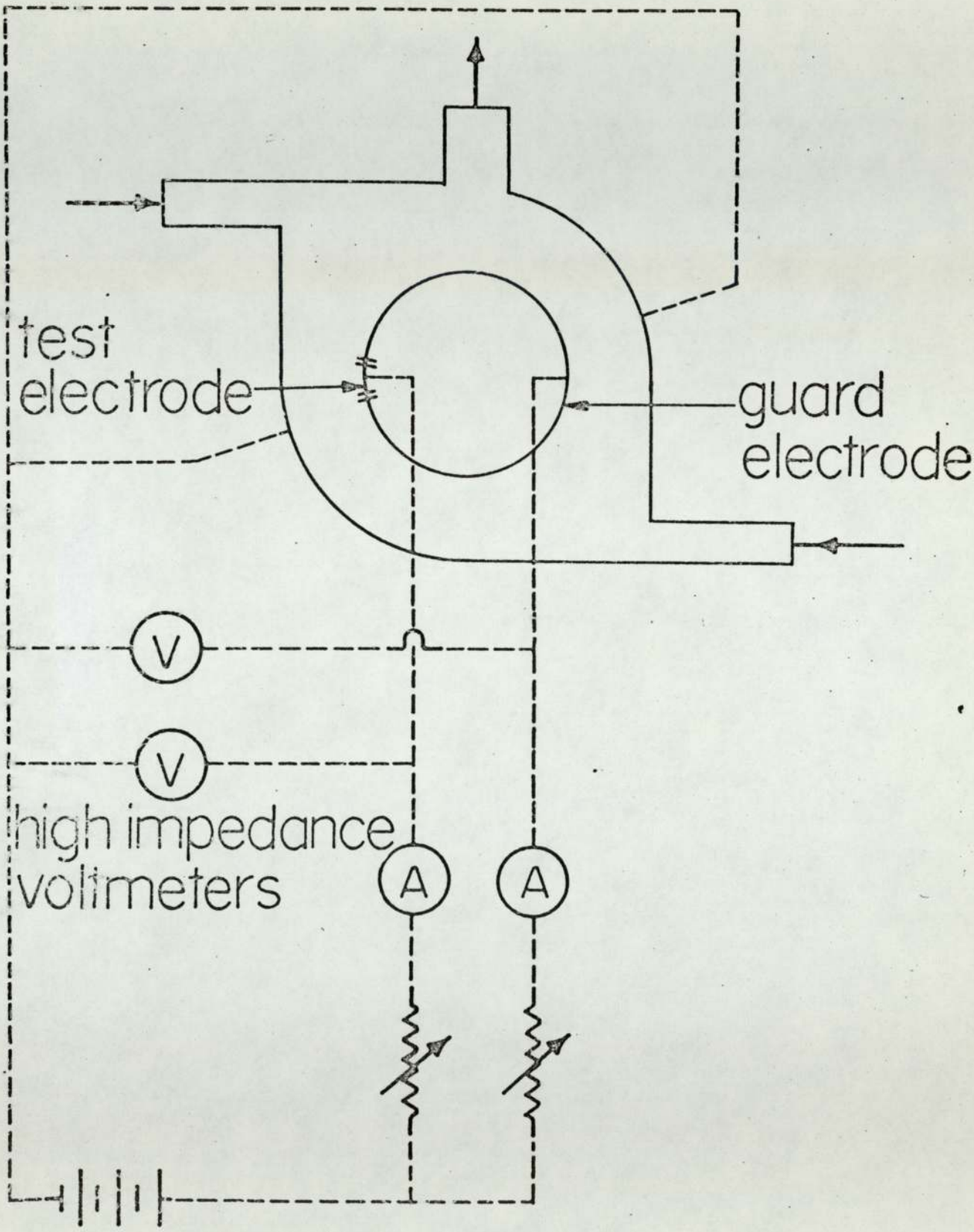

Fig. 2.6 Electrical circuit for measurement of local coefficients.

position relative to the burners and flue.

The experimental procedure was similar to that for measurement of average coefficients. The mass transfer coefficient at any point on the billet surface was found by first rotating the billet until the test electrode was in the desired position. The electrode potentials at both the guard and test electrodes were increased until limiting diffusion controlled conditions were reached and then both currents were measured. The billet was rotated until the test electrode was in a new position and the limiting currents remeasured. It was not necessary to obtain the complete polarisation curve at each position of the test electrode since it was found that diffusion controlled conditions could be maintained comparatively easily whilst the billet was rotated. At any position the local coefficient is obtained from the current to the test electrode and the average coefficient for the whole billet obtained from the current to the guard electrode.

2.3 Mass Transfer Measurements using the Naphthalene Sublimation Technique

A full description of this technique and its application to the single cell furnace has been given by Galsworthy[32]. For the sake of completeness a brief summary of the important aspects of this method will, however, be given here. In the technique, surfaces of the model corresponding to the heat transfer surfaces of the furnace are coated with naphthalene and air passed through the model to simulate the flow of combustion products in the furnace. The resulting weight losses from the naphthalene surfaces are used to obtain the average mass transfer coefficients for each surface using the equation:

$$h_D = \frac{WRT}{\Delta p\, NA} \qquad \ldots\ldots (2.26)$$

The driving force, Δp which causes the naphthalene to sublime is the difference between the vapour pressure at the surface and the partial pressure of naphthalene in the circulating air stream.

The partial pressure of naphthalene in the air stream is calculated from the total weight loss from all the surfaces and a mass balance which includes any data which may be available concerning flow patterns and mixing in the furnace. In the case of the single cell furnace the partial pressure will not be constant throughout the model due to the unsymmetrical positioning of the burners and flue. In addition flow visualisation studies have shown that a large proportion of the flow from the top burner passes directly out of the flue. These factors can easily be taken into account in the mass balance and naphthalene partial pressures in different parts of the model calculated.

The vapour pressure at the naphthalene surface is the saturated vapour pressure which, according to Sherwood and Bryant[33], is given by the equation:

$$\log_{10} p_s = - \frac{6777}{T_s} + 8.67 \qquad \ldots\ldots (2.27)$$

The temperature, T_s, in this equation is the surface temperature which will be lower than the circulating air temperature because of the latent heat of sublimation. The lowered surface temperature can be calculated using the analogy between heat and mass transfer if it is assumed that the heat required for sublimation is obtained from the air by convection through the boundary layer. Then a heat balance gives:

$$\frac{L_N \; h_D}{RT} \; (p_s - p_o) = h \; (T_c - T_s) \qquad \ldots\ldots (2.28)$$

applying the analogy to eliminate the transfer coefficients

$$(T_o - T_s) = \frac{L_N}{C_p \; \rho \; RT} \left(\frac{Pr}{Sc}\right)^{2/3} (p_s - p_o) \qquad \ldots\ldots (2.29)$$

from the Clapeyron Clausius equation

$$L_N = - R \; \frac{d \ln p}{d \left(\frac{1}{T}\right)} \qquad \ldots\ldots (2.30)$$

then from equation (2.27)

$$L_N = 6777 \; R \ln 10 \qquad \ldots\ldots (2.31)$$

finally substituting into (2.29)

$$(T_o - T_s) = \frac{6777 \ln 10}{C_p \; \rho \; T_o} \left(\frac{Pr}{Sc}\right)^{2/3} (p_s - p_o) \qquad \ldots\ldots (2.32)$$

Taking the case when the partial pressure of naphthalene in the air stream, p_o, is negligible and at 20°C equation (2.32) gives a temperature difference of 0.035°C which is generally not worth correcting for.

2.4 Heat Transfer Measurements in the Model

The use of the heat and mass transfer analogy to predict convective heat transfer coefficients in a furnace from mass transfer measurements in a model depends on two main assumptions:

1. The existence of geometric, kinematic and dynamic similarity between the furnace and model.

2. Under these conditions of similarity the dimensionless j factors for heat and mass transfer are equal.

The second of these assumptions has been tested by carrying out heat transfer measurements in an identical model as that used for the naphthalene and electrolytic experiments. The model used was of a 21.7 cm long section of the furnace.

2.4.1 Experimental Technique

Model billets of 2.9 cm, 3.8 cm, 4.45 cm and 5.1 cm diameter were constructed by winding 35 s.w.g. enamelled wire closely round a hollow perspex cylinder to form a single covering of wire. The billet was painted with clear varnish to maintain the wire in position and also to provide a smooth surface.

Each billet was placed in a water bath and a current of approximately 0.5 amp passed through the windings. The electrical resistance at several different water temperatures was then measured using a millivolt potentiometer. It was assumed that the temperature of the wire was that of the billet surface and also of the water and this was confirmed by calibrating at different currents, all of which gave the same resistance at the same water temperature.

After calibration the billet was mounted in the model furnace and air passed through the model. The billet was heated by passing through it a current of between 0.4 and 1.0 amp. Air inlet and outlet temperatures were measured with mercury thermometers and the resistance of the wire obtained from potentiometer readings. These measurements were continued until steady values were obtained. A diagram of the electrical circuit is shown in Figure 2.7.

2.4.2 Calculation of Heat Transfer Coefficient

The heat transfer coefficient, h, is obtained from the heat balance:

$$\text{Power dissipated} = hA\,(T_b - T_o) \qquad \ldots\ldots (2.33)$$

where T_b is the surface temperature of the billet obtained from the resistance measurements T_o is the average bulk temperature of the circulating air. The estimation of the latter quantity can present some difficulty since a significant proportion, e, of the cold air from the top burner passes straight out of the flue. The temperature T_o is then obtained from the inlet and outlet air temperatures using a heat balance, which gives:

$$T_o = \frac{2T_{out} - eT_{in}}{2 - e} \qquad \ldots\ldots (2.34)$$

This procedure is analogous to that for calculating the average concentration of naphthalene in the circulating air stream when using the naphthalene sublimation technique. In both cases, however, the temperature or concentration driving force is fairly insensitive to the value of e.

2.4.3 Analysis of Errors

Two main sources of error are likely in the heat transfer experiments and these arise from heat losses from the outside of the model and the effects of natural convection within the model. The errors resulting would be expected to be greatest when the temperature difference between the heated billet and the air is highest and at low air flow rates. Experiments were carried out using a constant flow rate and various temperature differences. Under such conditions equation (2.33) indicates that a plot of the temperature difference $(T_b - T_o)$ against the power dissipated should be a straight line through the origin.

Experimental results for a 4.45 cm diameter billet with a Reynolds number of 2800 are shown in Figure 2.8. This figure would appear to indicate little error in the experiments under these conditions.

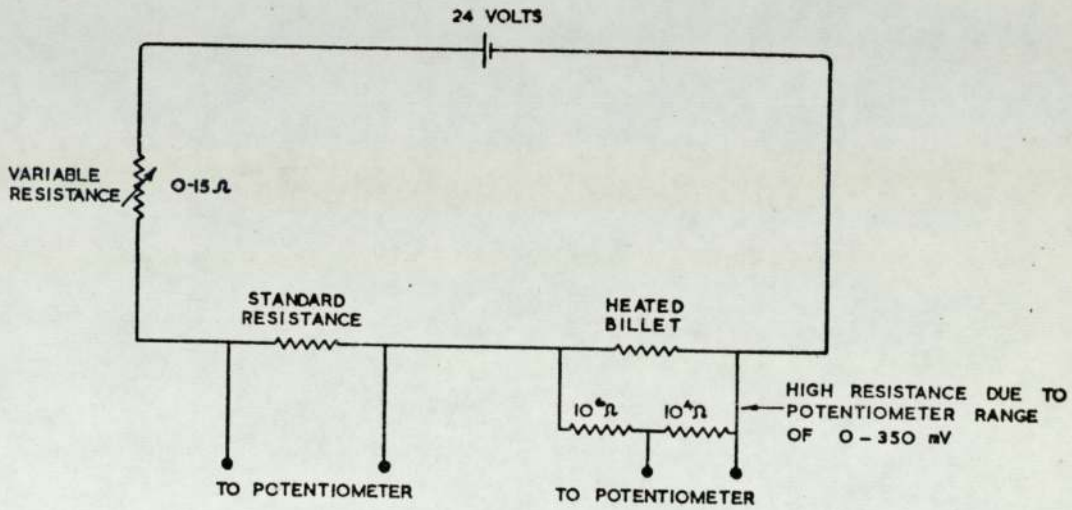

FIG. 2.7 DIAGRAM OF ELECTRICAL CIRCUIT

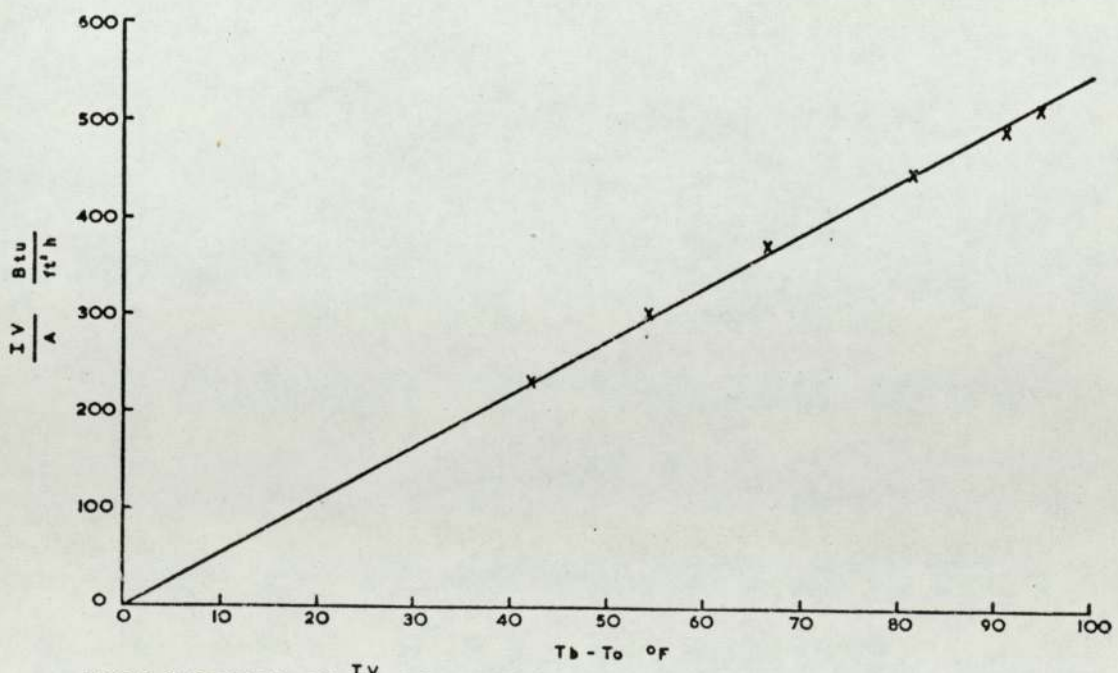

FIG. 2.8 GRAPH OF $\frac{IV}{A}$ AGAINST $T_b - T_o$ FOR THE 1·75 IN. DIAMETER BILLET

3. CORRELATION OF RESULTS

Convective heat transfer coefficients can be derived directly from mass transfer measurements as described in section 1.2.4. Generally heat transfer coefficients in a furnace are required over a range of thermal inputs and it is therefore necessary to carry out mass transfer experiments over a corresponding range of volume flow rates to the model. The experimental results can usually be correlated in a simple form allowing interpolation for flow rates not covered by model tests. In many cases heat transfer coefficients are required for a range of sizes of load in, perhaps, furnaces of various size. In these cases empirical correlation of model results can become cumbersome. However, in some instances the system is such that a simple expression can be found that will correlate all the results over a wide range of flow rates and sizes. Such a case is illustrated by the single cell furnace.

3.1 Solid Body Rotation

Preliminary examination of the mass transfer results indicated that coefficients at the walls were higher than at the billets. It was suggested that this might be explained if the fluid in the furnace and model rotated about the billet axis as if it were a solid body. If the boundary layers on the two surfaces are neglected the velocity distribution would then be given by:

$$v_r = kr \qquad (r_b < r < r_w) \qquad \ldots\ldots (3.1)$$

where

$$k = \frac{2V_{av}}{(r_b + r_w)} \qquad \ldots\ldots (3.2)$$

and $$v_{av} = \frac{1}{(r_w - r_b)} \int_{r_w}^{r_b} v_r . dr \qquad \ldots\ldots (3.3)$$

Under conditions of solid body rotation it would seem reasonable to characterise the flow near the billet by a Reynolds number in which

the length term is taken as the billet radius and the velocity is that obtained by substituting r_b into equation (3.1). It was thus found possible to correlate the mass transfer results reasonably well in the form

$$Sh = a\, Re^{b}\, Sc^{0.33} \qquad \ldots\ldots (3.4)$$

which on rearrangement gives

$$j = a\, Re^{(b-1)} \qquad \ldots\ldots (3.5)$$

Mass transfer coefficients at the walls of the model could be correlated in a similar manner using the wall radius and the velocity close to the wall.

The correlation of results on the basis of solid body rotation was not perfect and it was thought that it would be improved if more accurate data were available on the velocities. This led to a re-examination of the results of some earlier flow visualisation work by Francis, Moppett and Read[35] and it was found that the velocities derived from this enabled a better correlation to be obtained.

The rest of this Chapter is concerned with a description of the flow visualisation studies and also of some additional measurements taken using a pitot-static tube in a full size model. However, it is perhaps first worthwhile emphasising that although velocities calculated from the equations for solid body rotation have not been used for correlating any of the mass transfer results in this thesis they have nevertheless proved valuable in predicting the performance of other similar furnaces for which no detailed measurements were available. One example of this, which will be described in Chapter 7, is the investigation of the effect of size on the thermal response of furnaces.

3.2 Measurement of Velocity

In a single cell furnace high convective heat transfer coefficients and uniform heat fluxes are achieved by promotion of high mass circulation

in the furnace chamber. When these furnaces were first being developed it was recognised that the amount of circulation induced by the burner jets and the nature of the circulation would largely determine the convection in the system. As a consequence, in addition to the mass transfer experiments a programme of flow visualisation was undertaken to obtain both qualitative and quantitative information. Later this work was backed up by a limited number of measurements taken using a pitot tube in a full size model.

3.2.1 Flow Visualisation

The flow in the furnace model has been visualised using polystyrene beads as tracer. The flow patterns were recorded on ciné film at 750 to 2000 frames per second with a spark time marker for film speed measurement. By projecting these films at low speed the flow can easily be followed and the velocity of individual beads measured. The circulation within the furnace was originally characterised only by a mean recirculation ratio, c_m, defined by the ratio of the circulating mass flow through any cross section of the furnace chamber to the total mass input rate to the furnace. Then for a constant density fluid

$$c_m = \frac{v_{a\,v}\,(r_w - r_b)\,l_m}{Q} \qquad \ldots\ldots (3.6)$$

This work was later extended to include measurement of velocity profiles by taking velocities of particles travelling round narrow annular sections in the model. These profiles can be expressed in dimensionless form by a velocity ratio defined by

$$v_r^* = \frac{v_r}{v_{a\,v}} \qquad \ldots\ldots (3.7)$$

The velocity ratio is a function of radial position and for solid body rotation becomes:

$$v_r^* = \frac{2r}{(r_b + r_w)} \qquad \ldots\ldots (3.8)$$

Combining equations 3.6 and 3.7 the velocity at any point in the furnace is given by:

$$v_r = \frac{v_r^* \, c_m \, Q}{l_m \, (r_w - r_b)} \qquad \ldots\ldots (3.9)$$

The flow in the single cell furnace is complicated by the single flue whose position results in a greater mass flow round the side opposite to the flue (designated side 2) than round the side including the flue (side 1). In interpreting the flow visualisation results the mean recirculation ratio has been taken as the average for both sides of the furnace and the difference between the two sides is contained in the velocity ratio. Different velocity ratios are therefore obtained for different sides of the furnace.

The mass transfer measurements which have already been described result in mass transfer coefficients which are averaged over the entire billet surface. In this case the coefficients must be correlated using average velocity ratios: The Reynolds number and j factor for the model experiments can then be defined as:

$$Re_b = \frac{d_b \, Q_M \, \rho_M \, c_m \, v_b^*}{2 \, l_M \, b_M \, \mu_M} \qquad \ldots\ldots (3.10)$$

and

$$j_b = \frac{h_{D\,b} \, b_M \, l_m \, Sc^{\frac{2}{3}}}{v_b^* \, c_m \, Q_M} \qquad \ldots\ldots (3.11)$$

For the walls mass transfer measurements were taken for each wall separately so that individual Reynolds numbers and j factors can be defined as follows:

for wall 1

$$Re_1 = \frac{d_w \, Q_M \, \rho_M \, c_m \, v_{w1}^*}{2 \, l_m \, b_M \, \mu_M} \qquad \ldots\ldots (3.12)$$

$$j_1 = \frac{h_{D\,1} \, b_M \, l_m \, Sc^{\frac{2}{3}}}{V_{w1}^* \, c_m \, Q_M} \qquad \ldots\ldots (3.13)$$

for wall 2

$$Re_2 = \frac{d_w \, Q_M \, \rho_M \, c_m \, v_{w2}^*}{2 \, l_m \, b_M \, \mu_M} \qquad \ldots\ldots (3.14)$$

$$j_2 = \frac{h_{D2}\ b_M\ l_M\ Sc^{\frac{2}{3}}}{v^*_{w2}\ c_m\ Q_M} \qquad \ldots\ldots (3.15)$$

Values of recirculation ratio and velocity ratio obtained from the flow visualisation results are given in table 3.1. It is worth noting that a simple mass balance leads to the conclusion that the velocity ratios on each side of the furnace differ by 0.5. The results given in table 3.1 do not agree with this mass balance and this point will be considered later.

Apart from measurements of velocity the flow visualisation has been useful in revealing several aspects of the aerodynamics of the furnace which were not immediately obvious. Firstly several areas of nearly stagnant flow were noted and these go some way towards explaining the local variations of mass transfer. Secondly, and more important, it was found that a large fraction, e, of the flow from the top burner passed straight out of the flue without apparently mixing with the rest of the fluid in the model. This factor must be taken into account in the calculation of the naphthalene mass transfer results and also in the prediction of the performance of the actual furnace. Measured values of the fraction e are included in Table 3.1.

One of the advantages of the flow visualisation technique is that no probes are introduced into the models and that the flow is undisturbed by measurement of its velocity. This is especially important in models of the size which have been described up until now. Some work has however been carried out using pitot-static tubes in a full size model of the furnace.

3.2.2 Pitot tube measurements

Tangential velocities were measured for cold air flowing through a full size model of the furnace using a 2 mm diameter pitot - static tube. The measurements were taken at different radial positions between the billet and the walls at four stations round the circumference and at two

Table 3.1

Flow Visualisation Results for the Prototype Single Cell Furnace

Model Billet Diameter, cm	C_n	V^*_b	V^*_{w1}	V^*_{w2}	e
3.80	1.41	0.532	1.36	1.54	0.75
4.45	1.31	0.572	1.28	1.47	0.77
5.1	1.19	0.630	1.21	1.42	0.79
5.7	1.05	0.714	1.13	1.37	0.81
6.35	0.88	0.852	1.08	1.36	0.83

stations down the length of the model. For each velocity profile measured across the annular gap the corresponding volume flow rate was calculated assuming that the velocity profile remained unchanged down the length of the furnace. Volume flow rates obtained in this way for an input flow of 11.4 dm^3/s of air through each burner are shown in figures 3.1 and 3.2. In figure 3.1 the four measuring stations all lie on a line behind the middle of one of the four flues whilst in 3.2 the measuring stations are on the centre line between two flues.

The velocity measurements show, as did the flow visualisation, that a large fraction of the fluid entering the model from the top burner passes straight out of the flues. However this obviously occurs only for that portion of the burner which is actually opposite the flues (0.6 of the burner length - see Figure 3.3). This results in the flow rate of the air directly behind the flues being a lot less than that which passes between the flues. As the air passes on round the furnace the lengthwise distribution of the flow becomes gradually more uniform to the extent that it is almost constant before the top burner is reached. Under these conditions it is hardly surprising that flow visualisation of an illuminated section of a model gave recirculation ratios on either side of the furnace which could not be reconciled with a simple mass balance.

The three dimensional nature of the flow in the model suggests that the velocity measurements should be taken using a five hole pitot tube rather than with a simple pitot-static tube. Also a large number of measurements would have to be made to obtain a complete description of the flow conditions. This work has not been attempted but the results described in this section at least give some indication of the flow distribution.

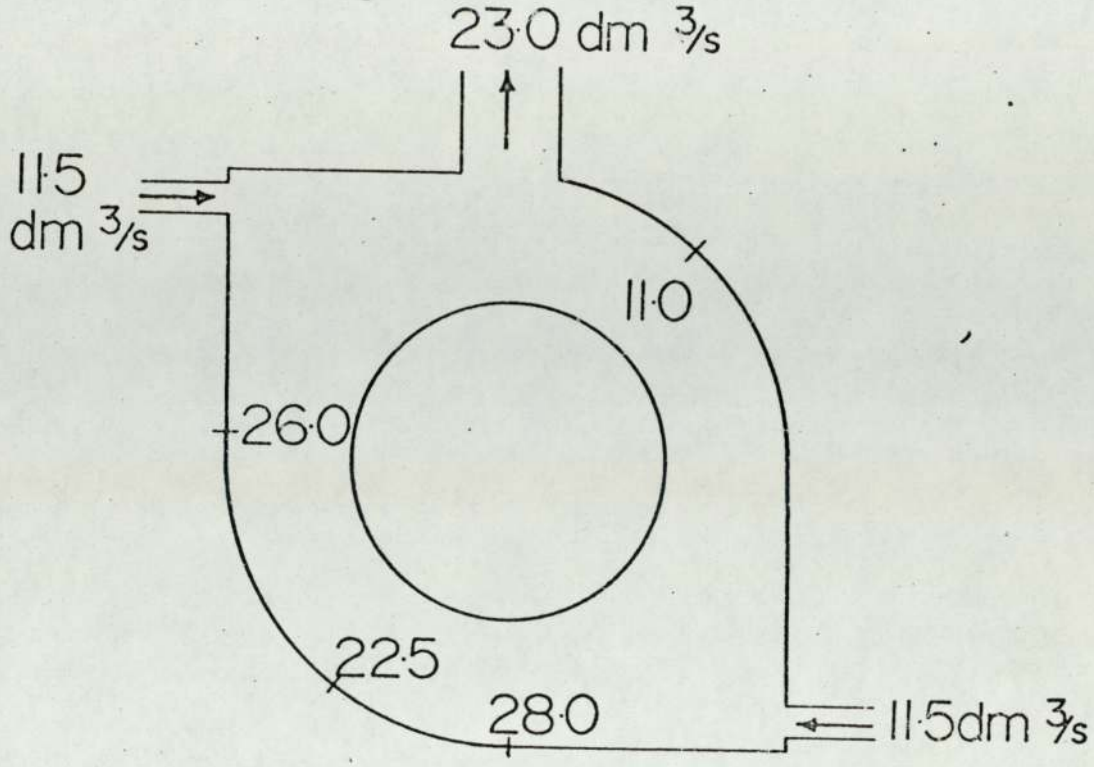

Fig. 3.1 Pitot tube measurements (in line with flue)

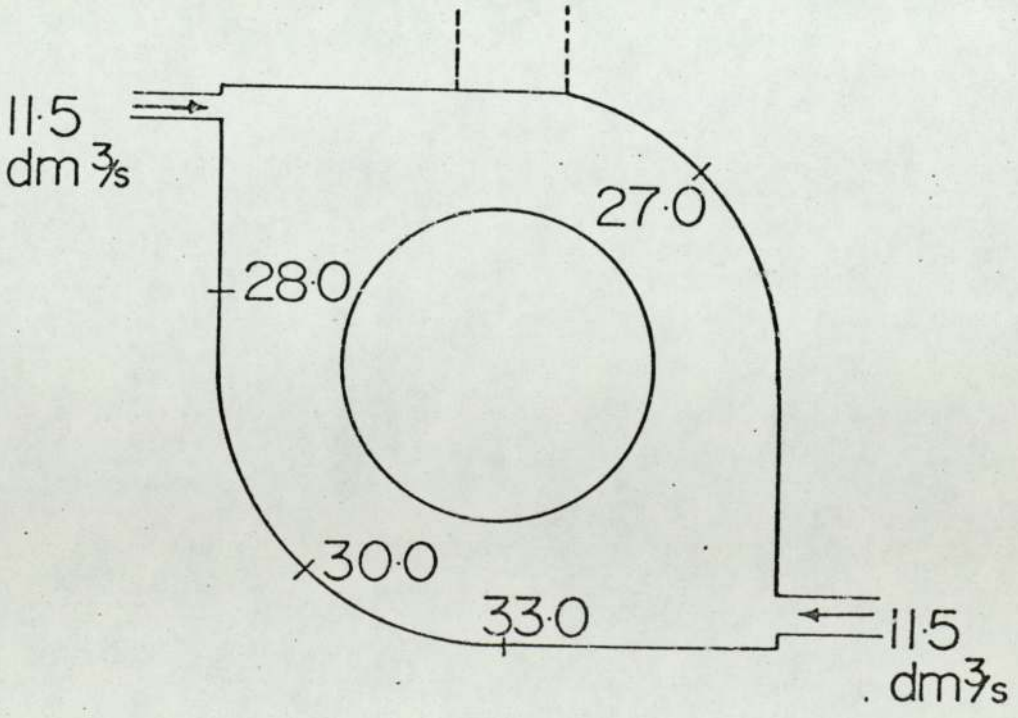

Fig. 3.2 Pitot tube measurements (between flues)

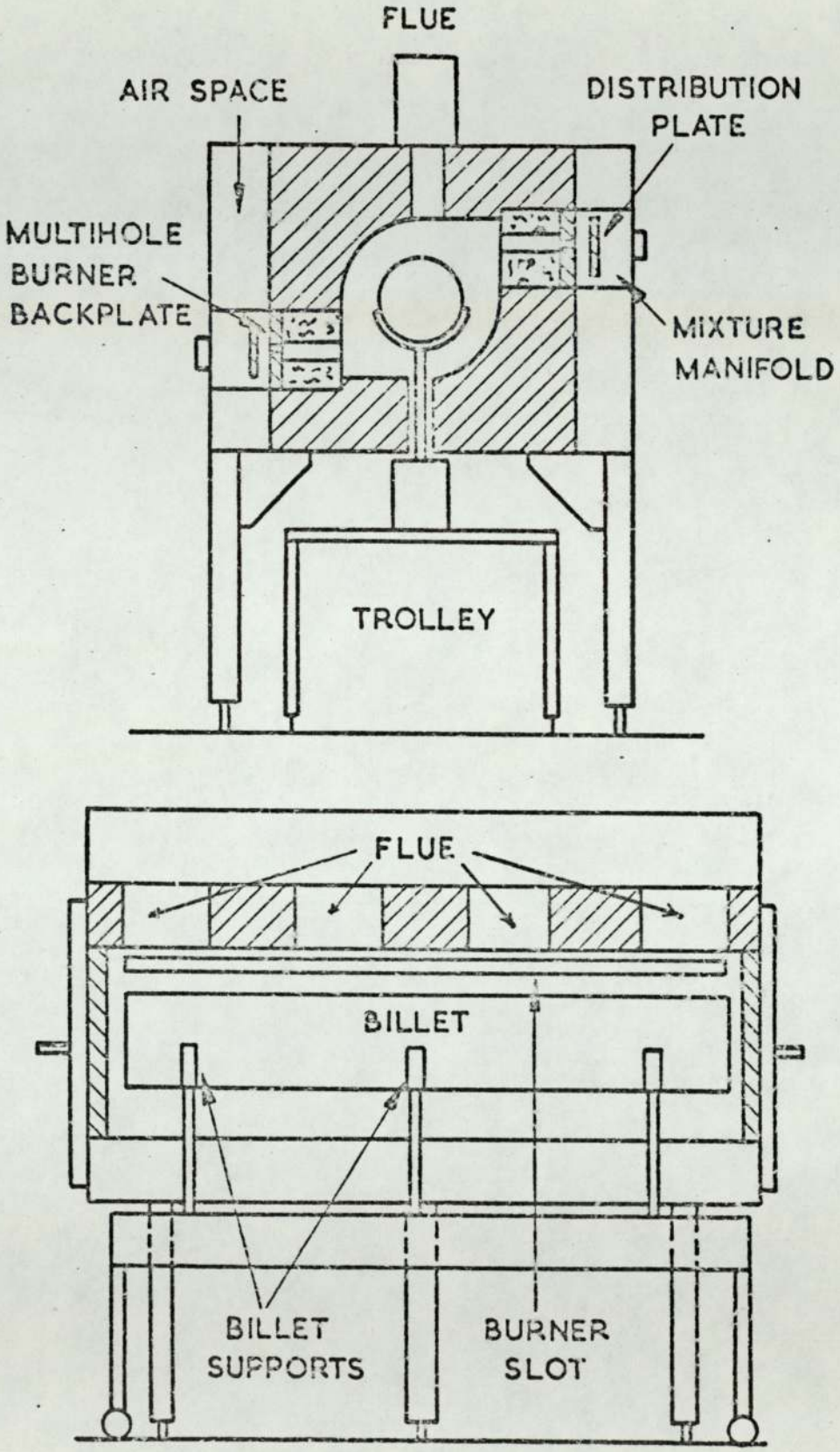

Fig 3.3 SINGLE CELL RAPID HEATING FURNACE

(4) RESULTS

In this chapter the results of the experimental measurements described previously are presented. The average coefficients obtained from the electrolytic technique are given in the first section and these are then compared with results obtained from the naphthalene and heated billet experiments. Finally the local mass transfer coefficients are given. All these results are discussed in the next chapter.

4.1 Average Coefficients obtained from the Electrolytic Technique

A typical set of experimental measurements for one billet size and several flow rates are given in detail in Appendix 2 and the results for the other billet sizes are summarised in Appendix 3. The mass transfer coefficients, for two billet sizes, are shown in figure 4.1. These same results, together with those for other billet sizes, are replotted in a dimensionless form in figure 4.2 using Reynolds numbers and j-factors calculated in the way which was described in chapter 3. Average coefficients at the walls obtained for the same range of billet sizes are given in figure 4.3. In this figure the results for the top and bottom walls of the model are shown separately and no distinction is made between different billet sizes.

4.2 Comparison of Average Coefficients for the Billets Obtained from the Three Model Techniques

In chapter 2 three experimental techniques were described; the electrolytic technique, the naphthalene sublimation method and direct heat transfer measurements. The results obtained from the electrolytic technique have been presented in the previous section. Average coefficients at the billet for various billet sizes using the other two techniques are shown in figures 4.4 and 4.5. In the case of the naphthalene results three separate sets of experiments are indicated (a) those for a model of a complete furnace, (b) those for a model of a

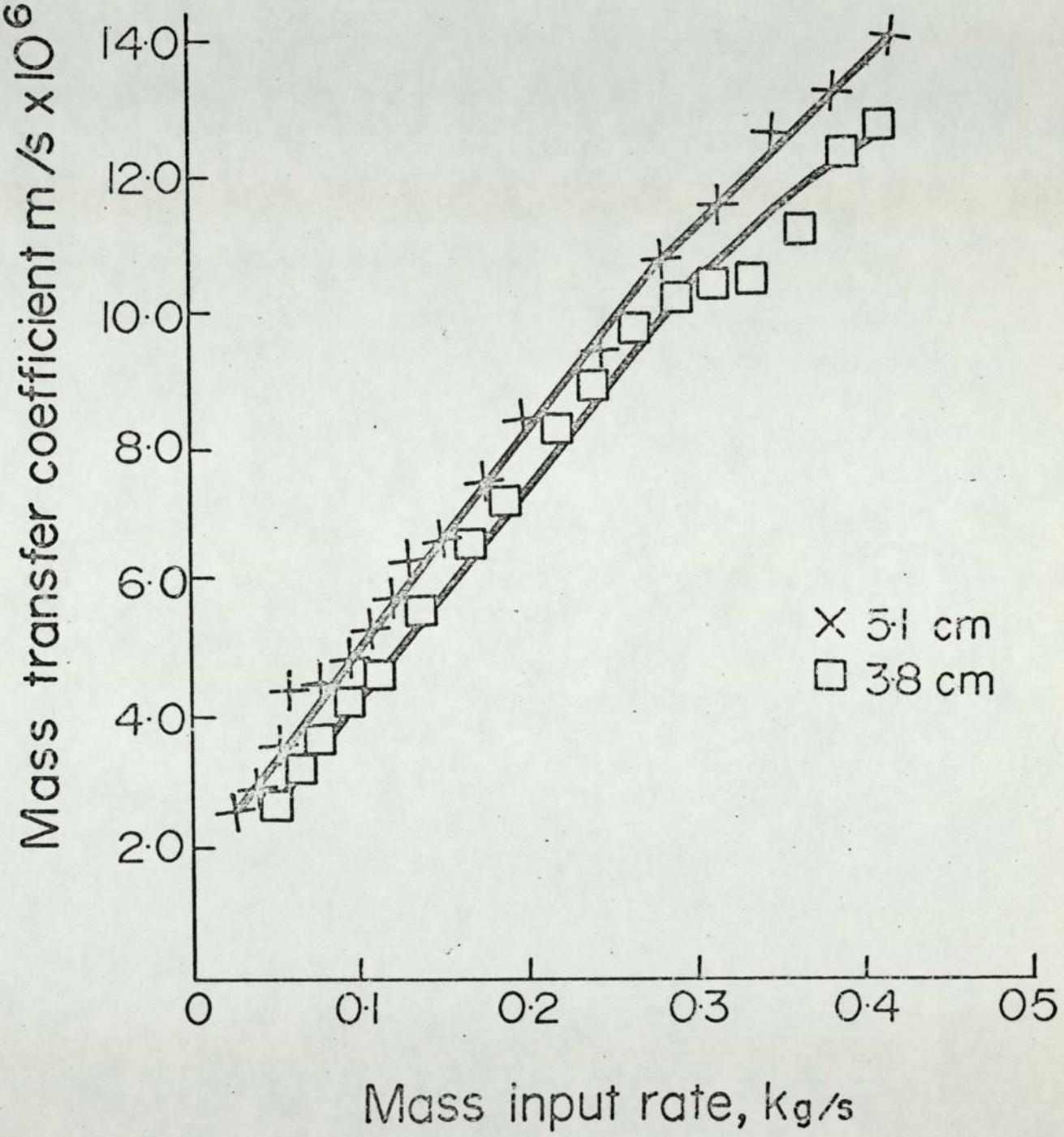

Fig. 4.1 Measured mass transfer coefficients for two billet sizes.

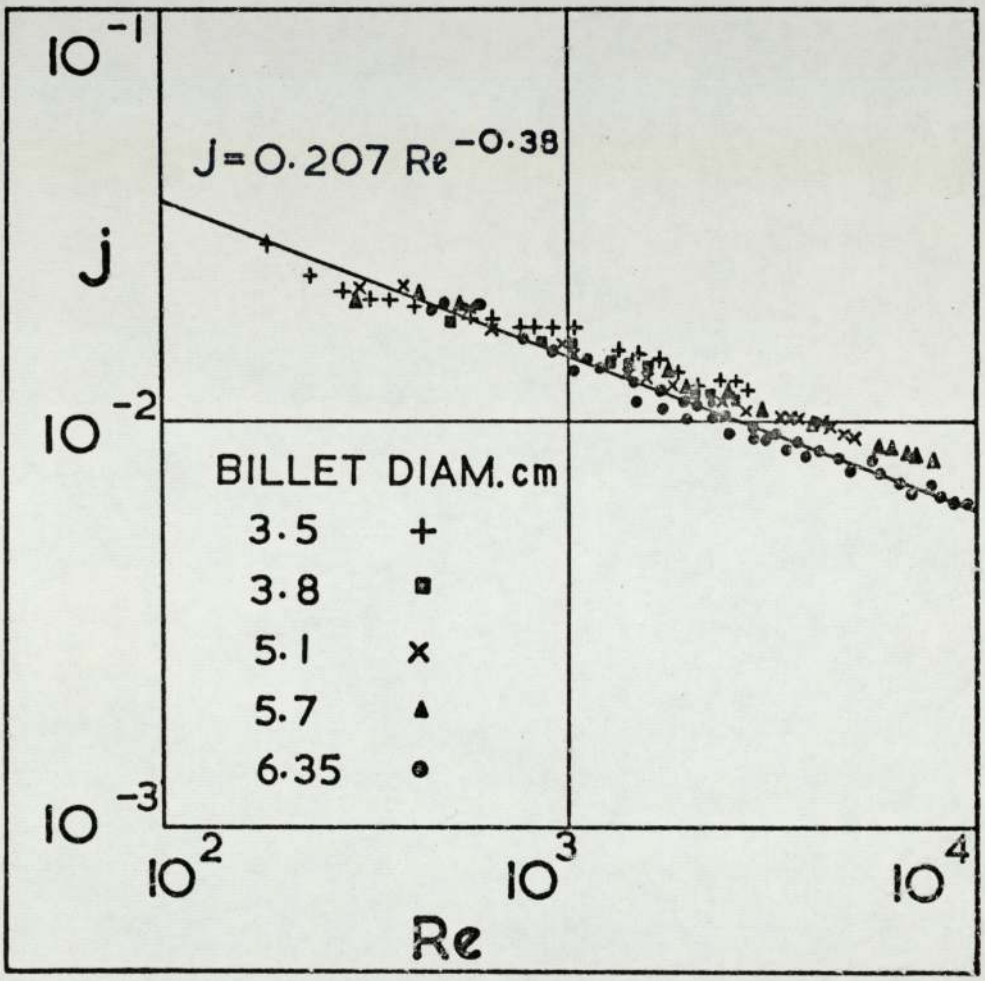

FIG. 4.2. ELECTROLYTIC RESULTS (BILLETS)

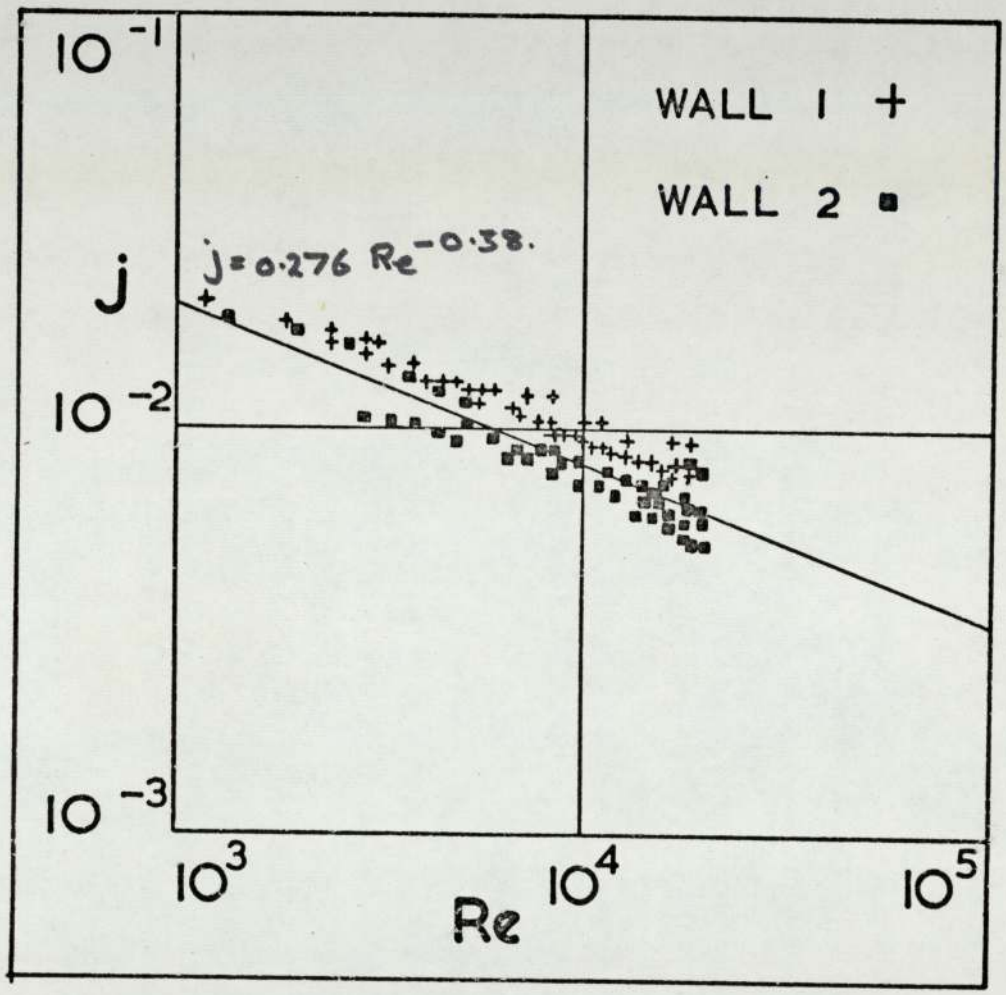

FIG. 4.3. ELECTROLYTIC RESULTS (WALLS)

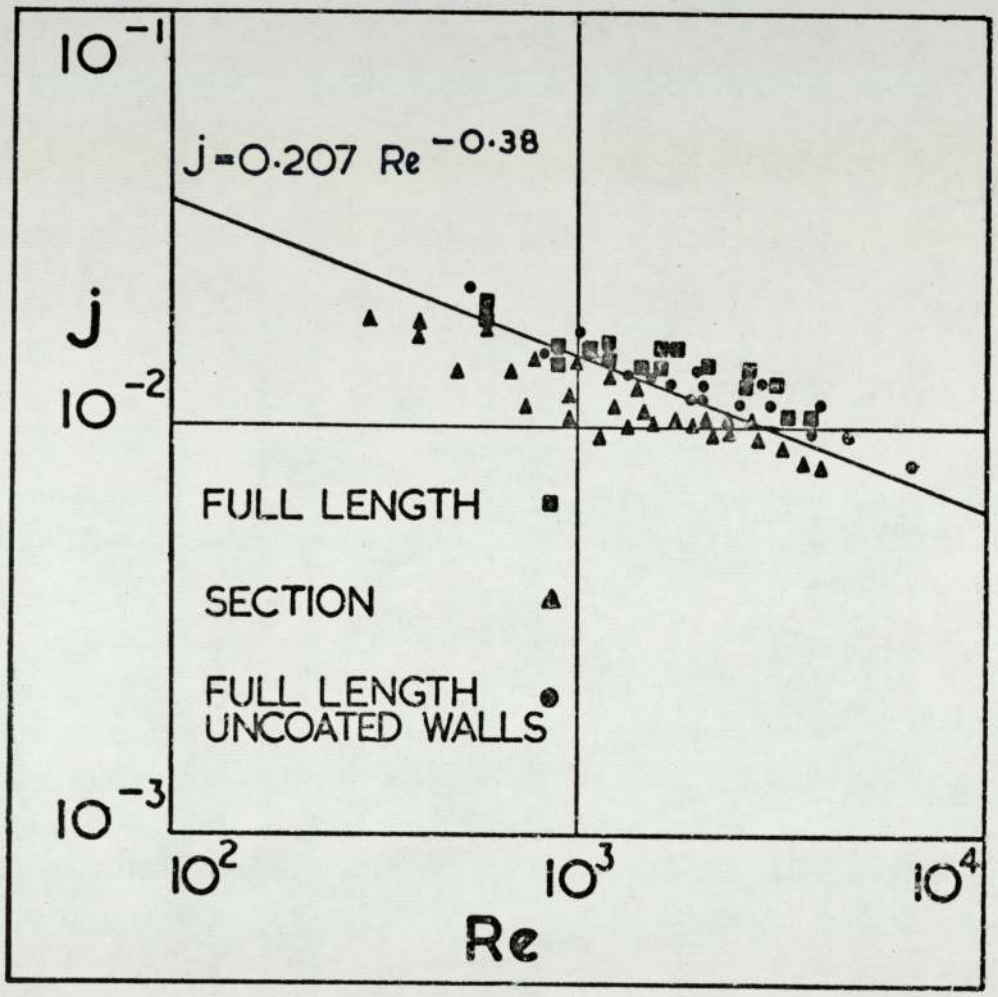

FIG. 4.4. NAPHTHALENE RESULTS (BILLETS)

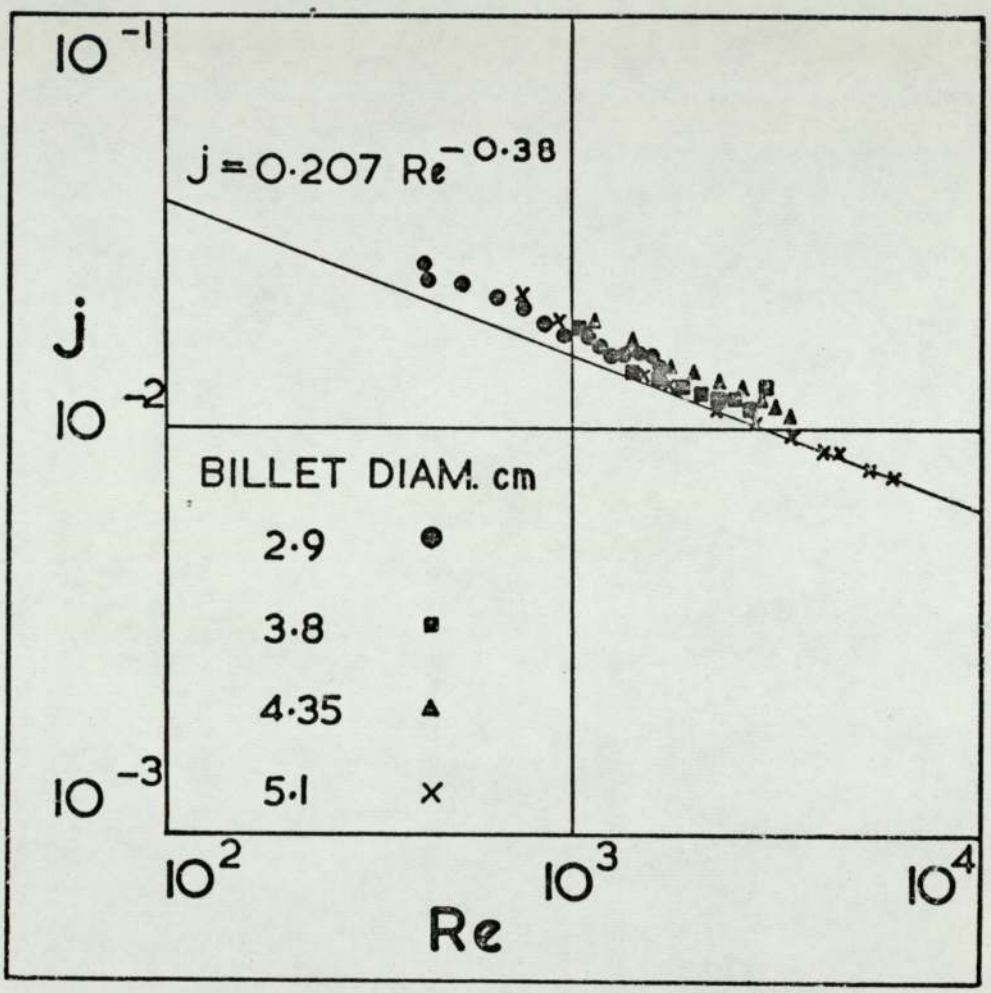

FIG. 4.5. WIRE WOUND BILLET RESULTS

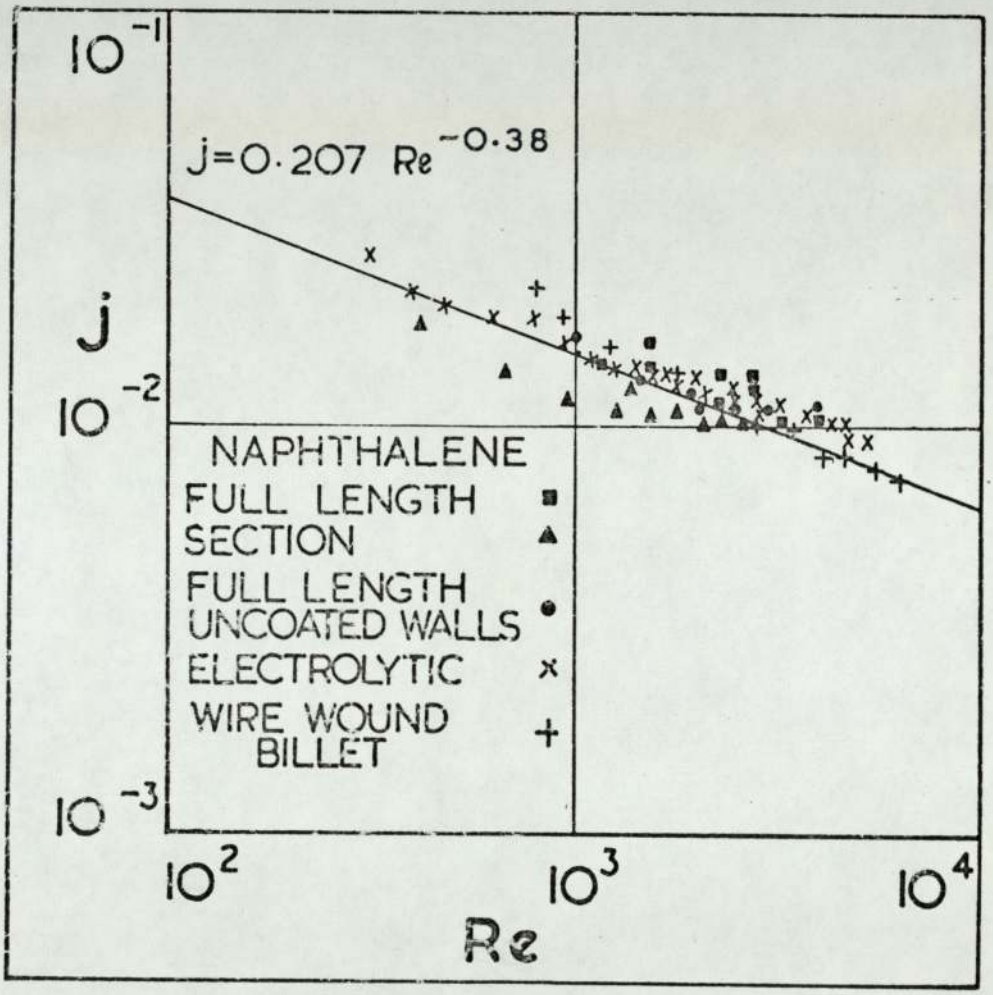

FIG. 4.6. COMPARISON OF DIFFERENT TECHNIQUES FOR ONE BILLET SIZE.

section of the furnace, (c) those for a model of a complete furnace in which the billet alone was used as a transfer surface. These measurements were made for three different billet sizes but for the sake of clarity no distinction is made between them in this figure.

A comparison of the results obtained from the three methods shown on the same graph is somewhat confusing since about 260 experimental points were obtained. However, in figures 4.2, 4.4, and 4.5 a common line is shown which represents the equation:

$$j = 0.207 Re^{-0.38} \qquad \ldots\ldots (4.1)$$

This equation was originally fitted to some early electrolytic results and was then incorporated into the mathematical model from which furnace performance was predicted. When more results from all three techniques became available their deviation from the original line did not justify the confusion which would have resulted from fitting a new correlation. In figures 4.2, 4.4 and 4.5,57% of all the experimental results lie between $\pm$ 10% of the line and 98% between $\pm$ 25% of the line. A clearer comparison can be obtained if the results for one billet size obtained from the three techniques are shown plotted together as in figure 4.6.

4.3 Local Coefficients obtained from the Electrolytic Technique

The measured local mass transfer coefficients obtained for one billet size and three different flow rates are given in figure 4.7. This figure is a polar diagram, the distance of the curve from the billet centre represents the mass transfer coefficient at any point. Results for the three flow rates can be reduced almost to a single line as shown in figure 4.8 by replotting as the ratio of the local coefficients to the average coefficient. Similar plots for other billets sizes are shown in figures 4.9 and 4.10.

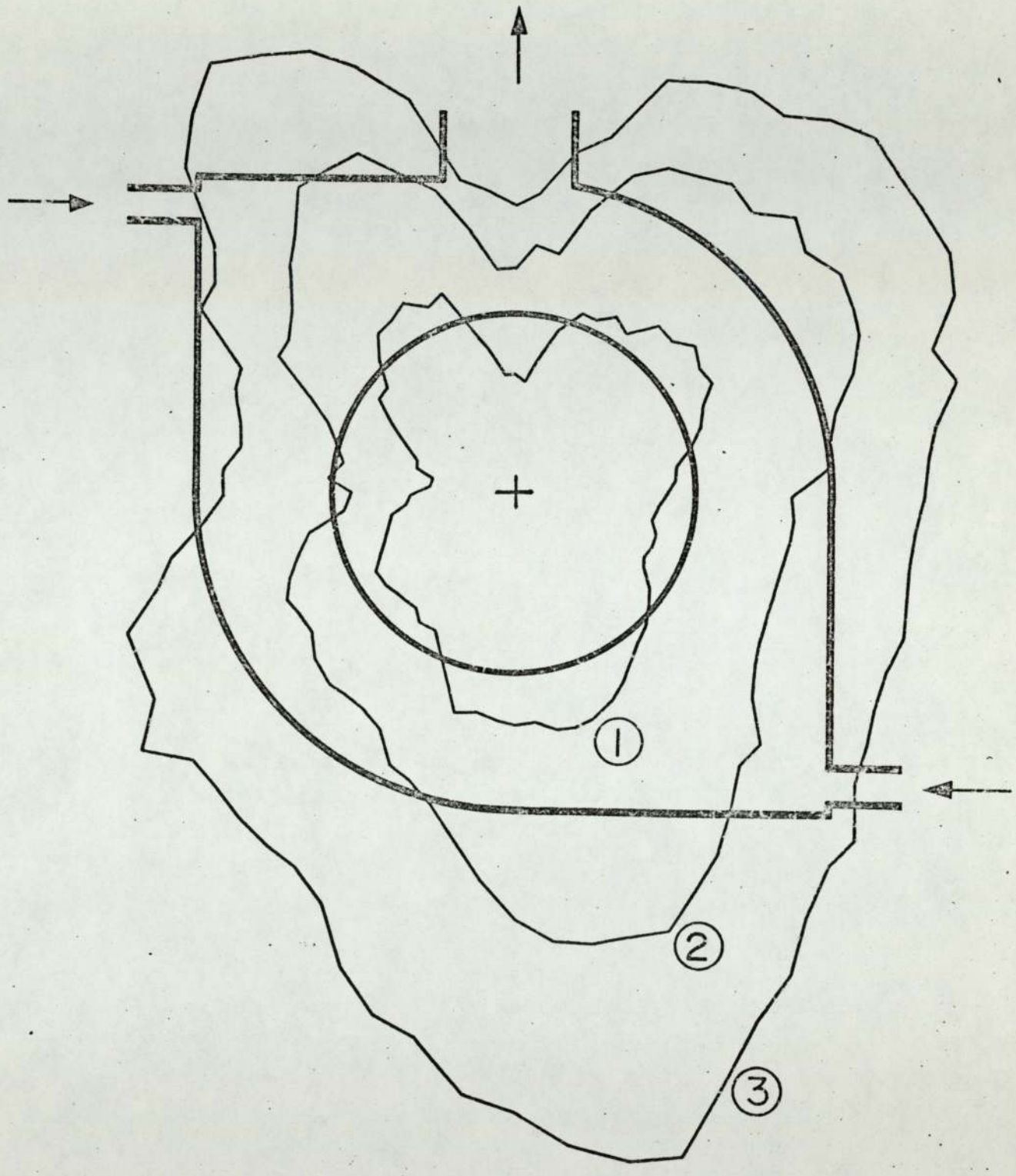

Fig. 4.7 Local mass transfer coefficients for a 5.1 cm diameter billet (1 cm radial distance represents 1.9×10^{-6} M/S)

(1) Flow rate = 0.119 kg/s

(2) Flow rate = 0.238 kg/s

(3) Flow rate = 0.358 kg/s

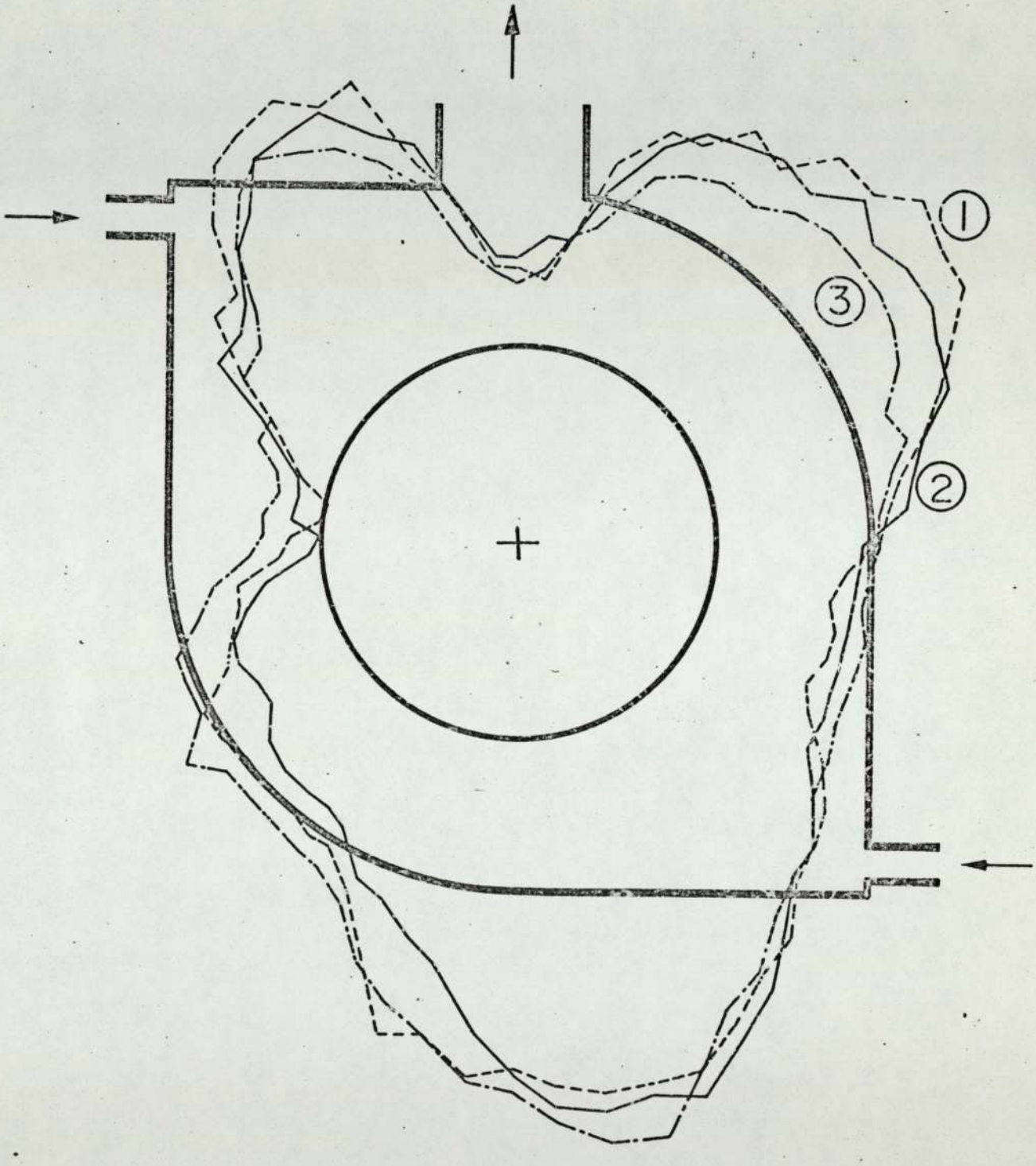

Fig. 4.8 Relative mass transfer coefficients for a 5.1 cm diameter billet (the average coefficient is represented by a radial distance of 6.25 cm)

(1) Flow rate = 0.119 kg/s

(2) Flow rate = 0.238 kg/s

(3) Flow rate = 0.358 kg/s

0.238 kg/s

0.119 kg/s

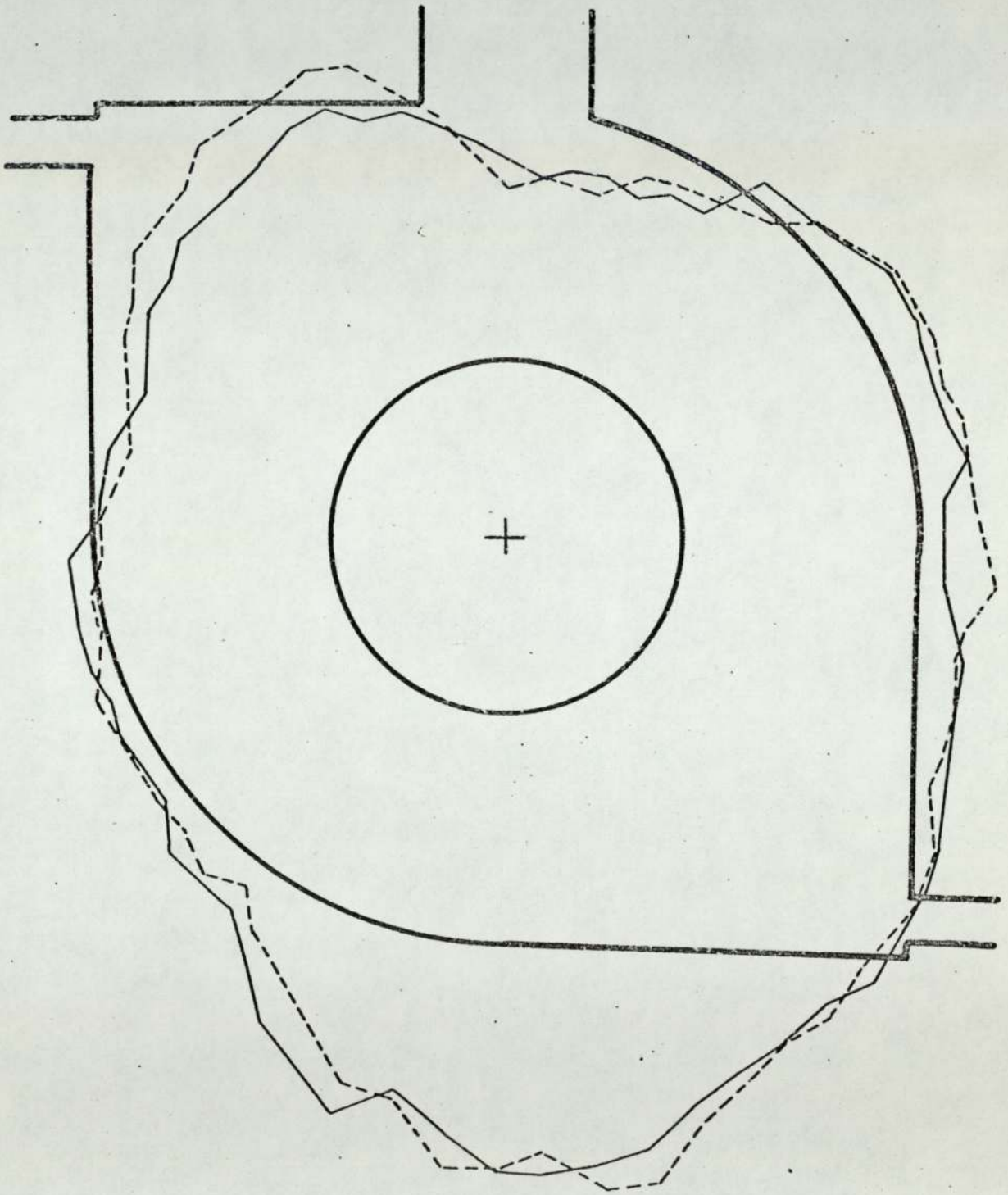

Fig. 4.9 Relative mass transfer coefficients for a 3.8 cm diameter billet (the average coefficient is represented by a radial distance of 7.3 cm).

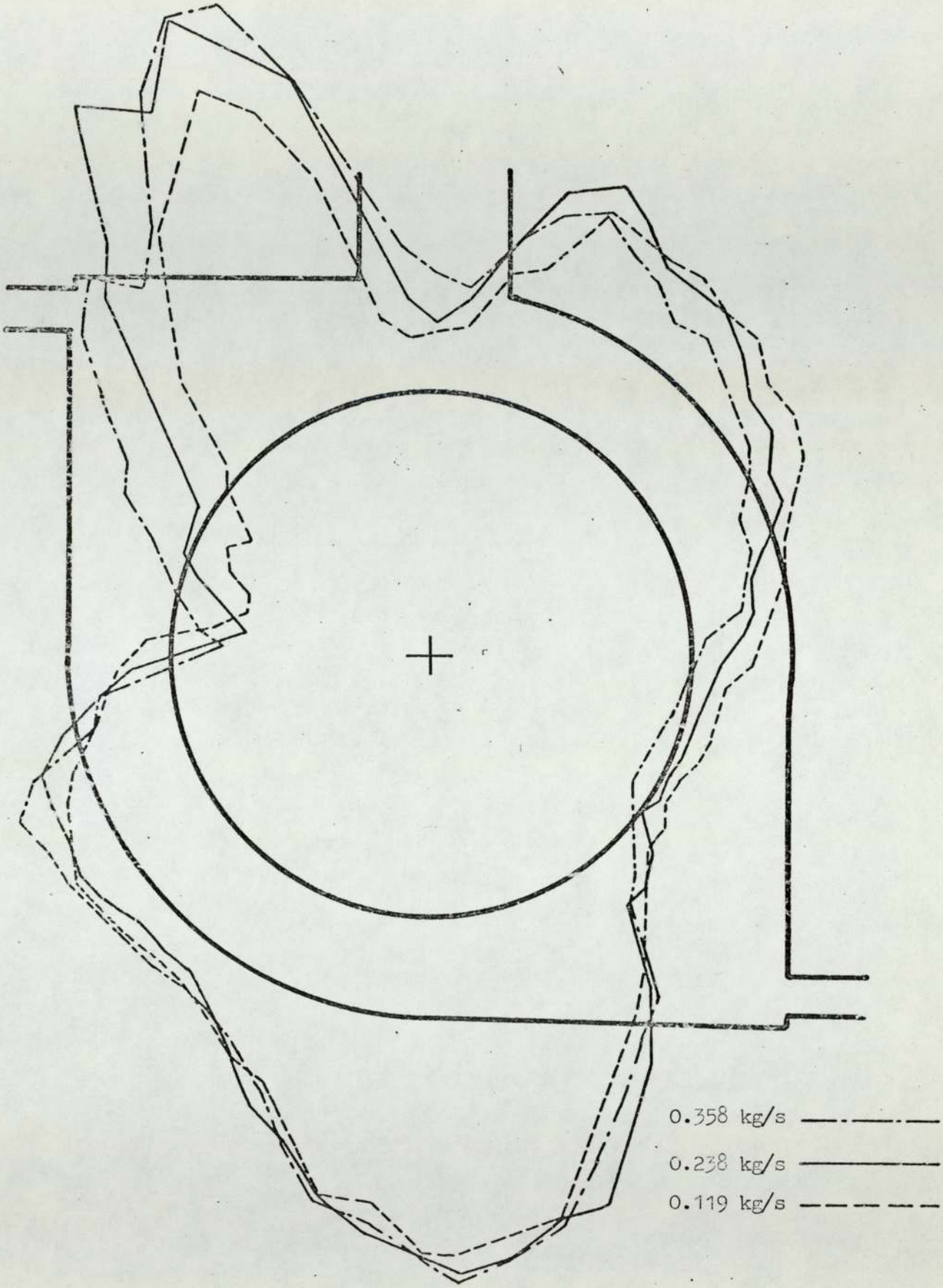

Fig. 4.10 Relative mass transfer coefficients for a 6.35 cm diameter billet (the average coefficient is represented by a radial distance of 7.3 cm).

5. DISCUSSION OF MASS TRANSFER MODEL WORK

The results given in the previous chapter show good agreement between the three sets of experiments and fully confirm the validity of the Chilton-Colburn heat and mass transfer analogy in the present case. A comparison of the results for one billet size only, such as figure 4.6, tends to show larger differences between the techniques. However, similar comparisons for other billet sizes show that there is no consistent ordering of the level of results according to the technique used. The scatter of results probably reflects the limits of accuracy of some of the experiments rather than indicating any inadequacies in the analogy.

In the case of the electrolytic technique the scatter of the results is less than that of the solid sublimation experiments. This arises from the fact that for any one billet size a large number of experimental results for the electrolytic technique can be obtained using the same billet and the same fluid at a constant temperature. This means that the surface condition of the billet and the physical properties of the solution are fixed and consequently the results show very little scatter. Duplicate runs using a freshly prepared nickel surface in each case and solutions of slightly different properties were found to produce results which were consistent within each run but which differed by 2 or 3% between runs. On the other hand, the solid sublimation experiments have to be carried out using a billet whose surface is continually changing as the solid is removed and the air temperature is difficult to keep constant during a run. Consequently the scatter of the solid sublimation results tends to be somewhat larger than that which occurs with the electrolytic technique.

The wire wound billet technique is similar to the electrolytic experiments in that a large number of experiments can be carried out using the same billet. However, the accuracy of the method is limited

by uncertain conduction losses and by the difficulty of obtaining steady state conditions. Both of these difficulties are of course absent from the mass transfer systems.

Coefficients for mass transfer at the wall measured using the electrolytic technique are shown in figure 4.3. The agreement between these and equivalent results obtained from solid sublimation is again fairly good. The strength of the method used for correlating the billet and wall results is confirmed by the closeness of the resulting j factors. The coefficients at the walls are much higher than those at the billet for the same input to the model but the calculated j factors for equal Reynolds numbers at the billet and wall are very close. The j factors are slightly higher for the walls than for the billet and this may result from the boundary layer on the concave walls being less stable than that on the convex billet. Despite the lower mass flow (see table 3.1) the j factors for the wall which includes the flue, wall 1, are higher than those for the other wall. This is probably due to the break up of the boundary layer and the general disturbance produced by the flue.

Chilton and Colburn derived their analogy between heat and mass transfer from empirical evidence taken from a number of different systems. From time to time there has been debate concerning the best exponent on the Schmidt and Prandtl numbers. The present work has been carried out on a novel system and gives further support to the Chilton-Colburn exponent of $^{2}/_{3}$. This is particularly significant since the range of Prandtl and Schmidt numbers investigated (0.7 for the wire wound billet, 2.46 for the solid sublimation and about 1600 for the electrolytic system) is large. The analogy can be deduced theoretically from the similarity of the differential equations describing heat and mass transfer across the boundary layer providing the boundary conditions are

similar. The similarity of boundary conditions can be important in some cases such as fully developed laminar flow in a pipe where quite different transfer coefficients are obtained for the two extreme cases of constant flux and constant surface temperature or concentration. The two mass transfer model techniques used are both constant surface concentration systems; any local variations in the mass transfer coefficient resulting in local differences in flux. The heat transfer experiments are carried out near to constant flux conditions so that any variations of coefficient lead to local surface temperature differences. It is important to note that under these conditions the analogy has still been found to be valid.

Local coefficients at the billet measured using the electrolytic technique were presented in Chapter 4. There is obviously considerable variation of the coefficient around the circumference of the billet and this can be explained to some extent by the nature of the fluid flow. In figure 5.1 a typical coefficient distribution is shown together with arrows indicating the observed flow patterns which were obtained by the flow visualisation method described in chapter 3. The highest coefficients are obtained at the point marked A in figure 5.1 and this corresponds roughly to the region in which the flow is increased to its maximum rate by addition of fluid from the bottom burner. From Points A to B the coefficient gradually decreases since, although the mass flow rate remains constant, the boundary layer on the billet thickens. The lowest coefficient is reached at point B before it rises to C due to flow separation from the billet surface. The flow in the region of the top burner and the flue is complex and the resulting changes in the coefficient aretherefore difficult to explain. The gradual drop from E to F though is probably due to the thickening boundary layer again. Flow separation and the consequent rise in coefficient occurs somewhere around F. Any more detailed correlation

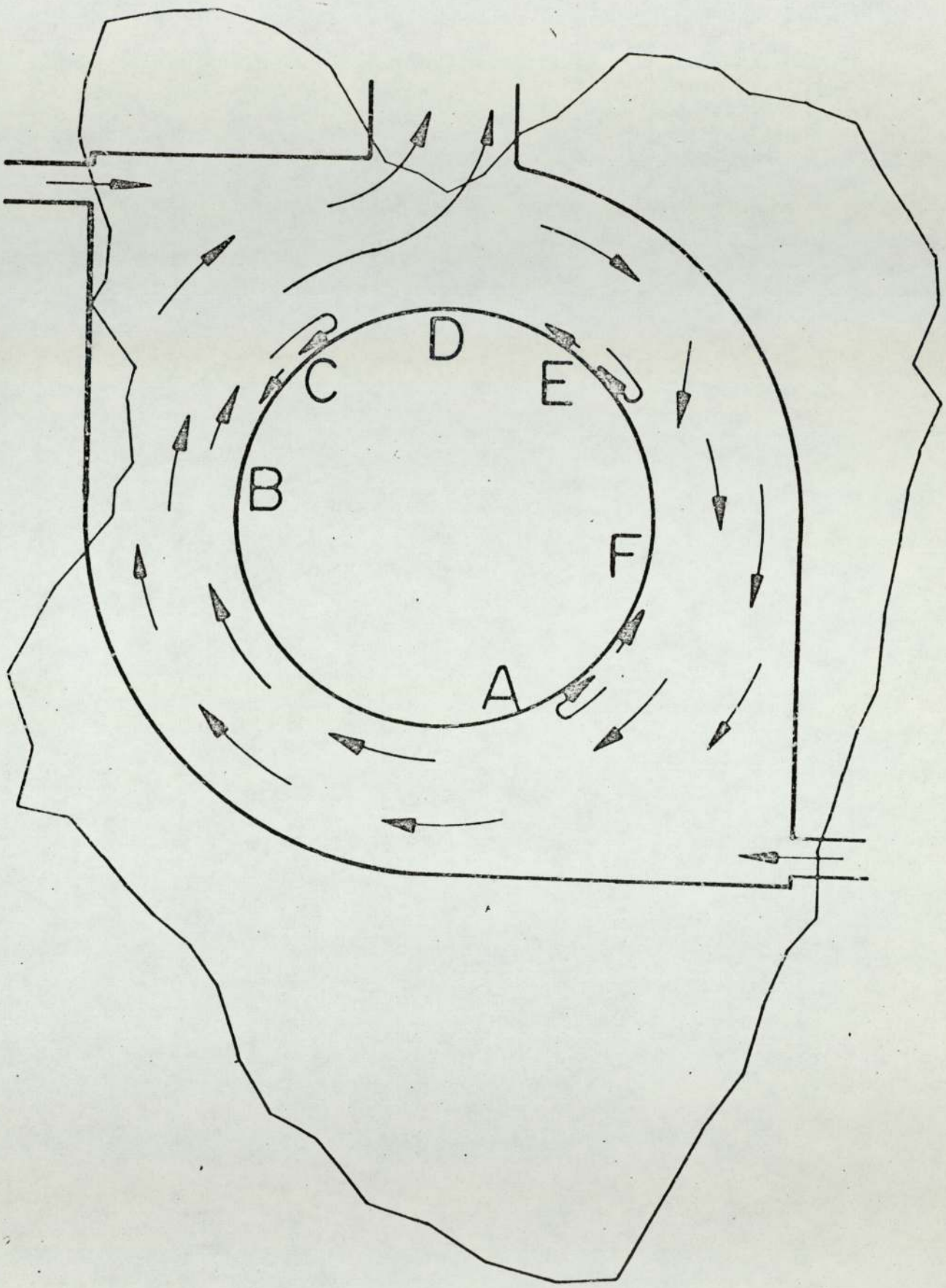

Fig. 5.1 Comparison of flow patterns with local mass transfer coefficients.

between the local flow conditions and coefficients is difficult to make since the flow is unstable in the regions of separation and the interpretation of the flow patterns from visual observation is somewhat subjective. These flow patterns, do however, seem to be independent of the flow rate over the range covered by the experiments and this is supported by the way that the coefficient distribution for different flow rates reduce to a single line when plotted in a dimensionless form as in figures 4.8 to 4.10.

Of the two mass transfer methods the solid sublimation is perhaps the most simple and versatile. A simple model may be constructed from perspex or any other suitable material and the surfaces to which the convective heat transfer coefficients are to be measured, painted with molten naphthalene. A smooth surface to the solidified naphthalene is easily obtained, and perspex, aluminium or tinned sheet have been used to form the initial shape of the surfaces onto which the naphthalene is painted. Modifications to the design may be easily made and their effect quickly assessed in the model. Other subliming solids apart from naphthalene may be used, for example, para-dichlorobenzene has a vapour pressure ten times higher than naphthalene and may profitably be used to limit the duration of an experiment when mass transfer rates are low.

The electrolytic technique is more difficult to perform experimentally than the solid sublimation method and it is less convenient to make design changes to the model. However, once the model and apparatus are assembled a large number of results for the chosen design may be obtained very quickly. The reproducibility of the results is greater than the solid sublimation experiments and the scatter is reduced. Both methods are capable of extension to the measurement of local coefficients, by the use of small electrodes in the electrolytic technique and by profilometry in the case of the solid sublimation method. The electrolytic technique is particularly suited to local

measurements on cylinders since in this case only a single test electrode need be made which can then be rotated to any chosen position. For local measurements on a flat surface the electrolytic method would probably be difficult to apply since a large number of small electrodes would be required. In this situation the solid sublimation method would be more suitable although the large number of surface measurements involved are laborious.

So far in the thesis only the application of, and the results obtained from, small scale isothermal models have been considered. The implication of this work in connection with the design and performance of rapid heating furnaces can only be deduced once the corresponding heat fluxes and temperatures in the furnace are calculated. This information can be obtained by incorporating the model data into suitable mathematical models, which describe the heat transfer processes in the furnace. These mathematical models are described in the following three chapters.

6. CALCULATION OF FURNACE PERFORMANCE

The performance of the furnace can be calculated by combining the results obtained from the physical models described in the previous sections with a mathematical model describing the heat transfer processes. Three mathematical models have been developed for this purpose and are described in the next three sections. These three models are basically very similar but provide increasingly more information concerning the furnace behaviour as certain assumptions are relaxed and the models become more complex.

The simplest model of heat transfer in a furnace is formed by two sets of simultaneous equations which describe the heat transfer from the furnace environment to the load surface and the conduction within the load. The heat transfer from the furnace environment provides the boundary conditions for the partial differential equation describing the transient conduction within the load. The solution of these equations gives the heat fluxes and temperatures at any position in the furnace system at any time.

6.1 The Heat Transfer Equations

The equations for the heat transfer from the furnace environment to the load surface are obtained by making three simple heat balances.

On the furnace system

Heat transferred to billet = heat loss by combustion products
- wall losses ..... (6.1)

On the billet

Heat transferred to billet = convection to billet + net radiation from walls to billet
+ net radiation from combustion products to billet ..... (6.2)

On the walls

Convection to walls + net radiation from combustion products to walls

= net radiation from walls to billet + wall losses

..... (6.3)

Each term in these equations is strictly formed from an area or volume integral. By making the assumptions of a well stirred furnace and uniform convective coefficients and radiation factors, position may be removed as a variable from each term to give the following equations:-

$$\Phi_b = (I_f - I_g)\, Q - \text{wall losses} \qquad \ldots\ldots (6.4)$$

$$\Phi_b = h_b A_b (T_g - T_b) + F_{bw} A_b \sigma (T_w^4 - T_b^4) + F_{bg} A_b \sigma (T_g^4 - T_b^4) \qquad \ldots\ldots (6.5)$$

$$A_w h_w (T_g - T_w) + A_w F_{wg} \sigma (T_g^4 - T_w^4) = A_b F_{bw} \sigma (T_w^4 - T_b^4) + \text{wall losses} \qquad \ldots\ldots (6.6)$$

Equation (6.4) may be rewritten more conveniently in terms of gas input rate as follows:-

$$\Phi_b = Q_g P \left(\frac{C_n}{P} - I_g\right) - \text{wall losses} \qquad \ldots\ldots (6.7)$$

For near to stoichiometric combustion of town gas

$$P = R_a + 0.7 \qquad \ldots\ldots (6.8)$$

Similarly for methane and North Sea natural gas

$$P = R_a + 1.0 \qquad \ldots\ldots (6.9)$$

The assumptions on which equations (6.4) to (6.6) have been based and their consequence in the case of single cell rapid heating furnaces are discussed below:-

(a) The combustion products temperature is uniform

Uniform combustion products temperature is promoted by high circulation of products within the furnace space. This is essentially the 'well stirred furnace assumption'. It allows the use of a single gas temperature, T_g, in equations (6.5) and (6.6) and the use of the heat

content of the recirculating combustion products, I_g, for the heat content of the flue gases, I_{flue}, in equation (6.4).

In the single cell furnace non-uniformity of combustion products temperature may occur in the circumferential, radial and axial directions. In the circumferential direction the possibility of temperature equalisation is bounded by two limiting conditions, plug flow and perfect mixing. No heat is transferred in plug heat flow by physical mixing, conduction or radiation in the direction of flow. The products of combustion circulating in the furnace annulus change in temperature as they either lose heat by convection or gain heat by entrainment with burner jets. These temperature differences are minimised by high recirculation and therefore the assumption of uniform temperature is more likely to be valid for the single cell furnaces with the highest recirculation ratios.

In the absence of radiation it would be logical to assume that, according to Reynolds analogy, there would be a radial temperature distribution in the combustion products following the radial velocity distribution. However intra-gas radiation tends to reduce any temperature differences; it has therefore been assumed in the calculations that these are negligible.

If the circumferential combustion products flow is constant along the length of the furnace then, in the absence of significant end effects, it is reasonable to assume that the temperature is uniform in the axial direction. The furnace doors will influence the fluid flow near them, but it is felt that the effect of this on the temperature distribution will be negligible for the single cell furnaces considered in this thesis.

(b) The convective heat transfer coefficients are uniform

Local variations of convective heat transfer coefficient result from local variations in fluid velocities and turbulence. Uniform convective

coefficients are therefore more likely to be obtained in furnaces of simple shape. Furthermore this assumption will introduce no serious error for conventional furnaces in which the contribution of convection to the total heat transfer from the combustion products is low.

The single cell furnace was designed to promote uniform convective heat transfer, although mass transfer studies of the original design have shown some circumferential variation of convective coefficient round the billet. However, for heating aluminium and copper stock, for which the furnace was designed, any non-uniformity in convective coefficients will have negligible effect on the furnace performance since the high conductivity of the stock eliminates any effects due to local heating. In the various modifications to the original design, higher recirculation and more uniform flow, and consequently more uniform coefficients, were obtained.

(c) The radiation factors are uniform

This assumption implies that the emissivities of the combustion products, the load surface and the wall surface are each uniform. For this to be possible the combustion must be complete in the burner tunnel, and the surfaces of the walls and load must each be homogeneous.

(d) The surface temperatures of the load and furnace wall are uniform

This assumption follows directly from the preceeding three since local temperature variations can only be caused by local variations in the combustion products temperature and heat transfer coefficients.

(e) The thermal inertia of the combustion products in the furnace chamber is zero

This assumption allows that term to be omitted from the first heat transfer equation which accounts for the increase of heat content of the combustion products within the furnace chamber. This assumption is

applicable to almost every furnace since the thermal capacity of the combustion products actually in the furnace at any time is low compared to that of the load.

6.2 Transient Heat Conduction Equation

The assumptions made in the heat transfer equations imply that the heat flux to the load is uniform over the load surface at any time. For cylindrical billets, therefore, only the radial heat conduction equation need to be considered, which is:-

$$\frac{\partial T}{\partial \tau} = \alpha \left[\frac{\partial^2 T}{\partial r^2} + \frac{1}{r} \frac{\partial T}{\partial r}\right] \qquad \ldots\ldots (6.10)$$

and at the surface of the cylinder

$$\Phi_b = A_b \lambda_b \left(\frac{\partial T}{\partial r}\right)_{r_b} \qquad \ldots\ldots (6.11)$$

Many analytical and numerical methods are available for the solution of these equations. The heat transfer within a furnace load must usually be calculated using numerical methods since the boundary conditions are non-linear and the thermal diffusivity and conductivity of the load vary with temperature. Using these methods the differential equations are replaced by a group of simultaneous finite difference equations each representing a heat balance on a small element of the load for a small increment of time. The elements and time increments must be so small that the boundary conditions, temperatures and physical properties can be considered constant for each step, the full solution comprising a number of successive steps.

In the case of uniform heat flux to cylindrical billets the elements into which the billet cross-section is considered to be divided are annuli. If the cross-section is divided into six elements as shown in Figure 6.1 all three finite difference forms give a series of six simultaneous

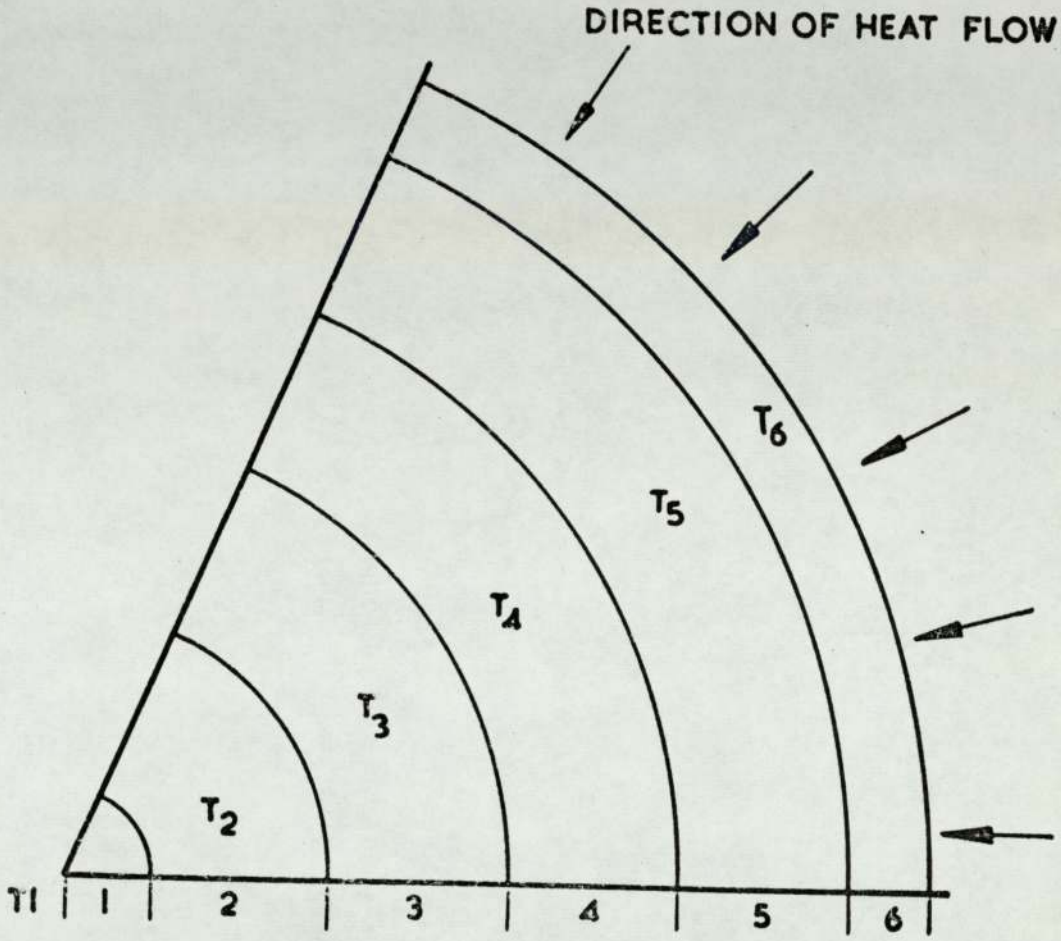

Fig. 6.1 Method of division of the cross-section of a cylindrical billet for the finite difference solution of the transient heat conduction equation.

equations which contain the surface heat flux and six unknown temperatures one of which is the surface temperature.

There are three generally accepted forms of finite difference substitutions, which were first presented by Schmidt[38], Liebmann[39] and Crank-Nicolson[40]. The Schmidt method is explicit in form and consequently a small amount of computation is involved but the method is unsuitable because very small time intervals are needed to keep the solution stable. The Liebmann and Crank-Nicolson formulations are implicit in form and unconditionally stable. Larger time intervals can be used that is possible with the Schmidt method, although the penalty for very large time intervals is a loss in accuracy due to truncation error. For engineering purposes there is probably little to choose between the implicit forms and for the work described in this section the Crank-Nicolson method has been used. Using this form the finite difference equation for a typical annular ring, j, is:-

$$\frac{T'_j - T_j}{\delta\tau} = \frac{\alpha}{2}\left[\left\{\frac{(T_{j-1} - 2T_j + T_{j+1}) + (T'_{j-1} - 2T'_j + T'_{j+1})}{\delta r^2}\right\} + \frac{1}{(n-1)\,\delta r}\left\{\frac{(T_{n+1} - T_{n-1}) + (T'_{n+1} - T'_{n-1})}{2\delta r}\right\}\right] \quad \ldots\ldots (6.12)$$

A heat balance on the outer element b gives:

$$\frac{V_b \lambda_b}{\alpha_b}\left(\frac{T'_b - T_b}{\delta\tau}\right) = \Phi_b - \frac{\lambda_{b,b-1} A_{b,b-1}}{2\delta r}\left(T_b - T_{b-1} + T'_b - T'_{b-1}\right) \quad \ldots\ldots (6.13)$$

A heat balance on the central cylindrical element gives:

$$\frac{V_1 \lambda_1}{\alpha_1}\left(\frac{T'_1 - T_1}{\delta\tau}\right) = \frac{\lambda_{1,2} A_{1,2}}{2\delta r}\left(T_2 - T_1 + T'_2 - T'_1\right) \quad \ldots\ldots (6.14)$$

For small highly conducting billets such as aluminium or copper it may be assumed that the temperature of the billet is uniform throughout at any time. A heat balance on the billet then gives:

$$\Phi_b = V_b \rho_b C_p \frac{dT_b}{d\tau} \qquad \ldots\ldots (6.15)$$

The group of finite difference equations then reduces to the single finite difference equation:

$$\Phi_b = V_b \rho_b C_p \left(\frac{T'_b - T_b}{\delta \tau}\right) \qquad \ldots\ldots (6.16)$$

6.3 Method of Solution

Before the equations described in the preceding two sections can be solved for a chosen load size and gas input rate the following parameters must be known : the convective heat transfer coefficients, the radiation factors and the wall losses, together with the relevant physical properties of the combustion products and load. It must be emphasised that as the temperature of the load surface changes so does that of the combustion products and the wall surface and consequently the heat flux to the load alters.

The initial temperature distribution in the load must be specified before the equations can be solved. For a cold billet this will be uniform ambient temperature, but any initial temperature distribution can be used, such as that resulting from an initial heating period in a soaking furnace. The specified surface temperature is put into the heat transfer equations to provide the corresponding combustion products temperature, wall surface temperature and heat flux to the surface of the load. The heat flux is used with the finite difference equations (6.12) to (6.14) or (6.16) to provide a new temperature distribution in the load after a chosen time interval, $\delta\tau$. The calculated surface temperature then provides a new combustion products temperature, wall surface temperature, surface heat

flux and subsequently a new temperature distribution in the load after a second time interval. Repeated solutions made in this manner will yield these temperatures at any time during the heating cycle. The mathematical operations include the iterative solution of non linear simultaneous equations at each time step and are best carried out on a computer.

The stepwise method of solution just described allows the convective heat transfer coefficients, radiation factors and wall losses to be re-calculated at each step so that the variation of these quantities and the thermal properties of the billet material may be taken into account as the temperatures in the system change.

The choice of a suitable time interval needs some comment. Firstly the main advantage of an implicit method in solving the transient heat conduction equation is that the solution is stable for any time interval, whereas the simpler Schmidt method becomes unstable if too large a time interval is used. Obviously the shorter the time interval chosen the more accurate is the solution of both the heat transfer and transient heat conduction equations. The penalty for increased accuracy is longer computation time and therefore higher computer costs. In calculations described in this chapter the computer programme has been written so that the time interval is adjusted to keep the difference in billet surface temperature between successive time increments within the range of 11°C to 55°C.

6.4 Data Required for Solution

6.4.1. Convective Heat Transfer Coefficients

The evaluation of convective heat transfer coefficients in a furnace formed the main part of the preceding chapters of this thesis.

6.4.2 The Radiation Factors

In gas fired rapid heating furnaces the combustion is essentially complete in the burner tunnel and the resulting combustion products are non-luminous. The problem of radiation, between surfaces separated by a non-luminous gas, and between a non-luminous gas and a surface, has been considered in some detail by Hottel and Sarofim[3]. A rapid heating furnace can be considered to be a system composed of a non-grey gas entirely enclosed by two grey sinks, i.e. the billet and walls. Applying the condition that the load cannot 'see' itself, it follows that:-

$$F_{bg} = \frac{\epsilon_g \epsilon_b}{y} \left[(1 - \epsilon_w) \frac{A_b}{A_w} + \frac{1}{z} \right] \quad \ldots\ldots (6.17)$$

$$F_{wg} = \frac{\epsilon_g \epsilon_w}{y} \left[(1 - \epsilon_b) \frac{A_b}{A_w} + \frac{1}{z} \right] \quad \ldots\ldots (6.18)$$

$$F_{bw} = \epsilon_b \epsilon_w \left[\frac{x}{y} + \frac{1-x}{y_{z=1}} \right] \quad \ldots\ldots (6.19)$$

where

$$x = \frac{\epsilon_g^{\,2}}{2\epsilon_g - \epsilon_{2_g}} \quad \ldots\ldots (6.20)$$

$$y = \left[1 - \epsilon_w\right]\left[1 - (1 - \epsilon_b)\, z\right] \frac{A_b}{A_w} + \frac{1}{z} - (1-\epsilon_w) \quad \ldots\ldots (6.21)$$

$$z = 1 - \frac{\epsilon_g}{x} \quad \ldots\ldots (6.22)$$

ϵ_{2_g} = gas emissivity evaluated for twice the beam length

The radiation factors change with temperature due to the temperature dependence of the emissivities of the combustion products and solid surfaces. This may readily be taken into account in the stepwise method of solution. The effect of temperature on the emissivity of combustion

products can be found in Gas Council Special Report No. 3[41]. However there is very little similar information concerning the surface emissivities of solids.

6.4.3 The Wall Losses

The evaluation of the wall loss term in the heat transfer equations should strictly require the solution of the transient heat conduction equation for the furnace structure to be carried out simultaneously with that for the load. However the problem may be simplified by neglecting any changes in the heat stored in the walls. This is valid for continuous furnaces and a reasonable assumption for batch furnaces which are fully warmed. In the latter case the wall surface temperature will fall at the start of the heating cycle, due to radiation to the billet, and rise as the billet is heated. The heat stored in the furnace walls will follow these surface temperature changes. The main effect of this will be to distort the heating profile by increasing the heat flux to the load at the start of the cycle, when the furnace walls are giving up stored heat, and reducing the heat flux towards the end of the cycle, when the walls are absorbing heat. When the furnace is fully warmed it may be assumed that the net heat lost and absorbed by the walls during a heating cycle is zero. The evaluation of the wall losses then reduces to a problem of heat conduction only.

The heat conduction through furnace walls is given by an equation of the form:

$$\text{Wall losses} = \frac{\lambda_m A_m}{\omega} (T_w - T_{wa}) \qquad \ldots\ldots (6.23)$$

where λ_m is a mean conductivity for the refractory materials forming the furnaces wall, ω is the average thickness of the furnace wall and A_m is a mean area normal to the direction of heat flow. Schemes for evaluating the mean area terms for simple shapes are suggested by McAdams[42].

In the calculations which follow the wall losses have been evaluated as

$$\text{Wall losses} = 5\,(T_w - 424) \qquad \ldots\ldots (6.24)$$

6.4.4 Physical Properties

The physical properties required for the combustion products are the heat content, emissivity, thermal conductivity, and viscosity. This data is given graphically for both towns gas and natural gas in Gas Council Sepcial Reports Nos 2[43], 3[41] and 6[44]. For the calculations described in this thesis polynomial expressions fitting this graphical data have been used.

For the billets the physical properties were taken from Spiers[45] and the surface emissivities assumed to be 0.15 for aluminium, 0.6 for copper and 0.8 for mild steel.

6.5 Comparison of Calculated and Experimental Heating Times

The procedure outlined in the previous section has been tested by predicting the time taken to heat various aluminium and copper billets to their forging temperature in a single cell billet heating furnace, and comparing these with the actual heating times obtained in the furnace. A diagram of the furnace in which measurements were made is shown in Fig. 2.1 and has already been described in section 2.1.

Town gas of gross calorific value 18.1 MJ/m³(st) was used in the furnace, and it was burnt with an air:gas ratio as near as possible to stoichiometric. The revelant properties of the fuel being:

$$R_a = 4.2$$

$$s = 0.52$$

$$C_n = 16.3 \text{ MJ/m}^3\text{(st)}$$

6.5.1 Model Work

The model work on this furnace has been described in detail in the previous sections. Summarising these results as far as the calculation of furnace performance is concerned, it was found that convective heat transfer coefficients to the billet could be given by the equation:

$$j_b = 0.207\ Re_b^{-0.39} \qquad \ldots\ldots (6.25)$$

and similarly for the walls

$$j_w = 0.276\ Re_w^{-0.38} \qquad \ldots\ldots (6.26)$$

When these correlations from the model experiments are applied to the furnace the Reynolds numbers for the furnace are:

$$Re_b = \frac{Q_g (R_a+S)\ \rho_o d_b c_m v_b^*}{(d_w-d_b)_F \mu_F\ l_F} \quad , \quad Re_w = \frac{Q_g (R_a+S)\ \rho_o d_w c_m v_w^*}{(d_w-d_b)_F \mu_F\ l_F} \qquad \ldots\ldots (6.27)$$

and the j factors are:

$$j_b = \frac{h_b (d_w-d_b)_F\ l_F}{2C_p Q_g (R_a+s) \rho_o c_m v_b^*} Pr^{2/3} \quad , \quad j_w = \frac{h_w (d_w-d_b)_F\ l_F}{2C_p Q_g (R_a+s) \rho_o c_m v_w^*} Pr^{2/3} \qquad \ldots\ldots (6.28)$$

For this particular furnace flow visualisation showed that a considerable fraction, e, of the hot combustion products entering from the top burner pass straight out of the flue without losing heat to the cooler combustion products circulating in the furnace space. Account must be taken of this in the first heat transfer equation which then becomes: (for town gas)

$$V_b \frac{\partial I_b}{\partial \tau} = Q_g (R_a + 0.7) \left(\frac{C_a}{R_a+0.7} - I_g \right) (1 - \frac{e}{2}) - \text{wall losses} \qquad \ldots\ldots (6.7a)$$

The fraction e is given for different billet diameters in Table 6.1 (arrangement 1) together with the mean recirculation ratios and the velocity ratios v_b^* and v_w^*.

TABLE 6.1

Flow Visualisation Results for Various Modifications of Single Cell Furnace

Single Cell Furnace Types	d_b cm	c_m	v^*_b	v^*_w	e
(1) Single Top Flue, Fired Tangentially to Walls	8·90	1·52	0·492	1·52	0·73
	9·5	1·49	0·503	1·49	0·74
	12·4	1·34	0·560	1·37	0·77
	12·7	1·31	0·572	1·37	0·77
	15·9	1·08	0·695	1·26	0·81
	17·8	0·87	0·860	1·27	0·825
(2) Twin Flue, Firing Tangential to Walls	9·5	2·6	0·323	1·79	0
	15·9	1·95	0·543	1·25	0
	19·0	1·7	0·941	1·18	0
(3) Twin Flue					
(a) burner inclined at 5°	9·5	2·81	0·314	1·48	0
	15·9	1·95	0·769	1·10	0
(b) burner inclined at 10°	9·5	2·72	0·382	1·30	0
	15·9	1·94	0·948	0·948	0
(c) burner inclined at 15°	9·5	2·6	0·485	1·06	0
	15·9	1·8	1·11	0·934	0
(3) Fitted with Self Recuperative Burners firing Tangentially to Walls	9·5	3·58	0·302	1·37	0
	15·9	2·5	0·840	1·15	0
	19·0	2·14	0·664	0·87	0

6.5.2 Predicted Performance

The performance of the furnace was predicted using the method described previously together with the information outlined above. It was assumed that the temperature of the billets was uniform throughout at any time. The times taken to heat aluminium and copper billets of various diameters to 550°C and 900°C respectively with several gas input rates were calculated. The predicted heating times are shown as solid lines and the experimental results as dashed lines in Figs. 6.2 and 6.3 The calculations were done on an ICT 1907 computer, the computation time for all the theoretical results shown in Fig. 6.2 being about 4 minutes. The agreement between experiment and theory is reasonable except for the 12.7 cm diameter copper billet. Generally the theoretical results are closest to the experimental at high heating rates and this is normally the region in which the furnace would be operated.

The theoretical results are based on assumed values for emissivities and a simplified wall loss term. There is also some doubt as to whether the convective heat transfer coefficients should be evaluated using the mean film or bulk temperatures. The effect of these uncertainties on the predicted heating times was therefore investigated, firstly to determine whether they could explain the discrepancies between theoretical and practical results, and secondly to determine whether the calculation was unduly sensitive to the choice of emissivity and wall loss data.

The value assumed for the emissivity of the aluminium billets heated in the furnace was 0.15. However recent measurements suggest that the true value may lie between 0.15 and 0.3 and therefore the heating times have been calculated using the extremes of this range. The results for the 8.9 cm and 17.8 cm diameter billets are shown in Figs. 6.4 and 6.5. In both cases the practical results generally lie close to the range of heating times predicted using the two emissivities.

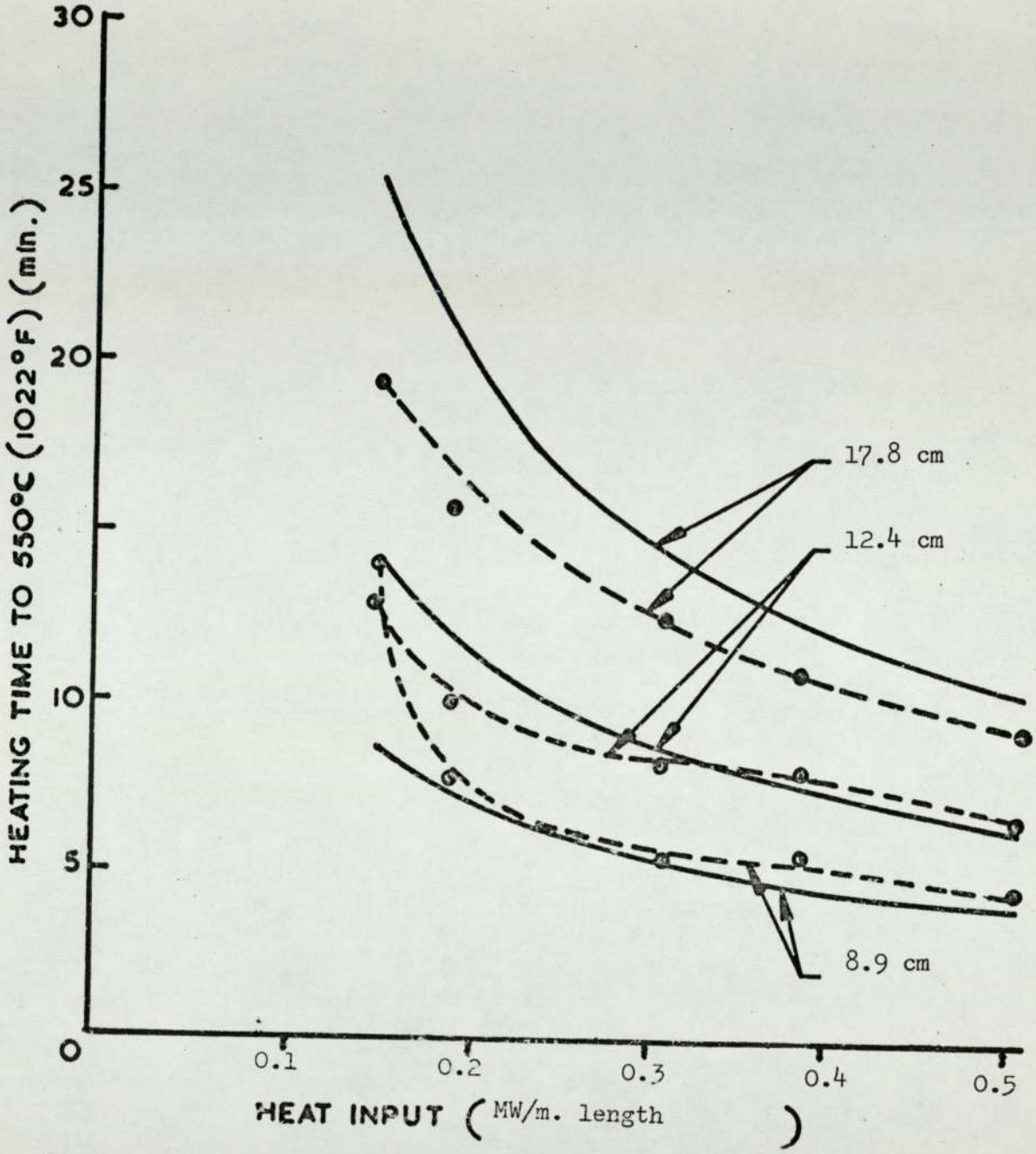

Fig. 6.2 Theoretical (solid lines) and experimental (dashed lines) heating times of aluminium billets in the single cell furnace

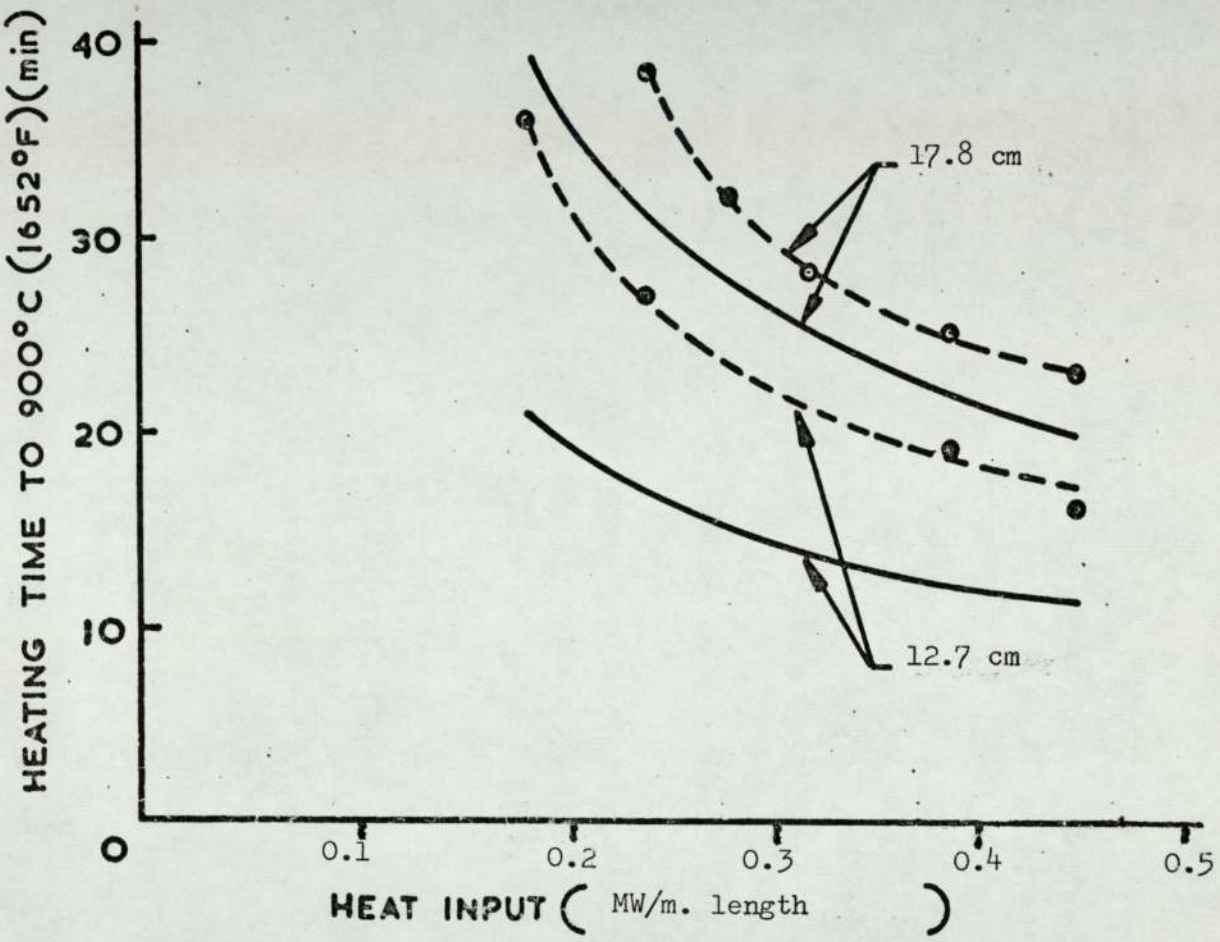

Fig. 6.3 Theoretical (solid lines) and experimental (dashed lines) heating times of copper billets in the single cell furnace.

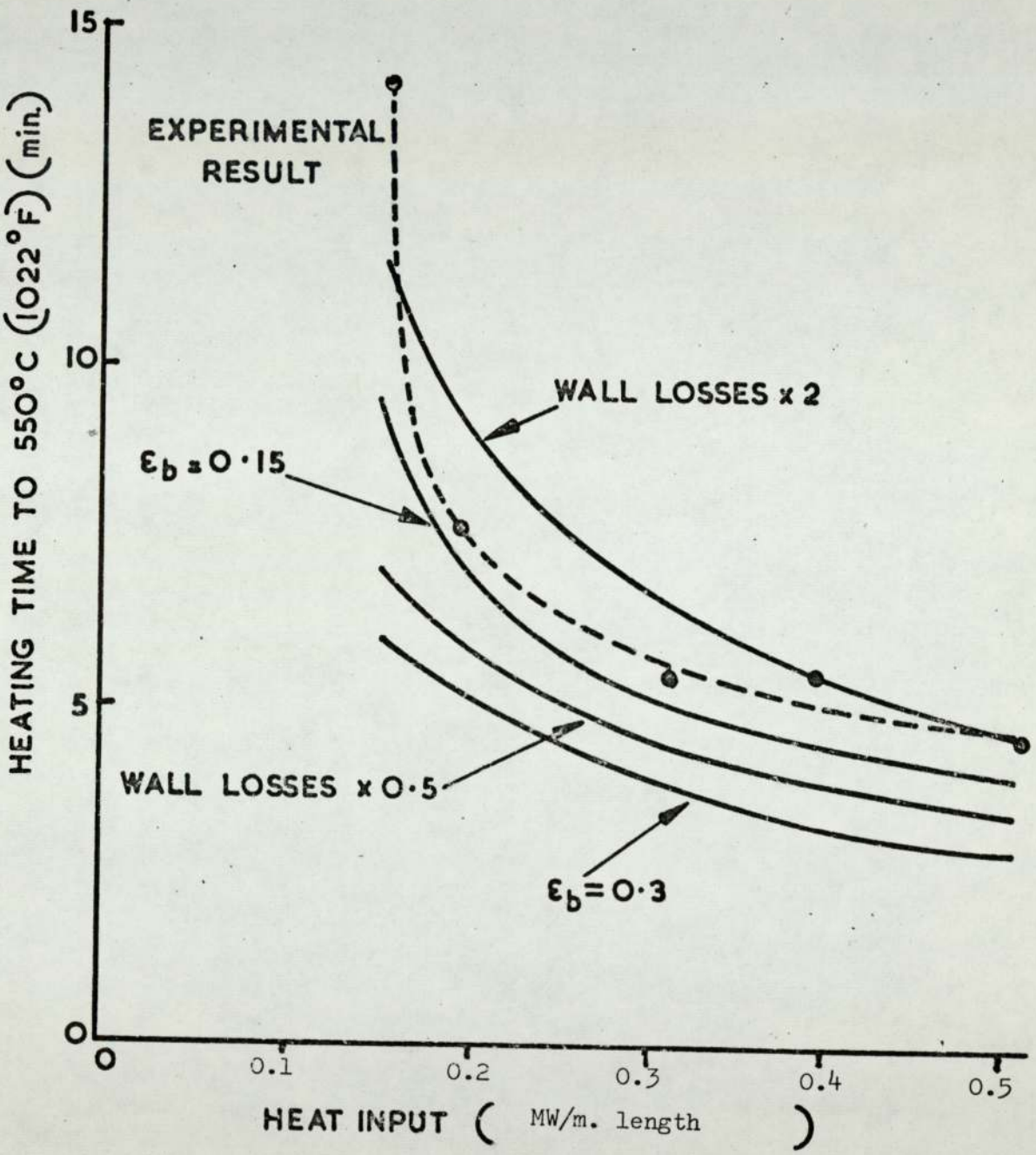

ig. 6.4 Theoretical (solid lines) and experimental (dashed lines) heating times of the 8.9 cm: diameter aluminium billet showing the effect of assuming different values for the emissivity and wall losses.

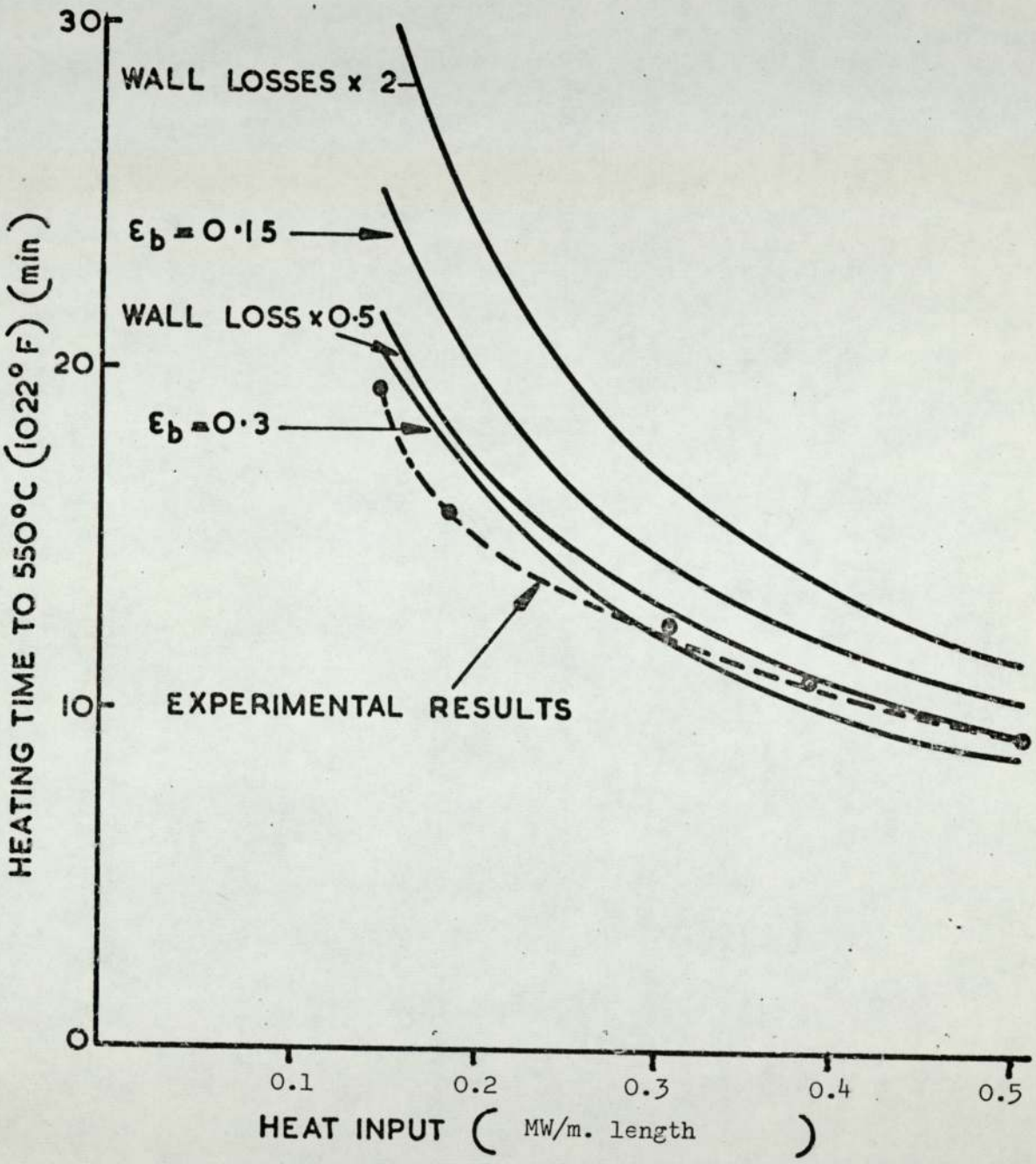

Fig. 6.5 Theoretical (solid lines) and experimental (dashed lines) heating times of the 17.8 cm. diameter aluminium billet showing the effect of assuming different values for the emissivity and wall losses.

The value assumed for the emissivity of copper billets was 0.6. However there is much uncertainty concerning this parameter since it is strongly dependent on temperature of the billet and on the combustion products. The heating times have therefore been calculated using emissivities of 0.3 and 0.5 as well as 0.6. The results are shown in Figs. 6.6 and 6.7 for the 12.7 cm and 17.8 cm diameters respectively. The practical results for the 17.8 cm diameter lie within the range of predicted heating times. However the practical and theoretical results for the 12.7 cm diameter still do not agree.

The assumption that the net heat content of the furnace walls during a heating cycle does not change limits the validity of the predicted results to furnaces which are fully warmed. It is likely that some of the practical results, especially those for copper, were obtained before the furnace had reached this state and this would considerably increase the wall losses. Also the conduction losses given by the simplified exppression, equation (6.24), may either over or under estimate the true conduction losses. Heating times have therefore been recalculated using both twice and half the wall losses given by equation (6.24) and assuming an emissivity of 0.15 for aluminium and 0.3 for copper. The results are included in Figs. 6.4, 6.5, 6.6 and 6.7. Once again the practical results generally lie within the range of predicted heating times except for the 12.7 cm copper billet.

The effect of evaluating convective coefficients using the mean film or bulk temperature has been investigated by calculating heating times using coefficients based on both temperatures. The heating times using the mean film temperature were 5% to 10% higher than the times obtained using the bulk temperature, the greatest differences obviously occurring where the direct convection to the billet becomes a significant mode of heat transfer.

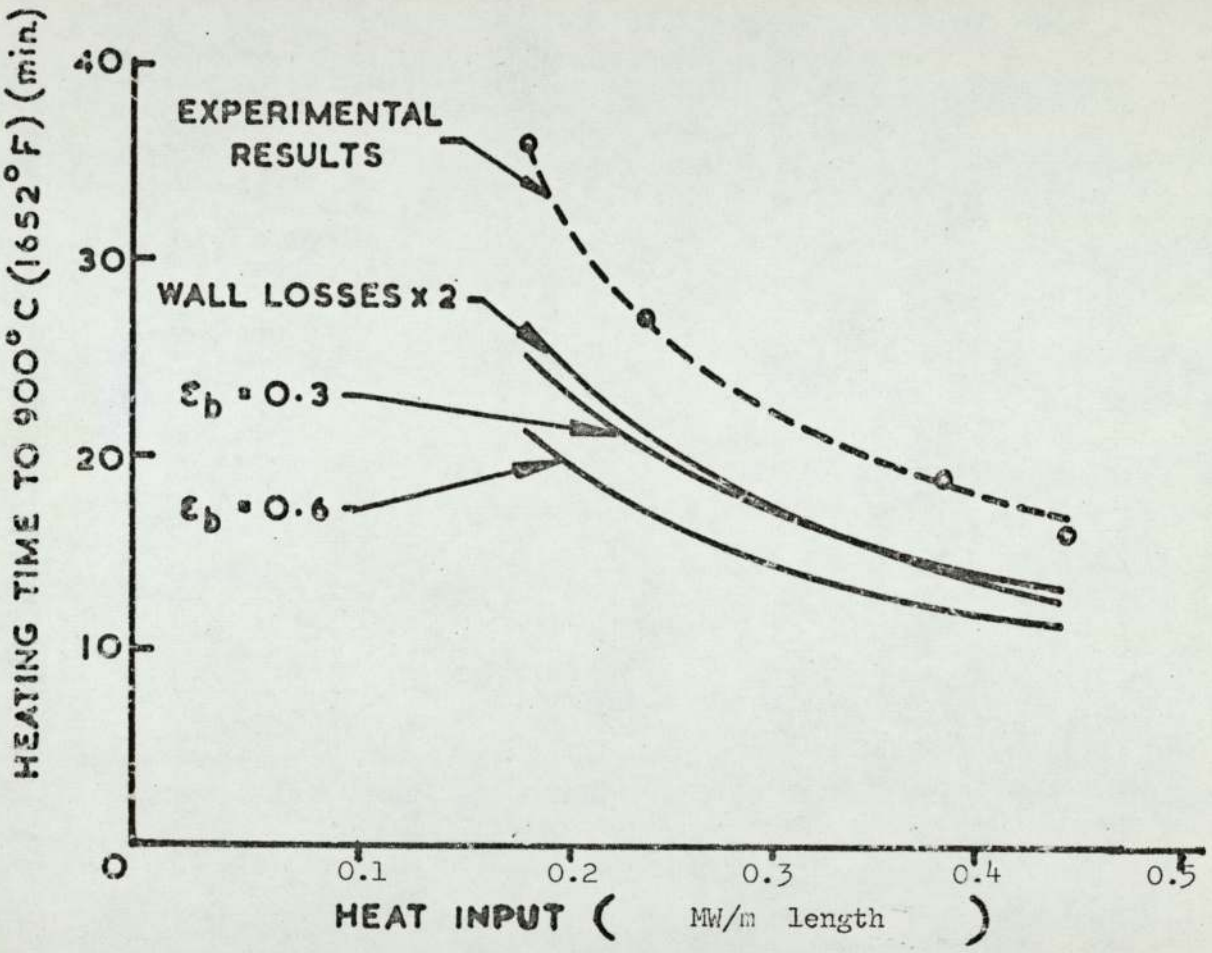

Fig. 6.6 Theoretical (solid lines) and experimental (dashed lines) heating times of the 12.7 cm. diameter copper billet showing the effect of assuming different values for the emissivity and wall losses.

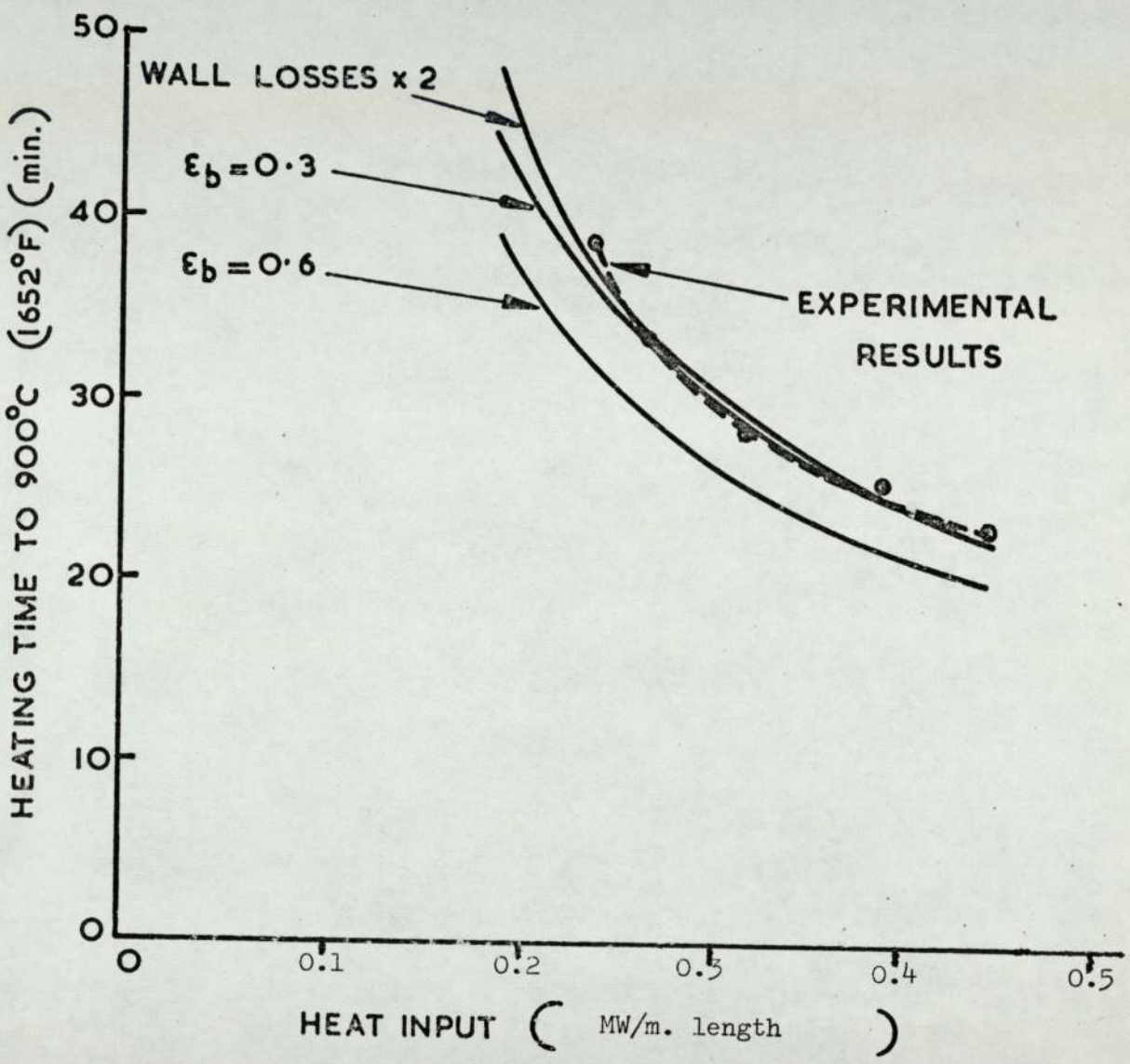

g. 6.7 Theoretical (solid lines) and experimental (dashed lines) heating times of the 17.8 cm. diameter copper billet showing the effect of assuming different values for the emissivity and wall losses.

It can be concluded from these investigations that the method is capable of predicting the performance of the single cell billet heating furnace accurately enough for practical purposes. The accuracy is limited chiefly by knowledge of the emissivity of the stock and by the estimation of the heat lost through the furnace structure.

The discrepancy between thepractical results and predicted heating times for the 12.7 cm diameter copper billet is difficult to explain unless it is due to excessively high wall losses in the experiments The practical and predicted heating times for the nearest size aluminium billet, i.e. 12.4 cm diameter, agree well. It would therefore appear that there are no significant errors in the heat transfer coefficients.

6.6 The Role of Conduction in the Rapid Heating of Steel

Rapid heating leads to temperature gradients within the stock. These are generally negligible with highly conductive metals such as copper and aluminium, but with ferrous stock they can be appreciable. In order that a valid comparison can be made between heating times achieved under different conditions, the final temperature profile in the load must be as nearly as possible the same in every case. It is impossible to obtain identical final temperature profiles under different conditions since the profile depends on the heating history of the load. However the final temperature profile may be conveniently specified by a final surface temperature and a maximum allowable temperature difference from surface to centre. Such a specification should be reasonably consistent with normal forging procedure, although the precise values will depend very much on the type of forging operation and the individual judgment of the forge operators. The total heating times for mild steel quoted in this paper are all for a final surface temperature of 1288°C (2350°F) and a maximum surface to centre temperature difference of 56°C (100°F).

At high heating rates, when the surface first reaches 1288°C, the surface to centre temperature difference is often greater than 56°C. The heat flux to the billet surface must then be reduced to maintain the surface at temperature until sufficient heat has been conducted into the billet to achieve the specified temperature uniformity. At this stage in the procedure the temperature profile is calculated solely from the transient heat conduction equation and no data on heat transfer from the furnace environment are used. This part of the calculation also gives the surface heat flux needed to maintain the surface temperature constant and this heat flux can be used to evaluate the equivalent heat input to the furnace and hence the furnace efficiency. In practice the condition of reduced heat flux may be obtained by holding the billet in the furnace with reduced heat input. However, if the period of reduced heat flux is short, acceptable temperature uniformity would probably be obtained during the removal of the billet from the furnace and subsequent handling. In addition the predicted values of the heat flux to the billet near the end of the cycle will be overestimated since in the simplified model used for the wall losses no account is taken of the increase in heat content of the walls. In practice, therefore, the condition of reduced heat flux to the billet may be produced naturally without the necessaity of turning down the furnace.

During the 'soak' period the heat input to the furnace can be calculated from the heat flux needed to maintain the surface temperature constant by using the heat transfer equations. However this problem may be simplified by assuming that the combustion products temperature and wall losses remain constant during the soak period at their values immediately prior to turn down. The gas used in the soak period is then calculated from the equation:

$$G\,P\left(\frac{C_n}{P} - I_g\right) = \left(I_b\right)_{final} - \left(I_b\right)_{soak} + \text{wall losses}\,(T_{final} - T_{soak}) \quad \ldots\ldots (6.29)$$

Any error in the assumptions on which this equation is based will have little effect on the calculated values of the total gas used and hence on the efficiency, provided that the soak is not too long.

6.7 Comparison of the Predicted Performance of Modified Single Cell Furnaces

It has already been shown that the prediction of furnace performance from model work can be carried out with reasonable accuracy. The main value of the technique lies in the ability to investigate and compare alternative furnace designs without the necessity of building expensive prototypes of each design. To this end the performances of 25.4 cm diameter single cell furnaces, fired with natural gas, with various burner and flue arrangements have been predicted and compared. Heating times were calculated for aluminium, copper and mild steel billets at 550°C, 900°C and 1250°C respectively for the following arrangements:

1. Single top flue, fired tangentially to walls, as described previously.
2. Twin flue, fired tangentially to the walls.
3. Twin flue, burner inclined at (a) 5°, (b) 10° and (c) 15°.
4. Fitted with self recuperative burners firing tangentially to the walls.

Line diagrams of these arrangements are shown in Fig.6.8.

The self recuperative burners shown in arrangement 4 were developed at the Midlands Research Station as a means of improving furnace efficiency by recuperating heat from the combustion products leaving the

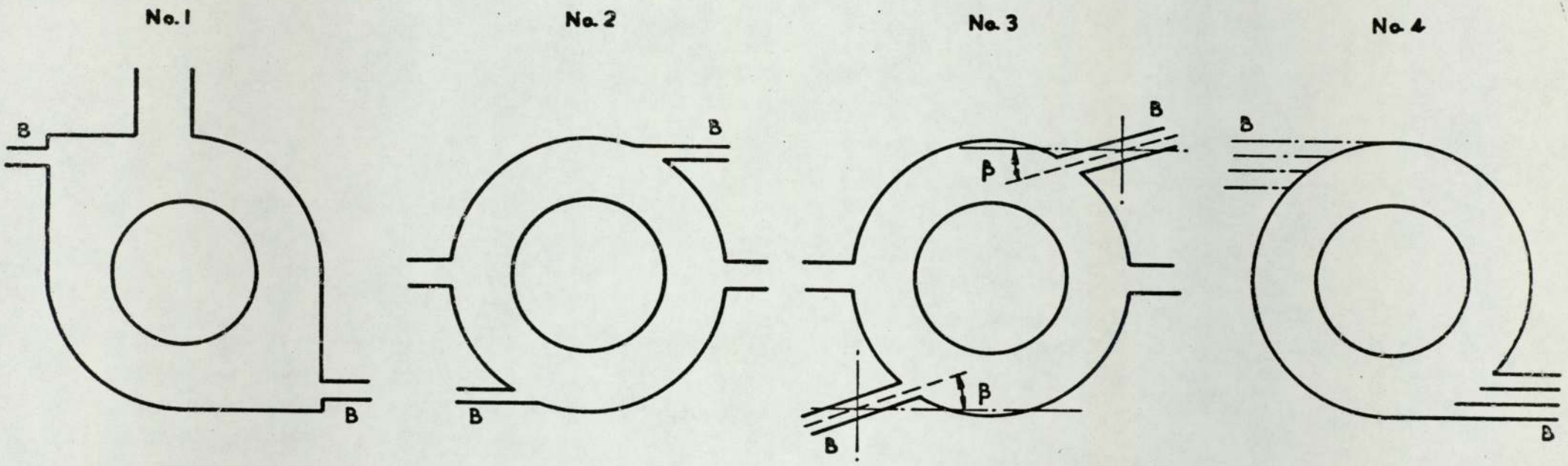

Fig. 6.8 LINE DIAGRAMS OF MODEL SECTIONS SHOWING DIFFERENT BURNER AND FLUE ARRANGEMENTS

(1) Single top flue, tangentially fired

(2) Twin flue, tangentially fired

(3) Twin flue, burner inclined at various angles

(4) Self recuperative burners

Burners are denoted by B, and in arrangement (3) the angle at which the burner is inclined is denoted by β.

furnace chamber. The heat exchanger section of these burners consists of three concentric tubes. The unburnt gas passes up the centre tube, the air passes up the adjacent annulus and the two streams mix and burn at the burner nozzle. The combustion products from the furnace chamber pass down the outer annulus counterflow to the air and gas streams. Typical dimensions for a burner rated at 10^{-3} m^3/s of natural gas would be 7.5 cm overall diameter and total length 40 cm.

6.7.1 Information from Model Work

The naphthalene sublimation technique was used to measure mass transfer coefficients in furnace models with burner and flue arrangements Numbers 1, 3(c) and 4 in the list above. Flow visualisation studies have enabled the mass transfer coefficients for the billet for these arrangements to be correlated by the equation:

$$j_b = 0.525\ Re_b^{-0.5} \qquad \ldots\ldots (6.30)$$

Similarly the mass transfer coefficients at the walls were correlated by the equation :

$$j_w = 1.13\ Re_w^{-0.5} \qquad \ldots\ldots (6.31)$$

In these equations the Reynolds numbers and j factors are defined as in Section 6.5.1.

The equations (6.30) and (6.31) should be valid for all furnaces which are essentially cylindrical in shape and which are fired tangentially or near to tangentially. These equations have therefore been used to evaluate the convective heat transfer coefficients in furnaces with the other burner and flue arrangements. The necessary values of recirculation ratios and velocity ratios were obtained from flow visualisation studies. These values are shown in Table 6.1.

In order to predict the performance of the furnace fitted with self recuperative burners the heat transfer equation (6.7) must be

modified to take account of the heat recuperated in the exchanger section. Equation (6.7) then becomes:

$$\Phi_b = Q_g P \left(\frac{C_n}{P} - I_{flue}\right) - \text{wall losses} \quad \ldots\ldots (6.32)$$

A theoretical analysis of the heat exchanger section of a self recuperative burner[46] has shown that its performance can be described by the simplified equation:

$$Q_g P \left(I_g - I_{flue}\right) = \text{'UA'} \left(T_{flue} - 288\right) \quad \ldots\ldots (6.33)$$

where

$$\text{'UA'} = \left[1.36 \times 10^{-6} \frac{Q_g (R_a + s)}{4.72\, n} + 1.59 \times 10^{-4}\right] t_g + 0.372 \ \text{W/K} \quad \ldots\ldots (6.34)$$

and n is the number of burners in the furnace, which has been taken as 10 for this theoretical comparison.

Equation 6.33 and 6.34 represent for a total natural gas input to the furnace of 10^{-2} m³/s an air preheat of about 470°C depending on the temperature of the combustion products in the furnace chamber.

During the soak period the gas used can be calculated by modifying equation (6.32) to the form:

$$G \ P \left(\frac{C_n}{P} - I_{flue}\right) = \left(I_b\right)_{final} - \left(I_b\right)_{soak} + \text{wall losses} \left(T_{final} - T_{soak}\right) \quad \ldots\ldots (6.35)$$

In using this equation it has been assumed that the heat content of the flue gases remain constant at their value immediately prior to turn down

6.7.2 Other Data

The radiation factors, emissivities and wall losses were taken to be the same as given previously. The performances of the furnaces were calculated when fired with North Sea natural gas at the stoichiometric

air/gas ratio. The relevant properties of this fuel are:

C_g = 37.8 MJ/m³ (st)

C_n = 34.4 MJ/m³ (st)

R_a = 9.72

s = 0.586

6.7.3 Predicted Performance

The heating times for aluminium, copper and mild steel billets of 9.5, 15.9 and 19.0 cm diameter in the various modifications of the single cell furnace have been predicted. The results for the 15.9 cm diameter aluminum and copper billets are shown in Figs. 6.9 and 6.10. The mild steel results for all three diameters are shown in Figs. 6.11 6.12 and 6.13. For the mild steel results the chain dotted curves indicate the time needed for the billet surface to reach 1288°C and the solid lines indicate the time needed for the centre to reach 1232°C. The shaded portion between these curves indicate the period for which reduced heat flux is necessary. The results for the 15.9 cm diameter mild steel billet have been replotted as efficiencies in Figs. 6.14 and an extract from a typical computer print out is shown in Table 6.2.

(a) Furnace No. 1

This is the furnace with which the thesis has been concerned so far. The flow visualisation model work described in Chapter 4 has shown that up to 80% of the combustion products flow from the top burner pass straight out of the furnace without apparently losing heat or momentum to the combustion products circulating in the furnace chamber. Consequently this furnace has the lowest recirculation ratios and longest heating times of the four arrangements investigated.

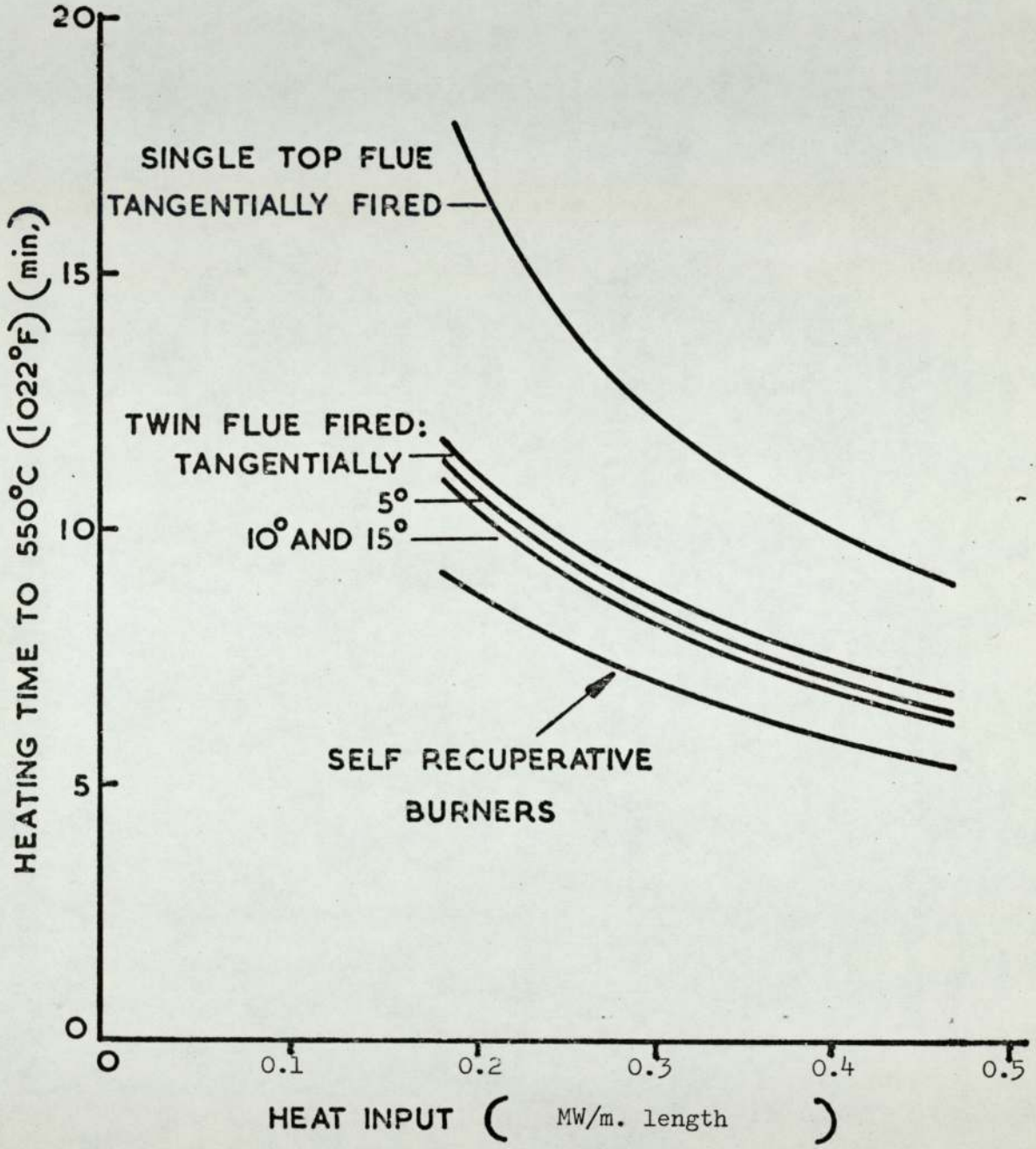

Fig. 6.9 Theoretical heating times for a 15.9 cm. diameter aluminium billet in various 25.4 cm. single cell furnaces.

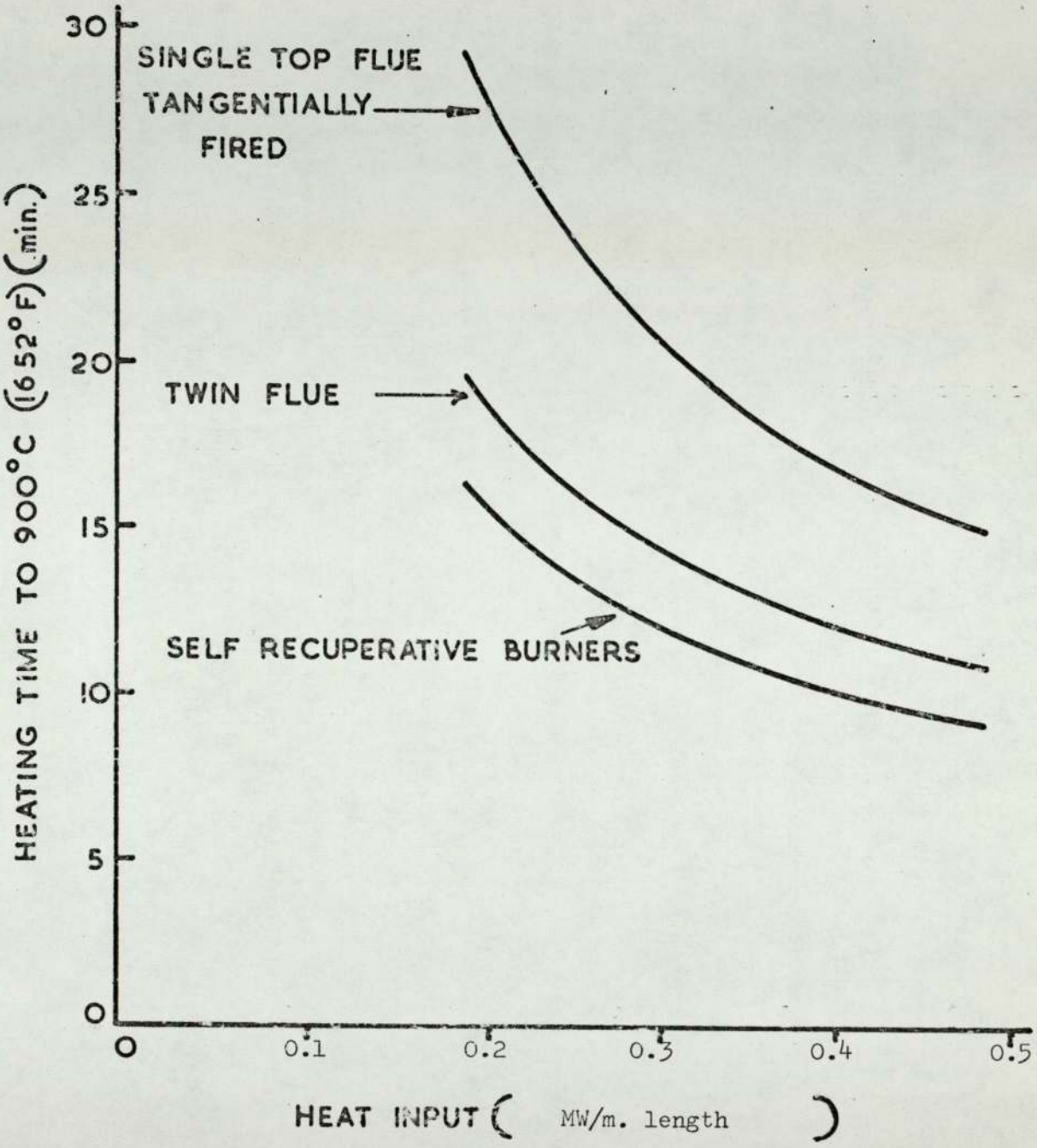

Fig. 6.10 Theoretical heating times for a 15.9 cm. diameter copper billet in various 25.4 cm. single cell furnaces.

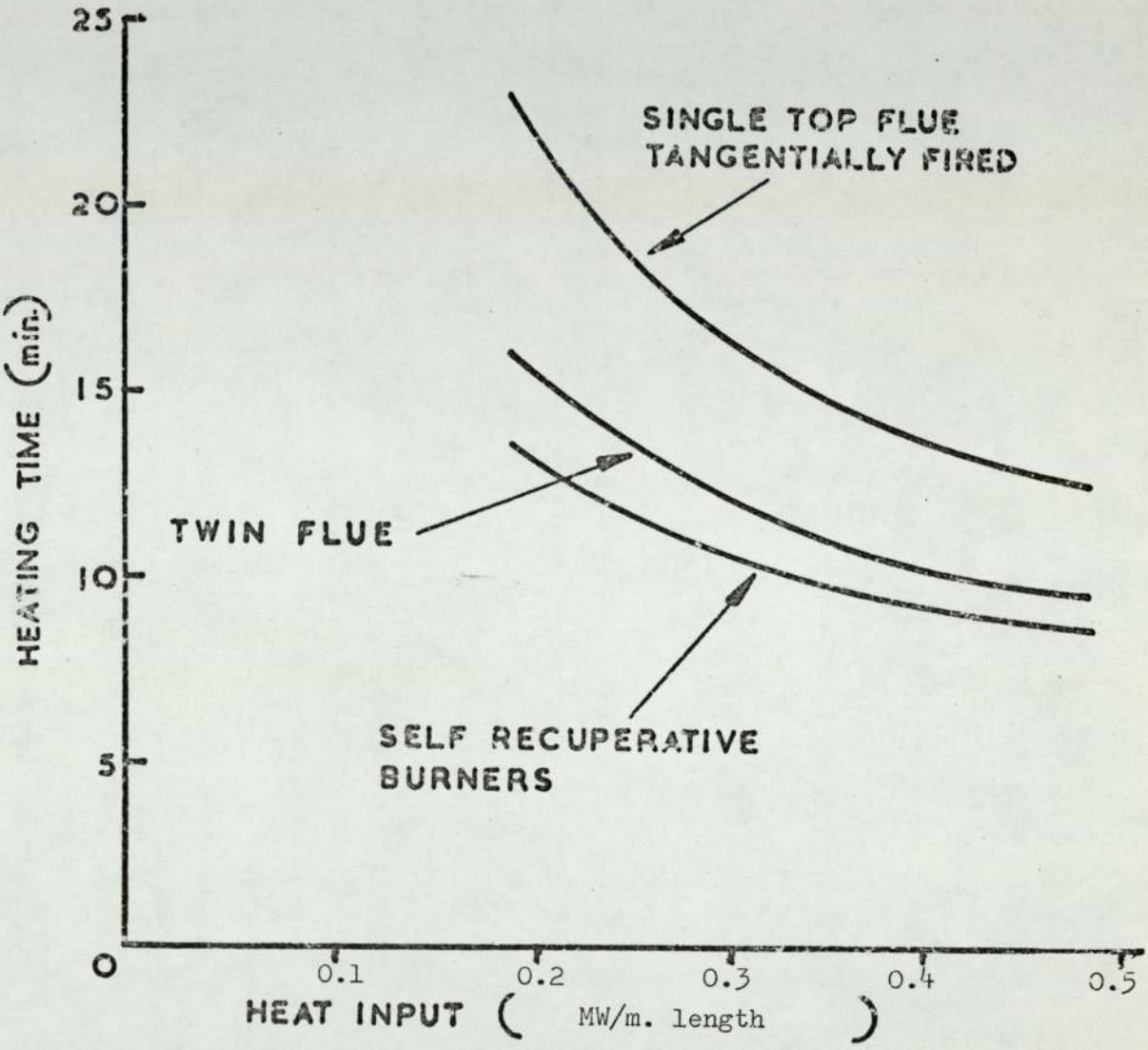

Fig. 6.11 Theoretical heating times for a 9.5 cm. diameter mild steel billet in various 25.4 cm. single cell furnaces.

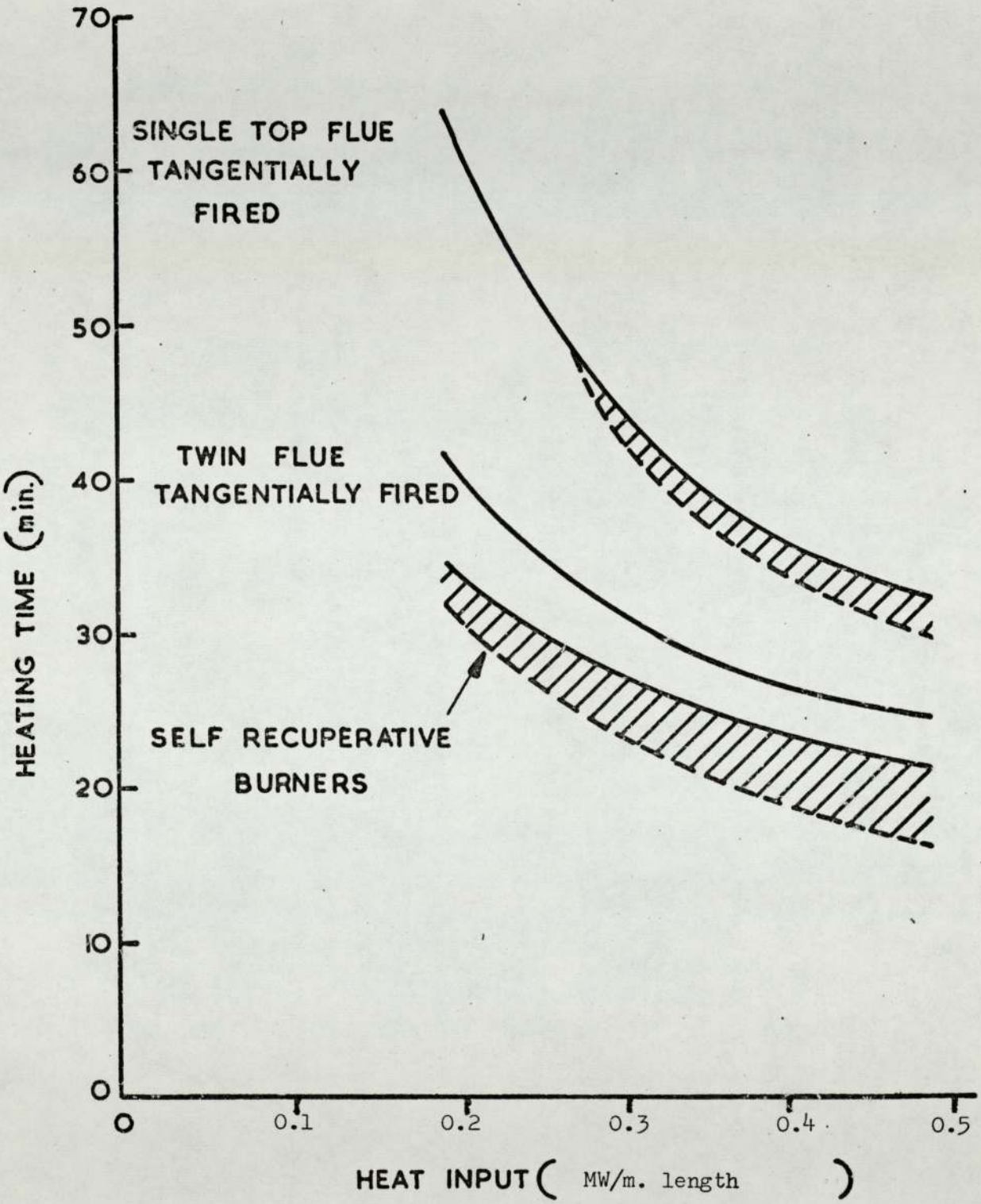

Fig. 6.12 Theoretical heating times for a 15.9 cm. diameter mild steel billet in various 25.4 cm. single cell furnaces.

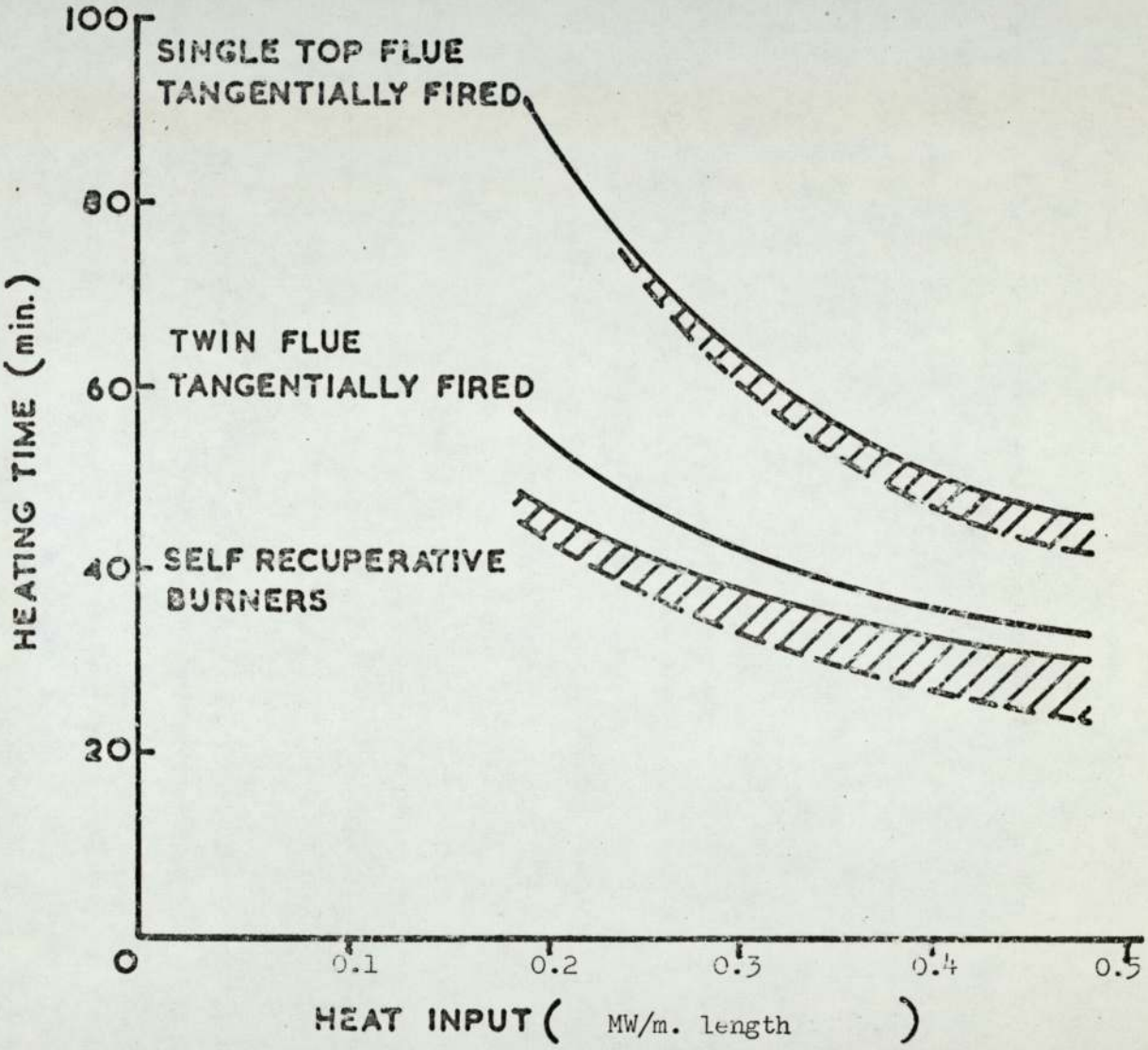

Fig. 6.13 Theoretical heating times for a 19.0 cm. diameter mild steel billet in various 25.4 cm. single cell furnaces.

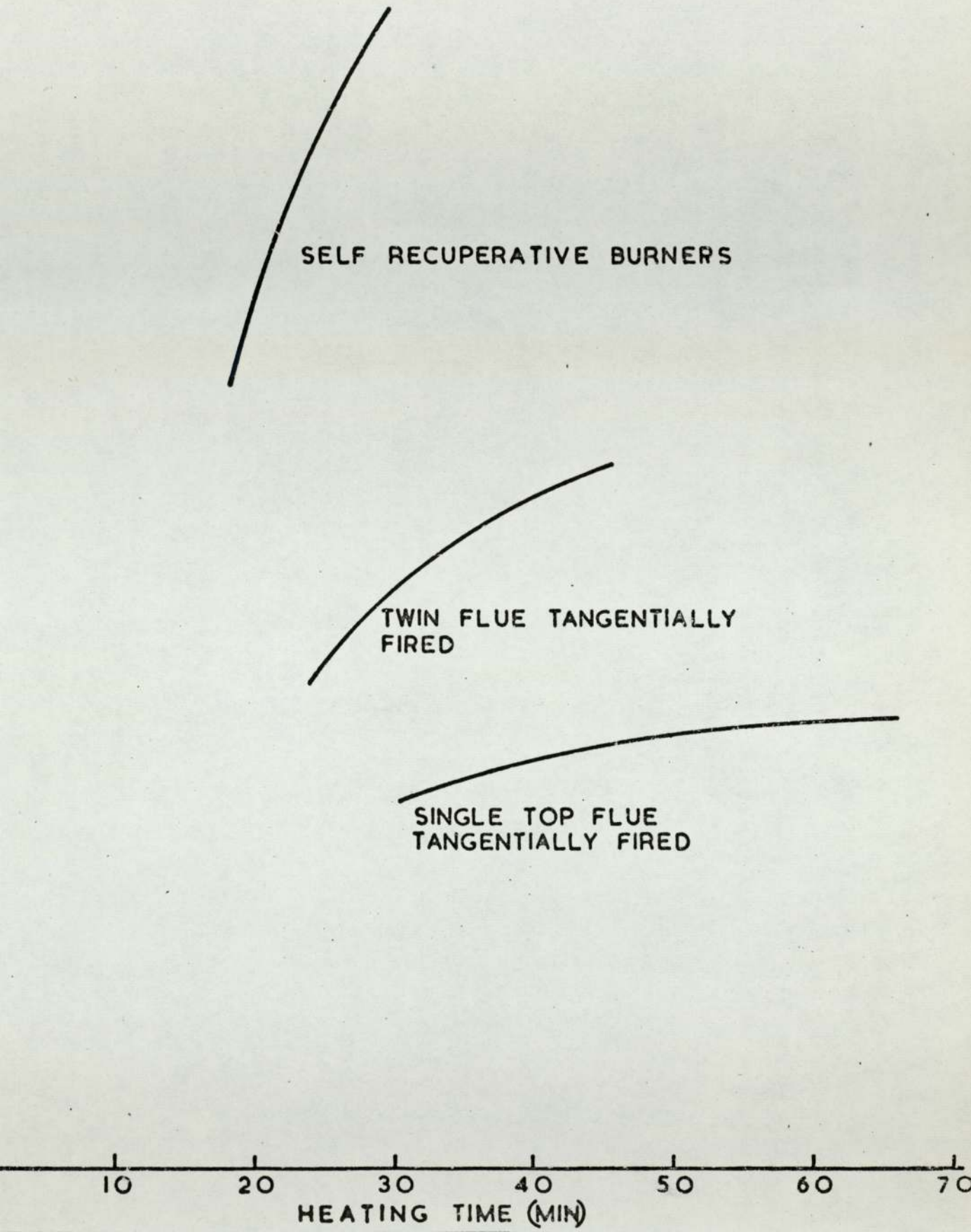

5.14 Theoretical thermal efficiencies for a 15.9 cm diameter mild steel billet in various 25.4 cm single cell furnaces.

Table 6.2

Extract from a typical computer print-out; single-cell furnace, twin flue, fired tangentially to walls. (No. 2 of figure 6.8).

Billet diameter = 19.0 cm; billet material: mild steel; heat input = 0.5 MW/m. length.

time		Temperatures °C								h_b	h_w	Wall Losses	ϕ_b
min.	sec.	T_1	T_2	T_3	T_4	T_5	T_6	T_g	T_w	w/m² K	w/m² K	kW/m length	kW/m length
0	0	15	15	15	15	15	15	1474	1010	50.7	150	10.9	124.6
0	5	15	15	15	15	18	42	1475	1010	51.1	150	10.9	124.4
0	10	15	15	15	17	24	62	1476	1011	51.3	150	10.9	124.2
0	15	15	15	16	19	31	77	1476	1012	51.5	150	10.9	124.0
0	20	15	16	17	22	39	90	1477	1012	15.8	150	10.9	123.8
0	25	16	16	18	25	47	101	1478	1012	52.2	150	10.9	123.6
0	30	16	17	19	29	55	111	1478	1013	52.4	150	10.9	123.4
0	40	18	19	24	38	71	129	1479	1013	52.5	150	10.9	123.2
0	50	21	22	30	49	85	147	1480	1014	52.7	150	10.9	123.0
26	10	1023	1033	1061	1107	1167	1241	1654	1355	72.0	172	15.3	72.0
26	50	1047	1056	1083	1127	1186	1258	1660	1367	72.8	173	15.4	70.4
27	30	1069	1078	1105	1147	1204	1273	1664	1377	73.1	173	15.5	68.9
28	10	1092	1100	1126	1166	1222	1288	1669	1387	73.6	174	15.6	53.1
28	50	1113	1122	1147	1185	1236	1288	-	-	-	-	-	-
29	30	1134	1143	1165	1202	1244	1288	-	-	-	-	-	-
30	10	1153	1164	1181	1213	1250	1288	-	-	-	-	-	-
30	50	1171	1185	1196	1224	1256	1288	-	-	-	-	-	-
31	30	1187	1192	1208	1232	1261	1288	-	-	-	-	-	-
32	10	1200	1205	1219	1240	1264	1288	-	-	-	-	-	-
32	50	1212	1216	1228	1247	1267	1288	-	-	-	-	-	-
33	30	1222	1226	1237	1252	1270	1288	-	-	-	-	-	-
34	10	1231	1234	1247	1257	1273	1288	-	-	-	-	-	-

(b) Furnace No. 2

In this arrangement the single top flue has been replaced by two flues so positioned that they eliminate any losses due to the combustion products passing straight out of an adjacent flue. This simple aerodynamic modification has resulted in an increase of recirculation ratio and a reduction in heating times of the order of 25%.

(c) Furnace No. 3

This burner and flue arrangement, with a variable burner angle, was suggested as a means of increasing direct convection to the billet. As the angle of firing is increased the velocity near to the billet increases and that near to the wall decreases as indicated by the values of the velocity ratio given in Table 6.1. This results in an increase in convection to the billet but a decrease in convection to the walls. Aluminium has a low emissivity and therefore a large proportion of the total heat transfer is by direct convection and only a small proportion by re-radiation from the furnace walls. In this case an increase of direct convection produced by increasing the angle of firing gave a significant reduction in heating times. However copper and mild steel have a high emissivity and a larger proportion of the heat transfer is by re-radiation. Consequently increasing direct convection to the billet at the expense of convection to the walls has very little effect on the heating times. In addition increasing the angle of firing limits the maximum size of ferrous billet that can be heated without impingement on the billet surface and the consequent risk of local overheating. It is interesting to note that the predicted wall surface temperatures were not appreciably lower than the tangentially fired furnaces. However these conclusions do not necessarily apply to the 19 cm billets or for angles of firing greater than 15° for the other two sizes, since, in these cases,

flow visualisation showed significant impingement of the combustion products on the billet surface. In this situation equations (6.30) and (6.31) do not apply and the assumption of uniform heat flux is no longer valid.

(d) Furnace No. 4

The single cell furnace fitted with self recuperative burners combines the aerodynamic advantages of the twin flue arrangement with the benefits to be gained by recovering heat from the flue gases. The predicted performance for this arrangement was the best of all the four cases investigated. The heating times in comparison with the single top flue design have been reduced by 50% to 60% for aluminium and copper and by 45% to 55% for mild steel depending on the gas input rate. In the case of steel the reduction in heating times that can be obtained are limited by the necessity of holding the billet at temperature to obtain acceptable temperature uniformity. In this case the improvements in design are best assessed by comparing efficiencies. For a heating time of 30 minutes for the 15.9 cm mild steel billet the single top flue single cell furnace is capable of an efficiency of only 13%. The twin flue gives 30% efficiency and the single cell fitted with self recuperative burners gives 40% efficiency for the same heating times.

A 30 cm diameter prototype single cell furnace fitted with self recuperative burners has been built at the Midlands Research Station. The practical aspects, such as the refractory materials, are still being developed but preliminary runs have shown that the performance is of the order expected from the theoretical analysis.

6.8 The Effect of Preheating the Combustion Air

One way of increasing furnace efficiency is to preheat the combustion air. Conventionally this has been achieved for large furnaces by using a regenerative system or an external heat exchanger.

The same benefits can conveniently be obtained by using self recuperative burners, which, because they are compact can also be used with advantage for small furnaces.

The performance of the single cell furnace fitted with self recuperative burners has been predicted assuming that the recuperators produce various degrees of preheat which remain constant during the heating cycle. The same results are then applicable to the tangentially fired twin flue furnace with external regeneration or heat exchange. The heat transfer equation (6.7) for this case must be modified to:

$$\Phi_b = Q_g P \left(\frac{C_g}{P} + \frac{R_g}{P} I_a - I_g\right) - \text{wall losses} \qquad \ldots\ldots (6.36)$$

and the gas used in the soak period of mild steel billets is calculated from the equation :

$$GP \left(\frac{C_n}{P} + \frac{R_g}{P} I_a - I_g\right) = (I_b)_{final} - (I_b)_{soak} + \text{wall losses}$$

$$(\tau_{final} - \tau_{soak}) \qquad \ldots\ldots (6.37)$$

The predicted heating times for the 15.9 cm mild steel billet when the air is preheated by 400°C, 600°C, 1000°C and 1200°C are shown in Fig. 6.15. The same results are plotted as efficiencies in Fig. 6.16. These figures show, for example, that using a gas input of 0.335 MW/m length and an air preheat of 400°C the heating time is 24 minutes at an efficiency of 28%. If an air preheat of 1200°C is obtained then the same heating time can be achieved at an efficiency of 48% using a gas input of 0.201 MW/m length, alternatively the heating time may be reduced to 18.5 minutes if the heat input is kept at 0.335 MW/m length.

6.9 Minimum Heating Times

The predicted heating times for the various furnace designs can be put into perspective by comparing them with the theoretical minimum

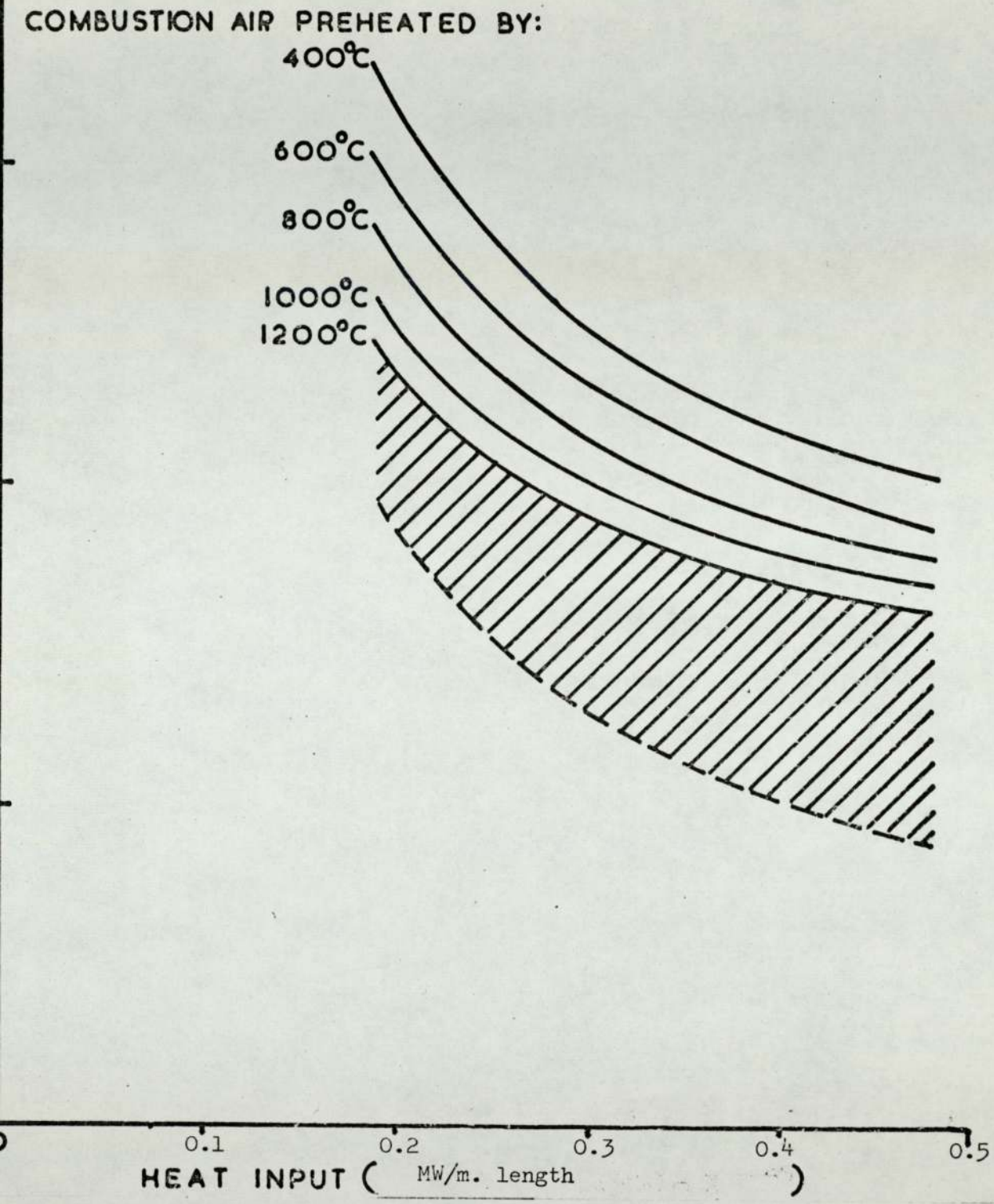

6.15 Theoretical heating times for a 15.9 cm diameter mild steel billet in a 25.4 cm single cell furance when the combustion air is preheated by various amounts.

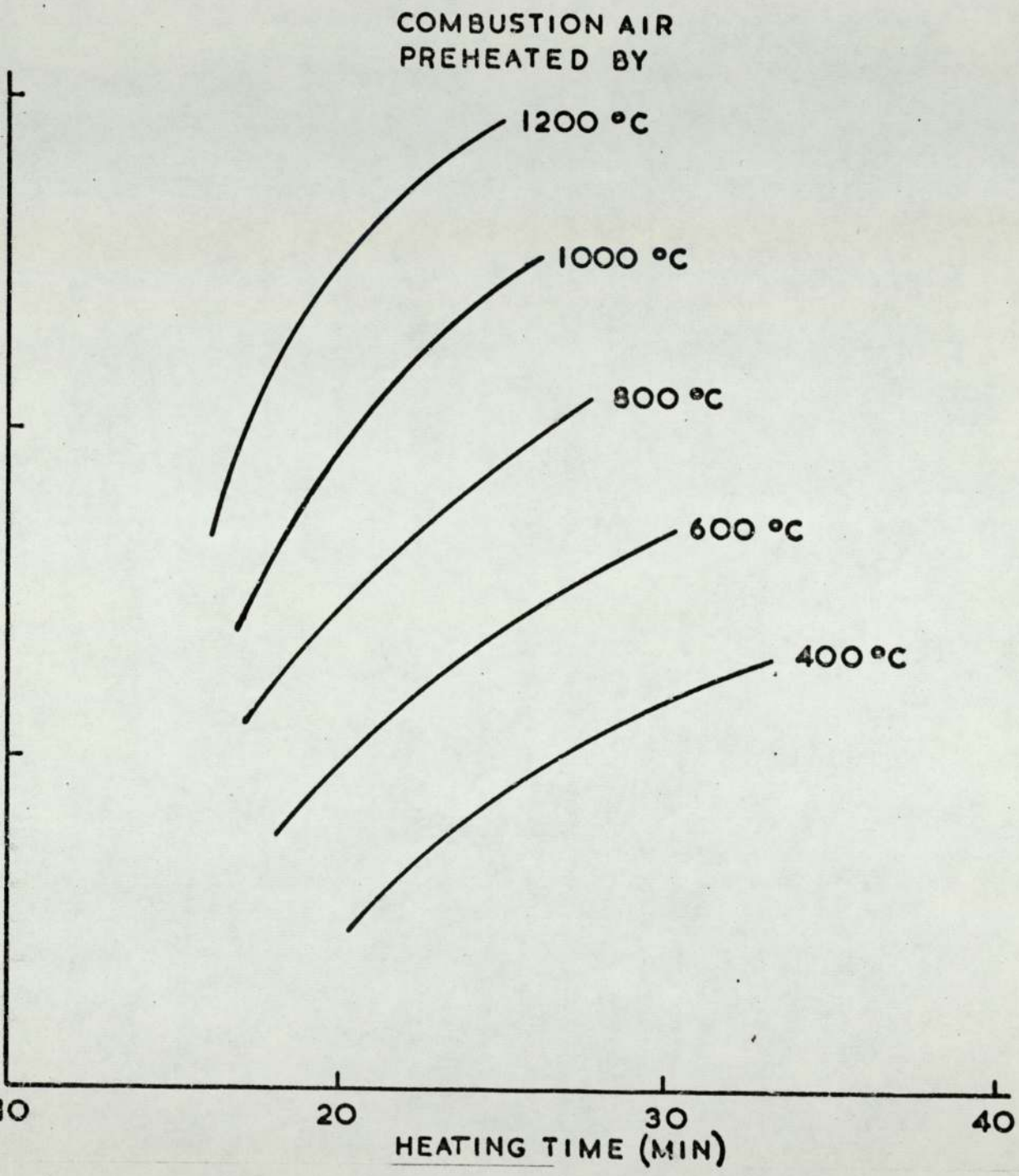

6.16 Theoretical thermal efficiencies for a 15.9 cm diameter mild steel billet in a 25.4 cm single cell furnace when the combustion air is preheated by various amounts.

heating time necessary to obtain the specified temperature uniformity for each billet size. The minimum could be reached when the initial heat flux to the surface is infinite so that the surface temperature reaches its specified value instantaneously whilst the centre is still cold. The heating time is then controlled only by the rate at which heat can be conducted from the surface into the interior of the stock. The asymptotic approaches to the minimum heating times for different billet diameters are shown in Fig. 6.17. This graph has been prepared by simplifying the heat transfer equations, giving the heat flux to the billet, to the form:

$$\Phi_b = H A_b (T_g - T_b) \quad \ldots\ldots (6.38)$$

It was assumed that the overall heat transfer coefficient, H in this equation was constant, until the billet surface reached its specified temperature of 1288°C, and that it was then progressively reduced to give the heating rate necessary to maintain the surface at temperature. It was further assumed that the gas temperature remained constant at 1650°C. The ordinate in Fig. 6.17 is the constant overall heat transfer coefficient used to calculate the heat flux in the initial stages of the heating cycle. The important thing to note in this figure is the limiting heating times for the different billet diameters. These are independent of the heat transfer characteristics of the furnace environment and consequently independent of the simplified heat flux relationship given by equation (6.38). The minimum heating times are the shortest times it is possible to heat a billet to the stated temperature profile in any furnace.

The closeness to which the minimum heating times are approached in the rapid heating furnaces considered in this paper are also indicated in Fig. 6.17. The numbered arrows in this figure show the

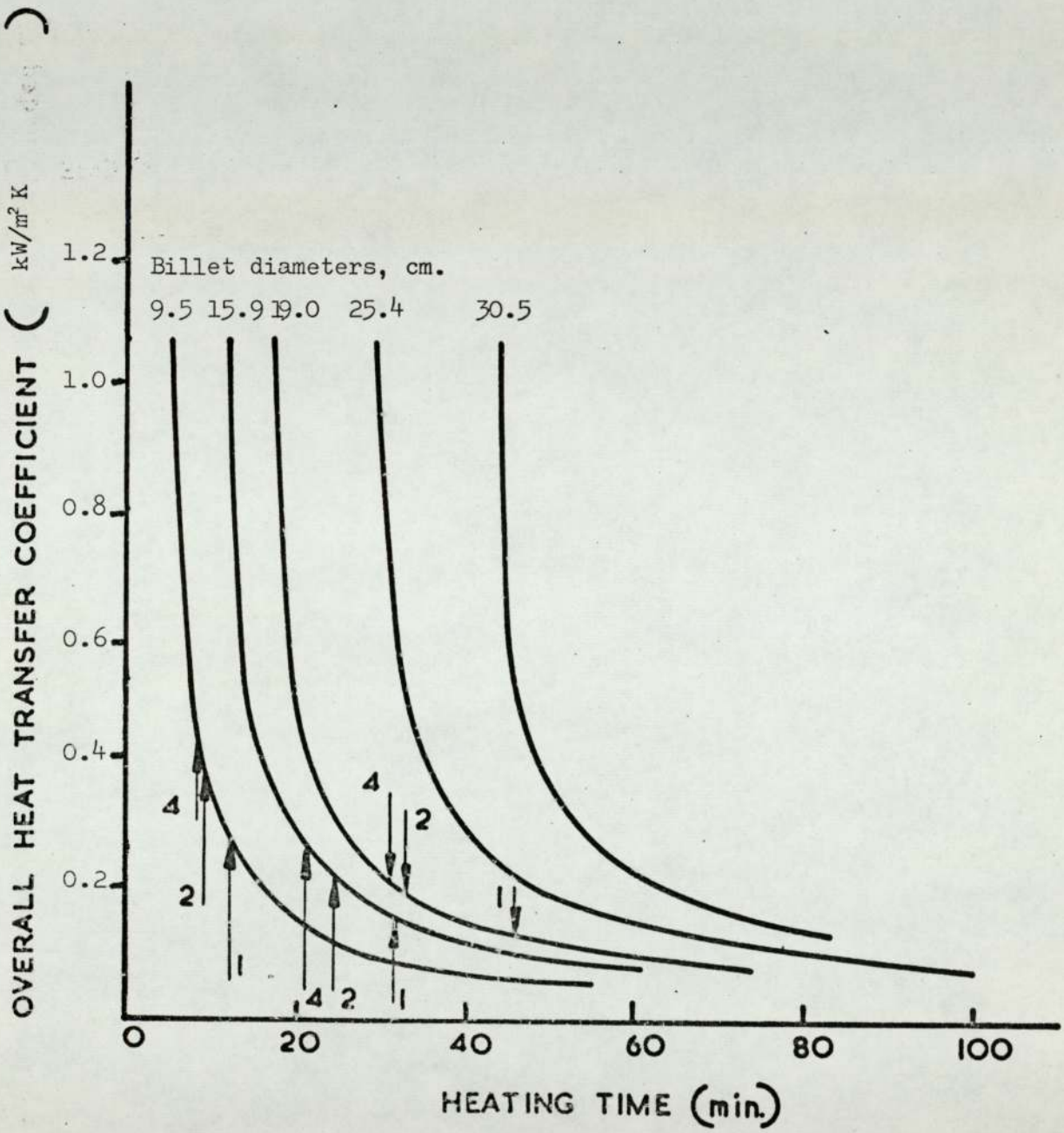

Fig. 6.17 Theoretical heating times for mild steel billets when the surface is heated to 1288° C and held until the centre reaches 1232° C.

heating times predicted for a heat input of 0.5 MW/m length in furnaces with the various burner and flue arrangements corresponding to the number indicated. These results show that if the overall heat transfer coefficient in the single cell furnace fitted with self recuperative burners could in some way be doubled then the heating time of the 15.9 cm billet would be reduced by only 30%. A further doubling of the coefficient would reduce the heating times by only about another 15%. The furnace therefore operates in a region in which conduction significantly limits the reduction in heating times which could be obtained by improving thermal aspects of furnace design.

One of the advantages of rapid heating over conventional heating methods is that the time for which the billet is above the temperature at which detrimental metallurgical effects can take place is minimised. The temperature above which these effects become significant is usually taken to be 800°C. For the sizes of billet shown in Fig. 6.17 i.e. up to 30 cm, the time for which the billet surface is above 800°C is always reduced as the heat transfer rate is increased. However this is not necessarily true for large billet sizes. In addition as the heating rate is increased the surface must be held at 1288°C for progressively longer periods. As oxidation and decarburisation increase with temperature as well as time it is possible that surface deterioration will not necessarily be minimised at the minimum heating times.

7. THE TRANSIENT THERMAL RESPONSE OF A RAPID HEATING CELL

Two main assumptions were made in the mathematical model used in the last chapter. These were that the furnace was well stirred and that the thermal inertia of the furnace walls was negligible and therefore no heat was lost or gained in the furnace structure during a heating cycle. In the mathematical model described in this chapter the second of these assumptions is relaxed. This allows certain transient aspects of the furnace performance to be investigated.

All the calculations in this section are made for furnace No. 2 of figure 6.8, the walls of which were assumed to be cylindrical. A diagram of the furnace is shown in figure 7.1.

7.1 The Mathematical Model

The mathematical model described in chapter 6 represented the heat transfer in a furnace by two sets of simultaneous equations which describe the heat transfer from the furnace environment to the load surface and the conduction within the load. The present model includes an additional set of equations which deal with conduction within the furnace wall. The solution of the three sets of equations provides the temperature distributions in the load and furnace wall, and the combustion products temperature at any time during the heating cycle.

7.1.1 Heat Transfer from the Furnace Environment

The equations for the transfer of heat from the furnace environment to the load surface are obtained by making simple heat balances on the combustion products in the furnace, on the billet and on the furnace walls. By making the assumptions that the combustion products within the furnace are well stirred (i.e. at constant temperature) and that the convective heat transfer coefficients and radiation factors are uniform the following equations may be derived

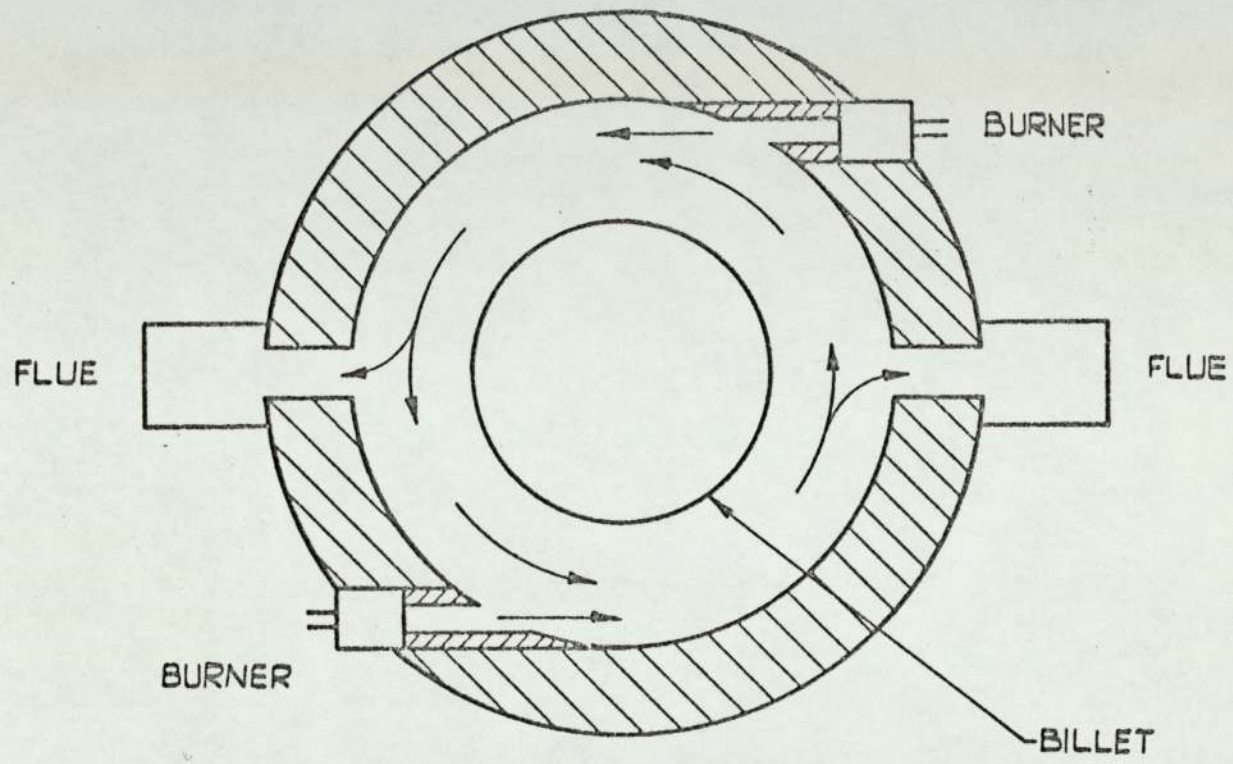

FIG. 7.1. LINE DIAGRAM OF FURNACE SECTION

(a) On the combustion products

$$\Phi_b = (I_f - I_g)Q - \Phi_w \qquad \ldots\ldots (7.1)$$

(b) On the billet

$$\Phi_b = h_b A_b (T_g - T_b) + F_{bw} A_b \sigma (T_w^4 - T_b^4) + F_{bg} A_b \sigma (T_g^4 - T_b^4) \qquad \ldots\ldots (7.2)$$

(c) On the walls

$$\Phi_w = h_w A_w (T_g - T_w) + F_{wg} A_w (T_g^4 - T_w^4) - F_{bw} A_b \sigma (T_w^4 - T_b^4) \qquad \ldots\ldots (7.3)$$

7.1.2 The Heat Conduction Equations

In this chapter we are concerned with a cylindrical billet heated in a cylindrical furnace with uniform surface heat fluxes, so that the transient heat conduction equation for this case then reduces to:

$$\frac{\partial T}{\partial \tau} = \alpha \frac{\partial^2 T}{\partial r^2} + \frac{1}{r} \frac{\partial T}{\partial r} \qquad \ldots\ldots (7.4)$$

The solution of this equation has already been discussed in section 6.2 and it was concluded that finite difference techniques must be used. In the present instance the Liebmann[39] substitution has been adopted. The first and second order space derivatives in equation (7.4) are then replaced by

$$\left(\frac{\partial T}{\partial r}\right) = \frac{T'_{j+1} - T'_{j-1}}{2\delta r} \qquad \ldots\ldots (7.5)$$

$$\left(\frac{\partial^2 T}{\partial r^2}\right) = \frac{T'_{j+1} - 2T'_j + T'_{j-1}}{\delta r^2} \qquad \ldots\ldots (7.6)$$

The resulting set of equations can be solved either exactly using Gaussian elimination or by an iterative technique. The method chosen was the Gauss - Siedel[48] iteration because of its simplicity and suitability to a fast digital computer. Its accuracy was tested by comparing calculated temperatures with an analytical solution for the same boundary conditions. Percentage differences were small and

decreased towards the end of the heating cycle. It was therefore assumed that equally accurate solutions would be obtained in cases where there was no analytical solution.

The solution of the transient heat conduction equation for the billet and for the furnace walls requires the specification of two boundary conditions in each case. For the billet these are the surface heat flux (Φ_b/A_b) and the fact that at the centre of the billet the temperature gradient is zero $\left[\left(\frac{\partial T}{\partial r}\right)_o = 0\right]$. In the case of the walls the inside boundary condition is the heat flux for the furnace environment (Φ_w/A_w) and at the outside the boundary condition is obtained by considering natural convection and radiation losses to the surroundings which can be given in the form:

$$\text{at } r = r_{wa} \quad \lambda\frac{\partial T}{\partial r} = h_a\,(T_{wa} - T_a) \qquad \ldots\ldots (7.7)$$

7.1.3 Method of Solution

Before the equations described in the preceeding sections can be solved for a given load size, furnace size and gas input rate, the following parameters must be known: the convective heat transfer coefficients, the radiation factors and the relevant physical properties of the combustion products, load and refractory. These factors are discussed in the following sections. The solution of the equations requires, first of all the specification of the initial temperature distributions in the load and wall. The load surface temperature and the temperature of the inside surface of the wall are then used in the heat transfer equations to provide the corresponding combustion products temperature and heat fluxes to the surface of the load and refractory. These fluxes are then used as the boundary conditions of the transient heat conduction equations to give new temperature distributions in the load and wall after a chosen time interval. Using the current values of the calculated billet and wall surface temperatures the solution is repeated for the next and subsequent time intervals.

The step-wise method of solution allows the convective heat transfer coefficients, radiation factors and physical properties to be recalculated at each step so that the variation with temperature of these quantities can be taken into account.

The size of the time interval was chosen to obtain a reasonable balance between accuracy and computing costs. For the calculations described in this chapter the computer programme was written so that the time interval was adjusted to keep the difference in temperature between successive time increments within the range 10°C to 20°C and 12°C to 24°C for the billet and wall surfaces respectively.

7.1.4 Other Data

The radiation factors and physical properties of the combustion products were evaluated as described in section 6.4. The convective heat transfer coefficients were obtained from the correlation given in section 6.7.1 i.e.,

$$j_b = 0.525\ Re_b^{-0.5} \qquad \ldots\ldots (7.8)$$

$$j_w = 1.13\ Re_w^{-0.5} \qquad \ldots\ldots (7.9)$$

These equations were obtained from mass transfer measurements on models of 25 cm diameter furnaces. In order that they may be used for furnaces of larger diameter fluid velocities close to the wall and billet surfaces must be available. These have been evaluated by assuming that the fluid is in solid body rotation (as discussed in Chapter 3) and by assuming that the mean recirculation ratio depends only on the ratio of the billet to furnace diameter.

7.2 The Effect of Furnace Size on Heating Times

Before dealing with the transient aspects of furnace operation it is first worthwhile considering the effect that furnace size has on heating times and consequently efficiency. The times taken to heat a 15.9 cm diameter mild steel billet to forging temperature in furnaces of the design of figure (7.1) have been calculated for a range of furnace

sizes at a fixed thermal input. These results are shown in figure (7.2) and are all based on the assumption that the furnace structure has become fully warmed so that heating times for succeeding billets will be constant. These results show that, for example, a heating time of 23 mins can be achieved in a furnace of either 17.2 cm diameter or in a furnace of 76 cm diameter. In the first case 39% of the heat gained by the billet is by convection, 3% by gas radiation and 58% by reradiation from the furnace walls, while in the second only 5.5% of the heat gained by the billet is by convection, 24% by gas radiation and 70.5% by reradiation from the walls.

In practice it is found that a furnace diameter of 17 cm, is too small since it becomes impossible to locate a billet centrally in a furnace of this size without damaging the walls. A furnace of diameter about 20-25 cm would therefore be used which leads to an increase in heating time and a drop in efficiency compared to the much larger furnace. However it will be shown in following sections that the modest loss in efficiency in the small furnace can be offset against a more rapid start up and better transient response than can be achieved in a larger furnace.

The calculations in this section have demonstrated the advantages to be gained from the use of very small gaps between billet and walls. Whilst these may not be achievable in the particular type of furnaces considered here they can easily be used in other types of rapid heating furnace such as those for strip and bar end heating.

7.3 Start-up

If a billet is charged to the furnace as soon as the burners are lit then both the billet and furnace structure must be heated simultaneously and consequently the time taken for the billet to reach the forging temperature will be longer than if the furnace had been in operation for some time. The performance of the furnace shown in Figure (7.1) has been calculated for the heating of a succession of billets to forging

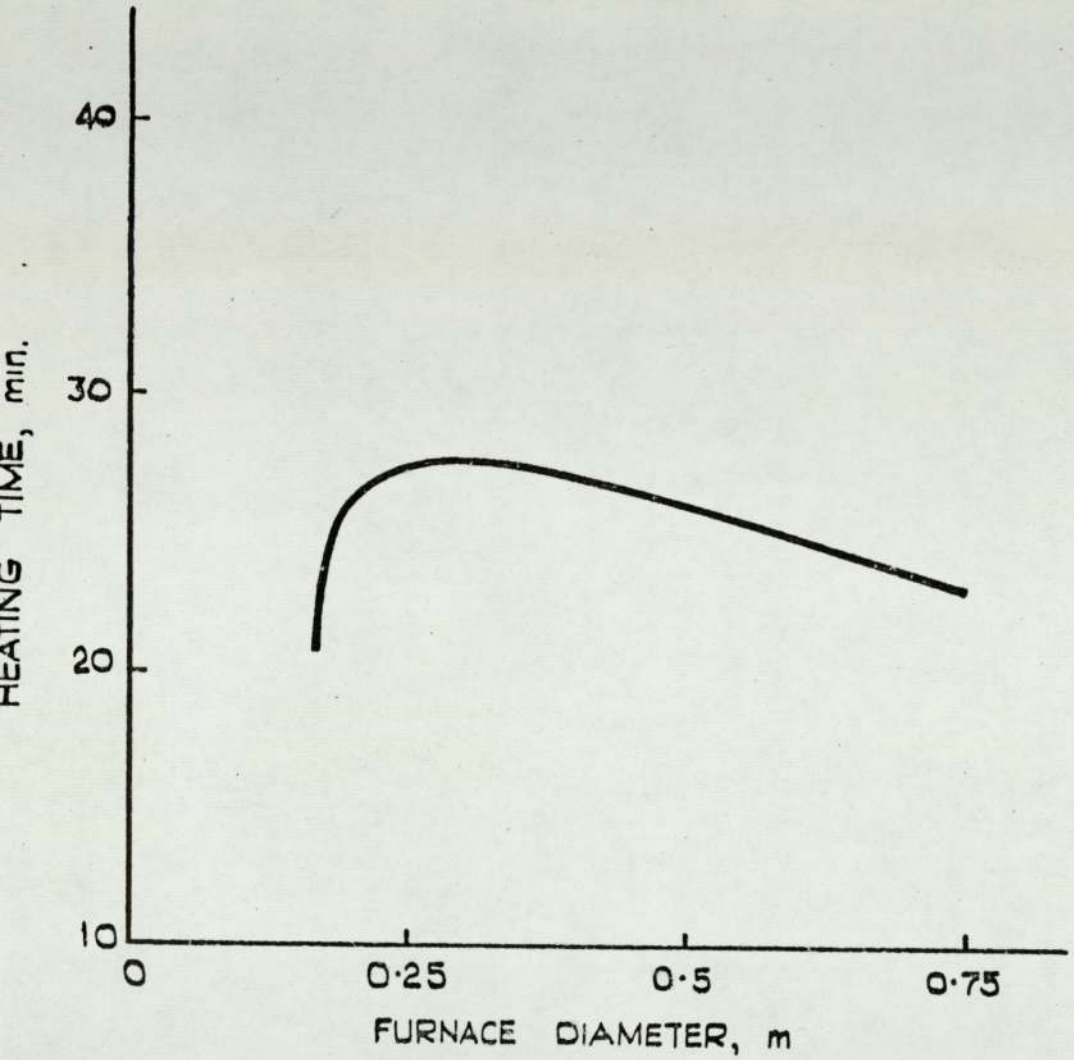

FIG. 7.2. THE EFFECT OF FURNACE SIZE ON BILLET HEATING TIME

temperature starting with a cold billet in a cold furnace. The results in Figure (7.3) show the time required to heat 15.9 cm. diameter mild steel billets in this manner to 1250°C in a furnace of 25 cm. diameter. As expected the billet heating times decrease progressively and reach a minimum when the refractory has become fully warmed. After the passage of only 3 or 4 billets the heating times are quite close to the minimum despite the fact that the outside temperature of the wall continues to rise even after 20 billets have been heated.

Also shown in Figure (7.3) are heating times calculated using a more simple mathematical model as described in Chapter 6. This model applies only to furnaces in which the walls have become fully warmed and it being thus assumed that the heat stored in the walls did not change during a heating cycle. It can be seen that the two mathematical models predict almost the same heating time once the furnace has become fully warmed.

The effect of furnace size on the time taken to heat the first few billets after start up has been investigated and the results are summarised in Table 7.1. If the heating times for the furnaces of 17.8 cm and 76.2 cm diameter with wall thicknesses of 12.7 cm are compared with each other it is seen that the heating time in a fully warmed furnace is slightly less for the larger size at the the same heat input.

The smaller furnace warms up much more quickly however, and, for example, the total time taken to heat the first five billets is 11% less than for the larger furnace. For the 25 cm diameter furnace the minimum billet heating time is 17% longer than in the 76cm furnace but, nevertheless, the first three billets are heated just as quickly in both furnaces.

A wall thickness of 12.7 cm is realistic for the smaller furnace sizes but its mechanical strength in a larger furnace is probably insufficient. The calculation for the 76 cm furnace have therefore been repeated using a wall thickness of 50 cm and the results shown in the last column of

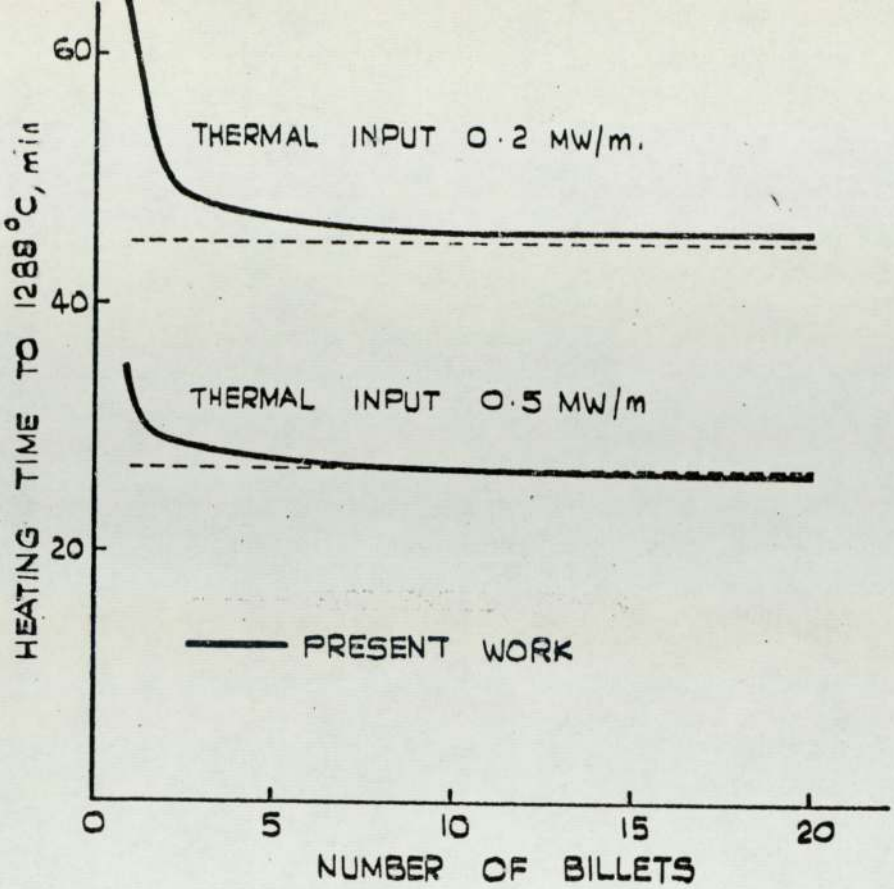

FIG. 7.3 HEATING TIMES INCLUDING WARMING OF FURNACE STRUCTURE

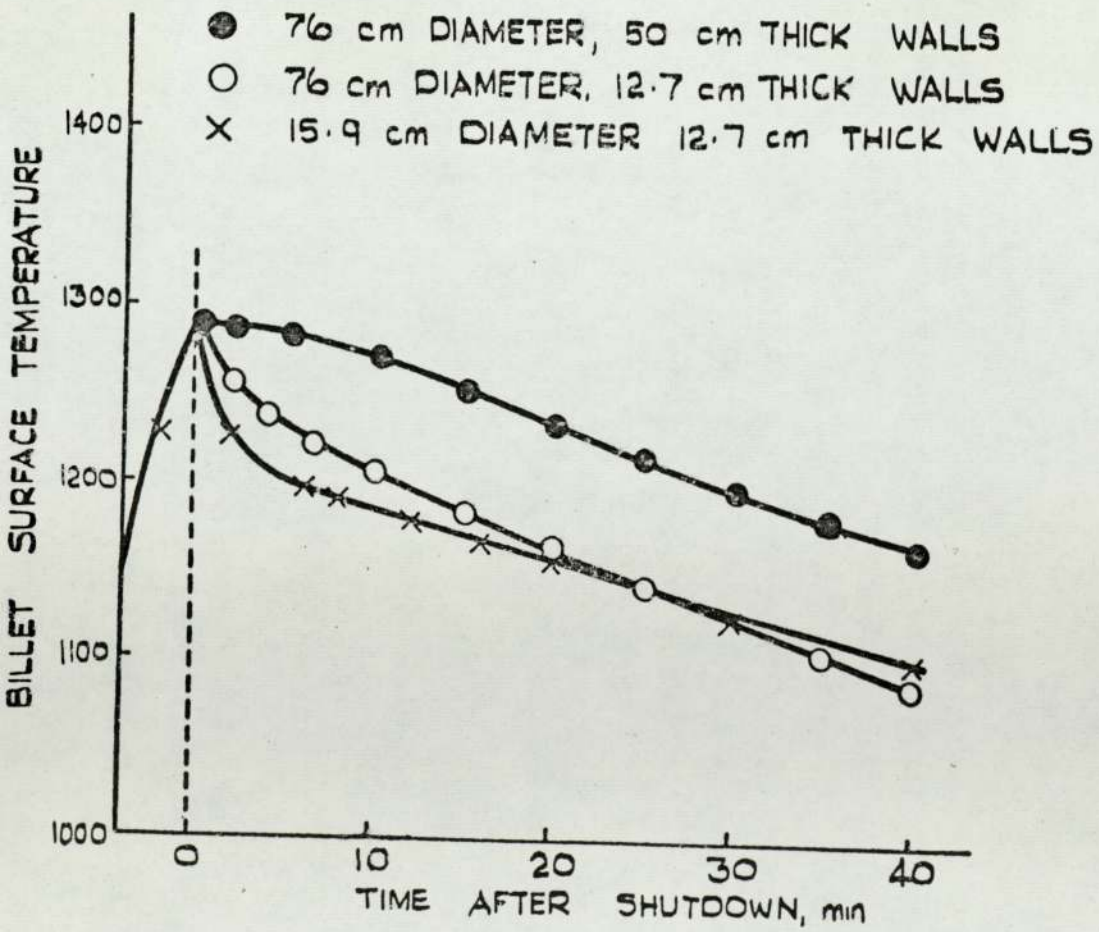

7.4 THE EFFECT OF FURNACE SHUTDOWN OF BILLET SURFACE TEMP.

Table 7.1 : Billet heating times during furnace start-up, min-s

Furnace diameter, cm	17.8		25.4		76.2		76.2	
Wall thickness, cm	12.7		12.7		12.7		50.8	
Heat input, MW/m	0.5		0.5		0.5		0.5	
Billet No.	Heating time	Cumulative time	Heating time	Cumulative time	Heating time	Cumulative time	Heating	Cumulative time
1	28-15	28-15	34-30	34-30	39-15	39-15	43-20	43-20
2	25-20	53-55	29-00	63-30	26-55	66-10	26-25	69-45
3	24-50	78-25	28-20	91-50	25-30	91-40	25-25	95-20
4	24-30	102-55	27-55	119-45	24-45	116-25	24-50	120-10
5	24-30	126-25	27-40	147-25	24-10	140-35	24-40	144-50
6	24-10		27-20		23-45		24-25	
7	24-5		27-10		23-30		24-00	
8	24-5		27-10		23-25		23-45	
9	24-5		26-55		23-15		23-45	
10	24-5		26-55		23-15		23-45	
15	24-5		26-45		22-55		23-15	
20	24-5		26-45		22-55		22-55	

table 7.1. Here, with such a large mass of refractory to be heated, the first billet takes 61% longer than in the smallest furnace considered. Even after 20 billets have been heated the structure is not fully warmed and the heating times for each successive billet is still slowly becoming less. Finally it is worth noting that the firing density of the largest of the furnaces considered in this section is 0.23 MW/m^3 and this is about twice that in many conventional reheating furnaces. Conventional furnaces are also very much larger and the time to warm the furnace structure is of the order of a few hours rather than a few minutes as in rapid heating cells.

7.4 Furnace Response

In this section the response of the furnace to changes in the heat input rate is considered. Two cases are dealt with, that of an increase in the heat input rate to meet a demand for an increase in work output and the shutting down of the furnace due to a mill stoppage.

7.4.1 Increase in Output

It is predicted that a 17.8 cm diameter furnace will heat 15.9 cm mild steel billets to forging temperature at a steady rate of 41 min 55 secs per billet for a thermal input of 0.2 MW/m length of furnace. On increasing the heat input to 0.5 MW/m length the next billet is heated in 24 min 5 secs which is the same as the heating time achieved under steady conditions using the same heat input. The response of the furnace is thus very fast and its control to meet output demands is very simple.

In the case of a 76.2 cm furnace heating the same billet, a steady rate of 41 min - 10 sec. for each billet can be obtained using 0.2 MW/m length of furnace. An increase in heat input to 0.5 MW/m length results in the next billet being heated in 23 min 40 sec. which is 3.3% longer than that achieved under steady conditions.

7.4.2 Furnace Shutdown

When there is a temporary stoppage in the production line the heat input to the furnace must be reduced or completely shut off to prevent overheating or melting of the stock in the furnace. If the stoppage occurs when the billet surface is approaching its forging temperature then even if the heat input is completely cut off the surface temperature may still continue to rise as the walls radiate stored heat. This process has been investigated for a range of sizes of furnaces heating a 15.9 cm mild steel billet and the results are shown in Fig. 7.4. It has been assumed throughout that the furnace is shut down when surface temperature of the billet first reaches 1288°C.

When the furnace is first shut down the hot walls radiate heat to the billet surface and the wall surface cools until its temperature becomes equal to that of the billet surface. This takes about 1 min. for the 17.8 cm furnace, 3 min. for the 76 cm furnace with 12.7 cm thick walls and $7\frac{1}{2}$ min. in the 76 cm furnace with 50 cm walls. During this period the surface temperature of the billet may either rise or fall depending on the temperature distribution within the billet and the amount of heat received from the wall. In all the cases shown in Figure 7.4 the billet surface temperature falls immediately since all the heat received can be conducted into the interior. However if, for example, a 15.9 cm aluminium billet heated in a 25 cm diameter furnace to an extrusion temperature of 550°C is considered, then, due to the low emissivity of aluminium, the temperature difference between the billet and walls will be larger than for steel. Also the high thermal conductivity of aluminium results in a nearly uniform temperature throughout the billet. In this particular case the billet temperature will continue to rise when the furnace is shutdown and the surface would probably melt.

After the load and wall surface temperatures have equalised the direction of heat transmission is reversed. The walls become cooler

than the billet and therefore the net radiation between them is towards the walls. The rate of heat transfer is dependent on the wall surface temperature and therefore on the rate at which heat can be conducted through the wall.

The calculated results show that the 76 cm furnace with 12.7 cm thick walls is able to accept and conduct away the heat received from the from the billet more readily than can the 17.8 cm furnace having the same wall thickness. The billet temperature therefore falls more rapidly in the former case so that eventually it will be at a lower temperature than it would be in the smaller furnace at the same time. In the case of the 76 cm furnace with 50 cm walls the heat is conducted away slowly so that the billet temperature falls slowly.

7.5 Transient Conditions within the Wall

In the preceeding sections the influence of furnace size on the heating times and temperatures of the billet under transient operating conditions has been considered. This section and that following are concerned with transient variations of temperature within the furnace wall. Only one furnace size is considered, that of 25 cm. diameter heating a 15.9 cm. billet to a forging temperature of 1250°C.

Wall and billet surface temperature profiles during a heating cycle for a furnace which has reached steady operating conditions are shown in figure (7.5). When the cold charge is put into the furnace the hot walls radiate to the billet, and its temperature rises rapidly whilst the wall surface temperature drops. During the rest of the heating cycle both wall and billet temperatures rise, the rate of rise of billet temperature diminishing as the temperature difference between it and the wall decreases. Towards the end of the cycle the surface temperature is held constant by reducing the heat input to the furnace in order to achieve acceptable temperature uniformity for forging. This is accompanied by a fall in the wall surface temperature to the same value

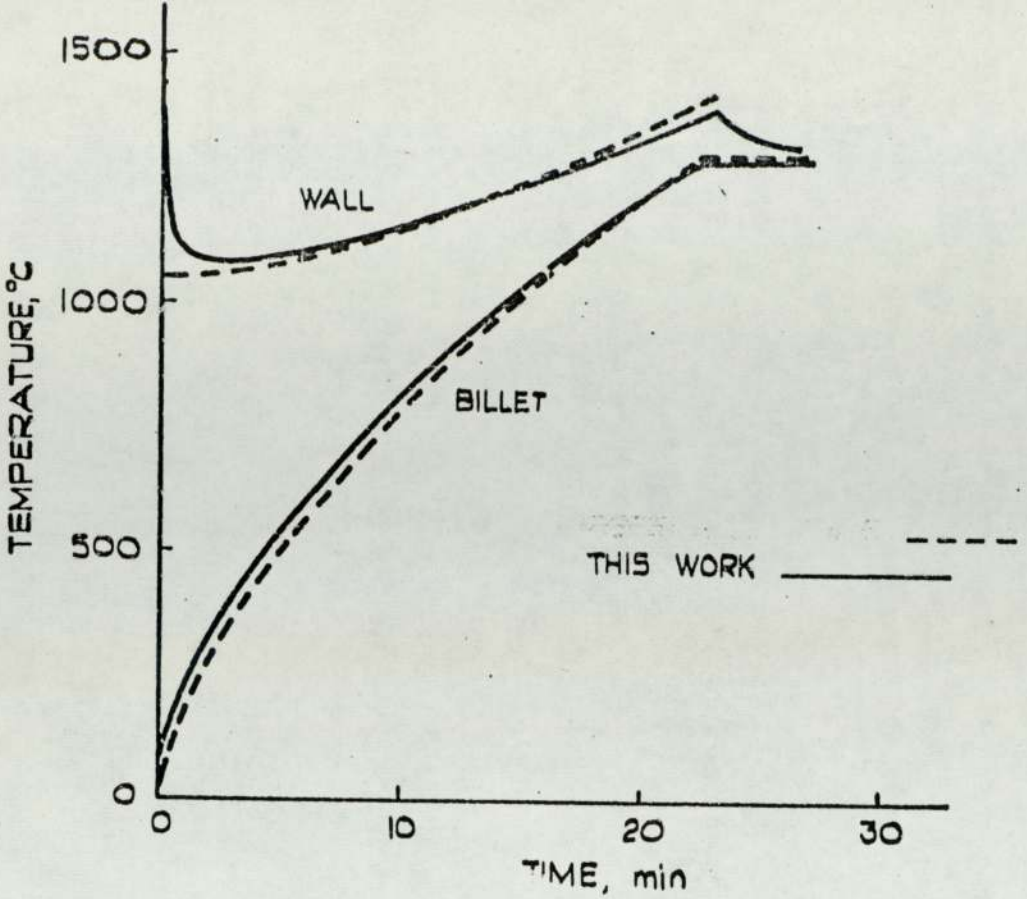

FIG. 7.5. WALL AND BILLET SURFACE TEMPERATURE VARIATION IN A FULLY WARMED SURFACE

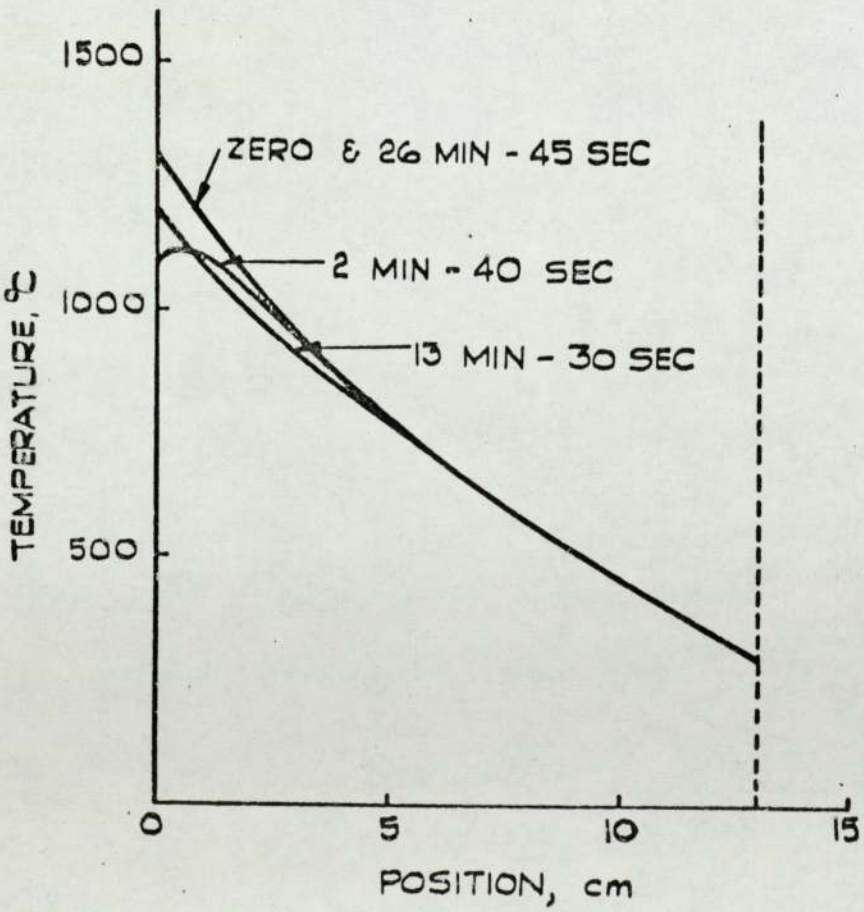

FIG. 7.6. WALL TEMPERATURE PROFILES DURING A HEATING CYCLE

that it was at the beginning of the heating cycle. This cycle is repeated during the heating of each billet causing the temperatures inside the wall to be fluctuating continuously.

Also shown in figure (7.5) are the billet and wall surface temperatures predicted using the simpler mathematical model of chapter 6 which does not take into account the changing heat content of the walls during the heating cycle. In the first part of the heating cycle the walls radiate stored heat to the billet and the calculated wall temperatures are therefore considerably in error. However, because of the low conductivity of the refractory, the temperature changes within the wall are significant only over a comparatively short distance as shown in figure (7.6). Hence over the greater part of the heating cycle the heat content of the walls only changes slowly and temperatures calculated from the simple model are close to those predicted from the present work. It is interesting to note that the temperature changes within the wall are out of phase with those at the surface.

7.6 Composite Wall

The fluctuations of temperature and change of temperature gradient within the furnace wall lead to changes in the stress pattern within the refractory. By the use of a composite wall made up of a dense cast inner refractory and an insulating brick these fluctuations may be confined to the dense face and any damage that they may produce is minimised.

The properties of the refractories in the wall were taken to be as follows:

	Dense Face	Insulating Brick
Main constituents Al_2O_3	53%	61%
SiO_2	41.5%	36.3%
Density (Kg/m^3)	2460	880
Specific heat ($J/Kg°C$)	960	1130
Thermal conductivity ($W/m°C$)	1.48	0.29

In order to calculate the temperature at the interface between the two refractories the finite difference form of the transient heat conduction equation contained in the mathematical model must be rewritten. If the interface, i, is between element j and (j+1) as shown in figure (7.7) then the temperature gradient in the first material at the interface can be expressed as $2(T_j' - T_i')/\delta r_1$, and in the second material as $2(T_i' - T_{j+1}')/\delta r_2$. The finite difference equations for the elements j and (j+1) are then:

$$V_j \rho_1 C_{p1} (T_j' - T_j) = \frac{k_1 A_{j-1\ j} (T_{j-1}' - T_j')\delta\tau}{\delta r_1} - \frac{2k_1 A_{j\ j+1}}{\delta r_1} (T_j' - T_i')\delta\tau$$

$$V_{j+1} \rho_2 C_{p2} (T_{j+1}' - T_{j+1}) = \frac{2k_2 A_{j\ j+1}}{\delta r_2} (T_i' - T_{j+1}')\delta\tau - \frac{k_2 A_{j+1\ j+2}}{\delta r_2} (T_{j+1}' - T_{j+2})\ \delta\tau$$

Temperature fluctuations within a composite wall have been calculated for different thicknesses of dense face and insulating brick. The results are shown in Fig. (7.8) for three walls each of total thickness 12.7 cm but with a dense face thickness of 2.54 cm, 3.81 cm and 5.08 cm. Temperature variations at the interface are reduced from 83°C with 2.54 cm of dense face refractory to only 16°C when 5.08 cm are used. The latter thickness seems to reduce thermal shock in the insulating brick to a negligible amount.

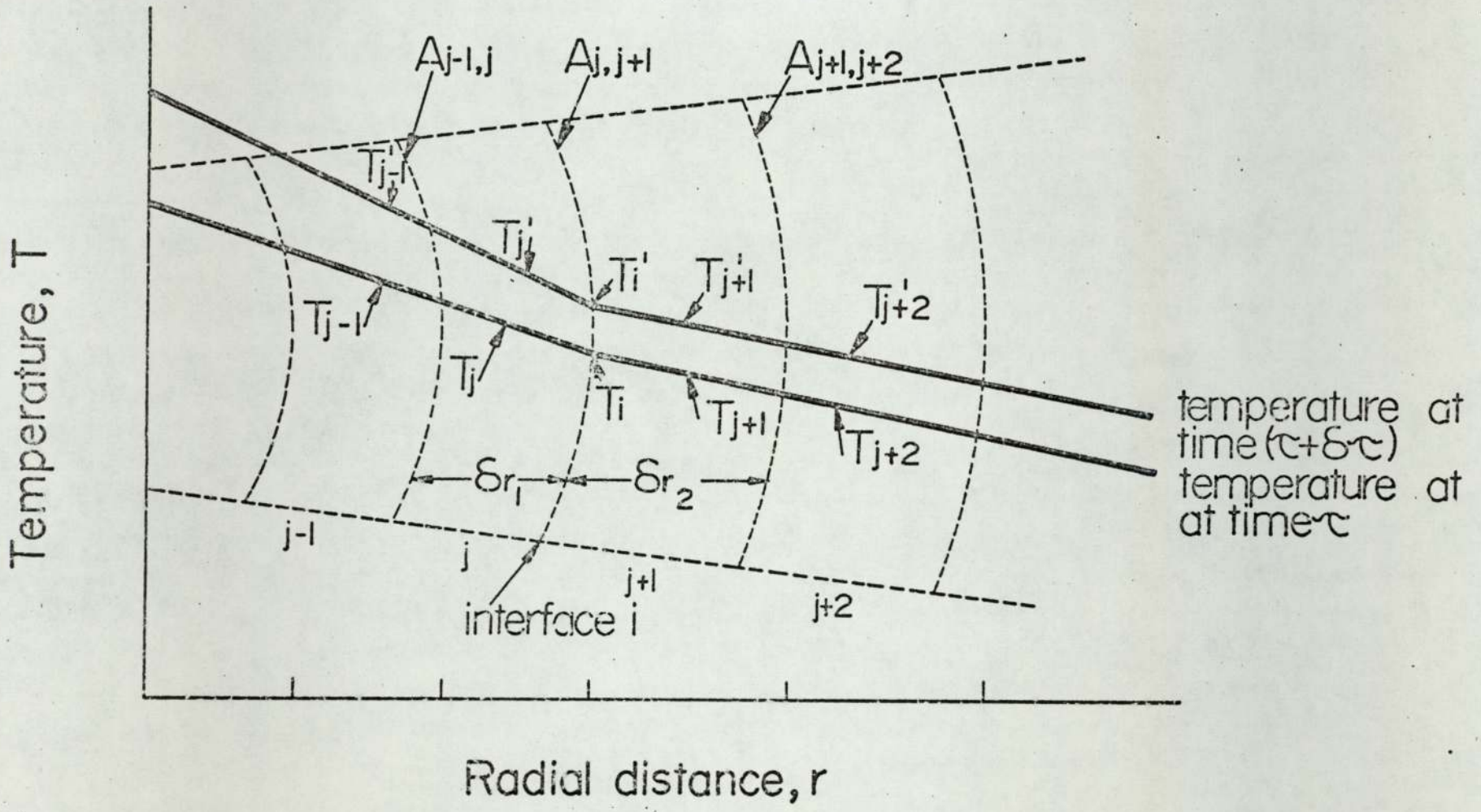

Fig. 7.7 Calculation of the temperature at the interface between two different refractories.

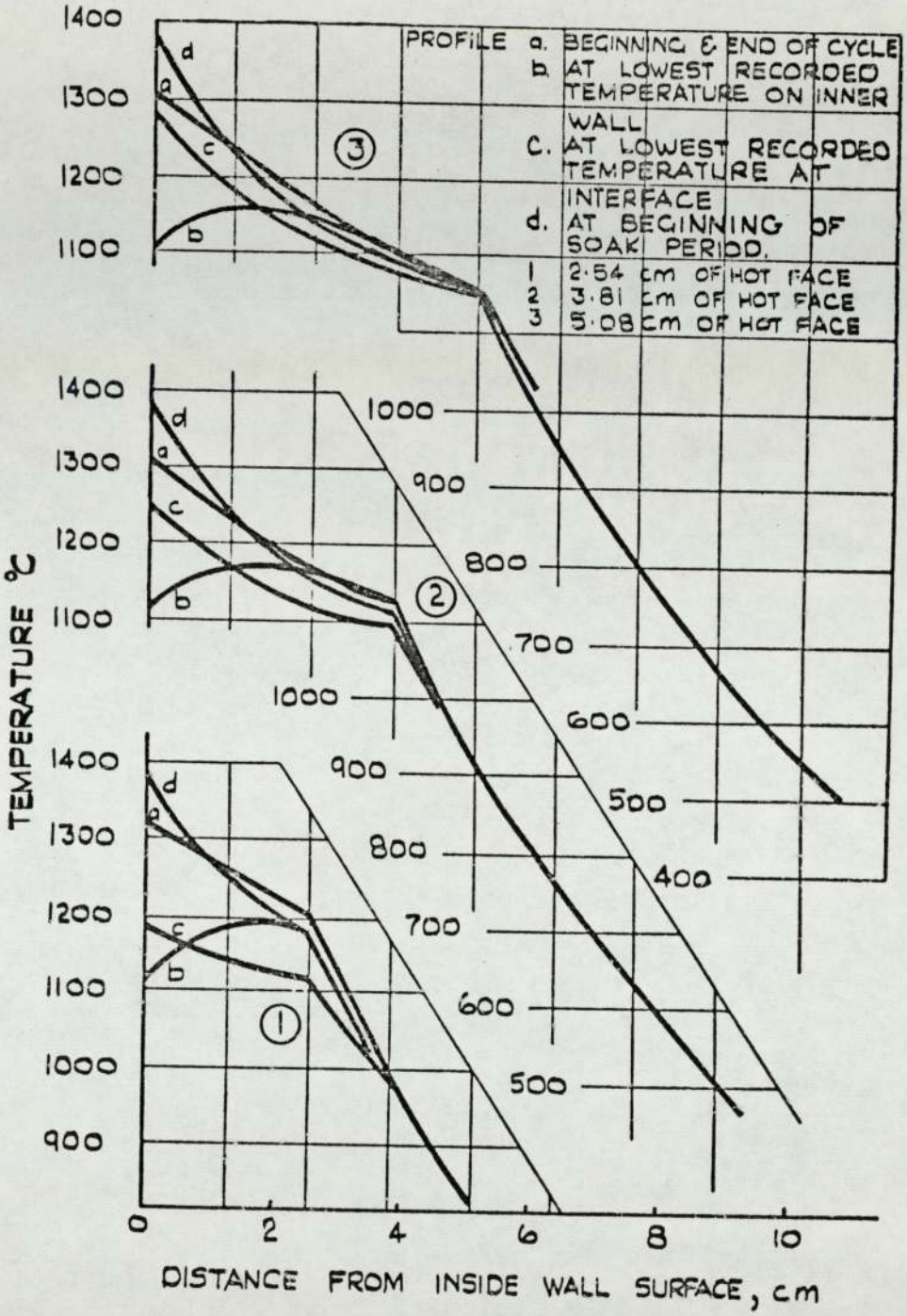

FIG. 7.8 TEMPERATURE PROFILES FOR THREE THICKNESSES OF HOT FACE REFRACTORY

The use of a dense hot face refractory slows the transient response of the furnace since the heat content of the entire structure is increased significantly by the comparatively large mass of dense material at high temperature. If a 76 cm diameter furnace with walls of 12.7 cm thickness including 5.08 cm of dense face is taken as an example then the heating time for the first billet is 45 min 30 secs compared with 39 mins 15 secs in a furnace with a bubble alumina wall using a heat input of 0.5 MW/m length of furnace. On shutting off the burners with a billet at forging temperature left in the furnace the billet surface temperature falls to 1225°C in 25 mins whilst in a furnace with bubble alumina walls it falls to 1106°C in the same time.

8. CALCULATION OF TEMPERATURE DISTRIBUTION IN THE BILLET USING THE LOCAL MASS TRANSFER COEFFICIENTS

The experimental measurements of local convective coefficents clearly showed that the distribution of convective heat transfer over the billet surface is not uniform. This may result in significant temperature differences around the circumference of the billet which may in turn affect the quality of the final product formed from the billet. It is therefore important to be able to predict the local temperature distribution and a method is described in this chapter which enables this to be achieved.

8.1 The Mathematical Model

The mathematical models which were described in the preceeding two Chapters are both based on the assumption that the heat flux to the billet was uniform over the surface and therefore only contained the one dimensional radial heat conduction equation. The method described in this Chapter assumes that the furnace is fully warmed and is therefore similar to that in Chapter 6 except that it contains the two dimensional heat conduction equation for a cylinder. The model is built up from two sets of simultaneous equations describing heat transfer from the furnace environment and conduction within the load.

8.1.1 Heat Transfer from the Furnace Environment

It is assumed that the temperature of the combustion products and the furnace wall are uniform at any instant in time and also that the convective heat transfer coefficients to the wall and the radiation factors are uniform. The only spatial variations taken into account are the convective heat transfer coefficient and temperature at the surface of the billet. The following heat balances can then be derived:

(a) On the combustion products

$$\phi_b = (I_f - I_s)Q - \phi_w \qquad \ldots\ldots (8.1)$$

(b) On the billet

$$\phi_b = \int_0^{2\pi} q_\theta \, r_b \, l_b \, d\theta \qquad \ldots\ldots (8.2)$$

where $q_\theta = h_{b\theta} (T_g - T_{b\theta}) + F_{bw} \sigma (T_w^4 - T_{b\theta}^4)$

$$+ F_{bg} \sigma (T_g^4 - T_{b\theta}^4) \qquad \ldots\ldots (8.3)$$

(c) On the walls

$$\phi_w = \frac{A_w k_w}{x_w} (T_w - T_{wa}) \qquad \ldots\ldots (8.4)$$

$$\phi_w = h_w A_w (T_g - T_w) + \sigma F_{wg} A_w (T_g^4 - T_w^4)$$

$$- \int_0^{2\pi} \sigma F_{bw} (T_w^4 - T_{b\theta}^4) \, r_b \, l_b \, d\theta \qquad \ldots\ldots (8.5)$$

Since the transient heat conduction part of the mathematical model requires a finite difference solution it is logical to rewrite the integral terms of (8.2) and (8.5) as sums of finite elements. If the billet surface is divided into t, equal elements in the circumferential direction equations (8.2) and (8.5) become:

$$\phi_b = \sum_{j=1}^{t} \frac{q_j A_b}{t} \qquad \ldots\ldots (8.6)$$

where $q_j = h_{bj} (T_g - T_{bj}) + F_{bw} \sigma (T_w^4 - T_{bj}^4)$

$$+ F_{bg} \sigma (T_g^4 - T_{bj}^4) \qquad \ldots\ldots (8.7)$$

and $\phi_w = h_w A_w (T_g - T_w) + \sigma F_{wg} A_w (T_g^4 - T_w^4)$

$$- \sum_{j=1}^{t} \sigma F_{bw} A_{bj} (T_w^4 - T_{bj}^4) \qquad \ldots\ldots (8.8)$$

These heat balance equations are similar to those of sections 6.1 and 7.1. For example, equation (8.8) differs from (6.6) and (7.3) only in that the term:

$\sum_{j=1}^{t} \sigma F_{bw} A_{bj} (T_w^4 - T_{bj}^4)$ replaces $\sigma F_{bw} A_b (T_w^4 - T_b^4)$.

But we can put:

$$\sum_{j=1}^{t} \sigma F_{bw} A_{bj} (T_w^4 - T_{bj}^4) = \sum_{j=1}^{t} \sigma F_{bw} A_{bj} T_{bj}^4 - \sum_{j=1}^{t} \sigma F_{bw} A_{bj} T_{bj}^4$$

$$= \sigma F_{bw} T_w^4 \sum_{j=1}^{t} A_{bj} - \sigma F_{bw} \sum_{j=1}^{t} A_{bj} T_{bj}^4$$

$$= \sigma F_{bw} T_w^4 A_b - \sigma F_{bw} \sum_{j=1}^{t} A_{bj} T_{bj}^4 \qquad \ldots\ldots (8.9)$$

The solution of the mathematical model proceeds from one time level to the next by calculating the combustion products and wall temperatures and the heat flux to the billet from the known billet surface temperatures. Under these conditions we can write (8.9) in the form

$$\sum_{j=1}^{t} \sigma F_{bw} A_{bj} (T_w^4 - T_{bj}^4) = \sigma F_{bw} A_b T_w^4 - \sigma F_{bw} k_1 \qquad \ldots\ldots (8.10)$$

Similarly equations (6.6) and (7.3) can be written:

$$\sigma F_{bw} A_b (T_w^4 - T_b^4) = \sigma, F_{bw}^4 A_b T_w^4 - \sigma F_{bw} k_2 \qquad \ldots\ldots (8.11)$$

Equation (8.8) therefore differs from (6.6) and (7.5) only in the value of the known constants k_1 and k_2. Similarly it can be shown that the equation (8.6) reduces to the same form as (6.5) and (7.2).

8.1.2 The Heat Conduction Equation

The differential equation for transient conduction in a cylinder with non-uniform heat flux in the circumferential direction is:

$$\frac{\partial T}{\partial \tau} = \alpha \left[\frac{\partial^2 T}{\partial r^2} + \frac{1}{r} \frac{\partial T}{\partial r} + \frac{1}{r^2} \frac{\partial^2 T}{\partial \theta^2} \right]$$

The solution of this equation for the boundary conditions obtained from the equations of the furnace environment must be made by finite difference methods. Most previous work on finite difference solutions of two dimensional heat

conduction problems has been limited to systems which can be described by rectangular co-ordinates. For these applications it has been found that explicit solutions require very small time intervals to prevent the solution becoming unstable and these intervals are much less than those necessary for one dimensional problems. Implicit or Crank-Nicolson formulations appear not to be used since the necessary algorithm for their solution is extremely complex. The technique which is most widely used is therefore a combination of explicit and implicit formulations which is known as the Peaceman-Rachford[5] or alternating direction implicit (A.D.I.) method. With this scheme the solution proceeds from one time level to the next through two stages in each of which the finite difference formulation is explicit in one direction and implicit in the other. The time interval for each stage is half the full time interval and the direction in which the implicit formulation is made alternates from one stage to the next. The equations for each stage then reduce to a similar form to those for one dimensional conduction and can therefore be solved by the standard algorithm.

Little work appears to have been done in applying the A.D.I. method to systems involving cylindrical co-ordinates and non uniform circumferential heat flux. In this case the closed nature of the solution in the circumferential direction causes difficulty in handling the matrix of coefficients. Some degree of iteration seems to be inevitable and in calculating the results presented in this thesis an entirely iterative technique has been used.

The finite difference equations have been set up so that a half radial element is obtained at the billet centre and surface. If the calculated temperatures are taken to represent the temperature of finite elements of the billet then the corresponding physical subdivision is shown in figure 8.1. This results in a large number of small elements near to the billet centre all of which might be expected to have

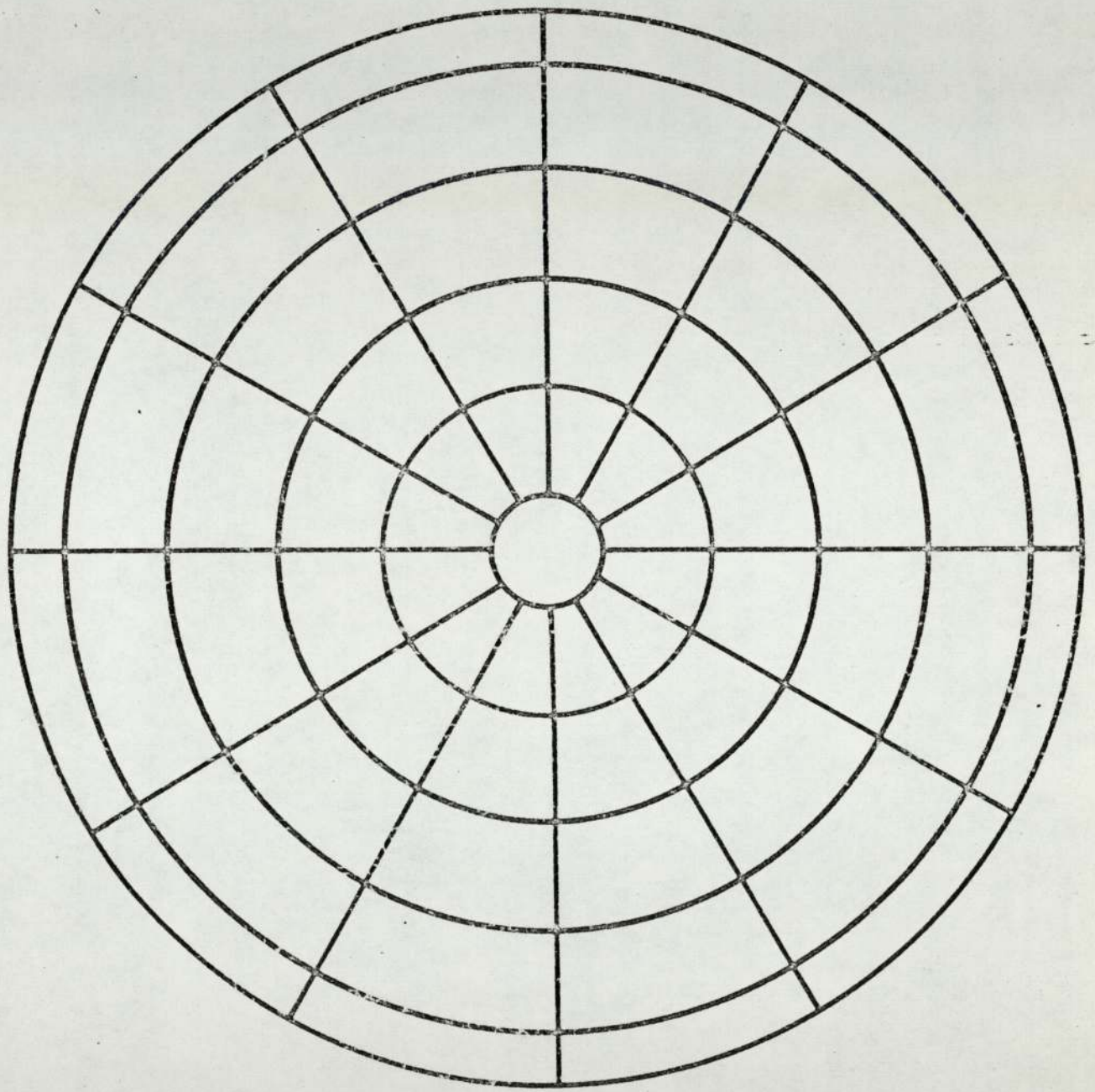

Fig. 8.1 Division of billet into 61 elements.

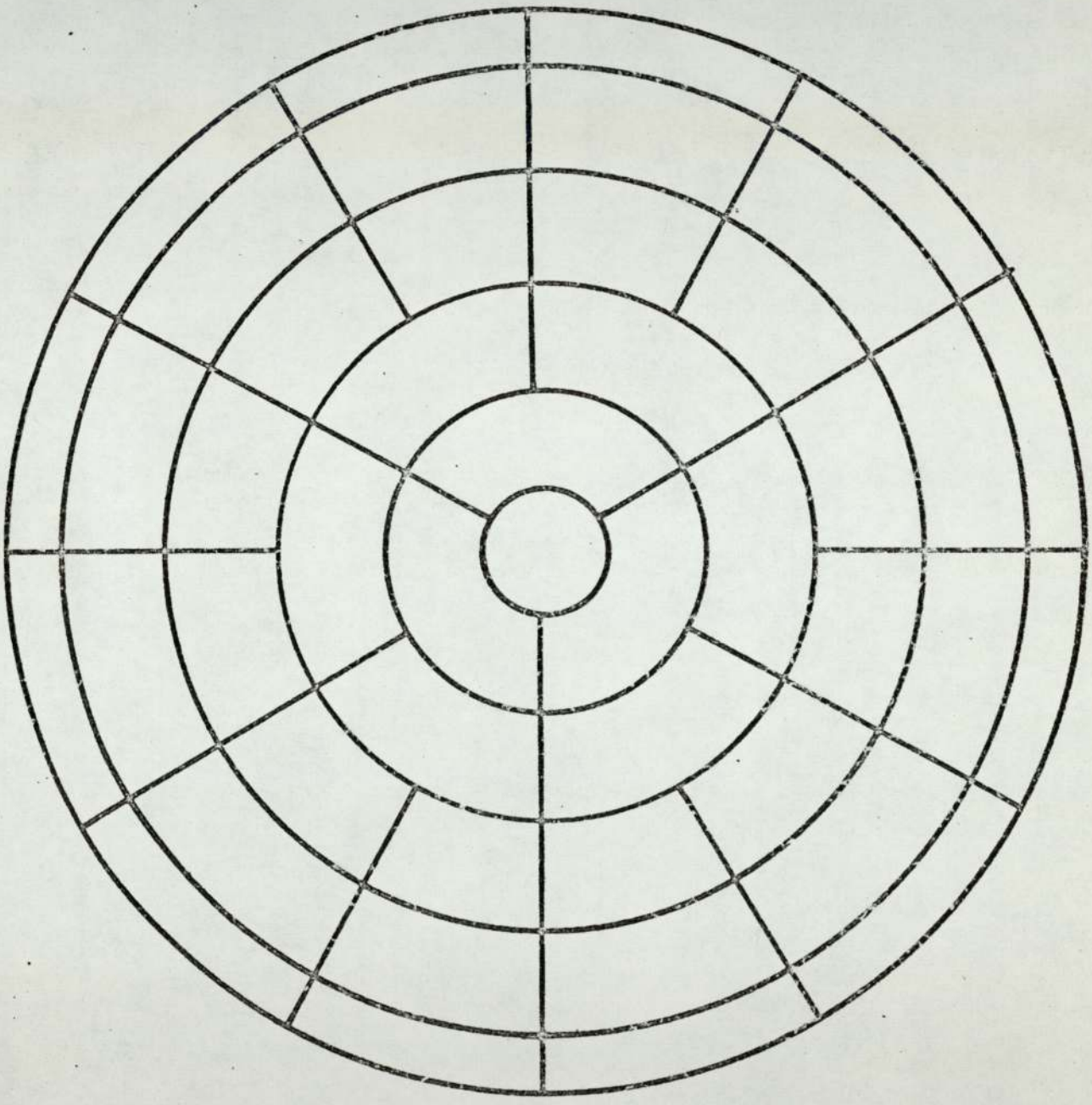

Fig. 8.2 Division of billet into 46 elements.

very similar temperatures. There is therefore a large number of unnecessary calculations but this may be reduced by grouping some of the elements together as shown in figure 8.2. The number of temperatures to be calculated at each half stage has thus been reduced from 61 to 46.

8.1.3 Method of Solution

The method of solving the equations forming the mathematical model is similar to that described in chapter 6 and therefore will not be explained again here.

8.1.4 Other Data

The radiation interchange factors between the billet and the wall were taken to be the same for every element of the billet surface. Similarly the interchange factors between the combustion products and the billet surface were assumed to be uniform. These two sets of factors are therefore identical to those for the whole billet surface and can hence be evaluated from the equations in section 6.4.2.

The average convective heat transfer coefficients were obtained from the correlations given in section 6.7.1 i.e.,

$$j_b = 0.525\ Re_b^{-0.5}$$

$$j_w = 1.13\ Re_w^{-0.5}$$

The local coefficients for each part of the billet surface were obtained from the average coefficient and the coefficient distributions given in figures (4.8) to (4.10).

Calculations in this chapter were made for natural gas and the properties of this fuel and its combustion products are given in section 6.7.2.

8.2 Overall Performance

The time taken to heat various mild steel billets to forging temperature in the single top flue furnace have been calculated using

the method described in this chapter. These values are shown in table (8.1) and ineach case the heating time is that until the highest temperature at the surface reaches 1300°C and no soak time is included. Also shown in the table are heating times calculated assuming uniform convective heat transfer coefficient distribution but still using the two dimensional programme. It is apparent that heating times are not affected significantly by the variation in coefficients. Thus if only overall performance is required to be predicted then measurement of average coefficients and the use of a one dimensional heat conduction programme are sufficient for this particular furnace.

8.3 Calculated Temperature Distributions

Calculated temperature distributions for three different billet sizes are shown in figures (8.3) to (8.5). In each case local temperatures are shown at the centre and surface of the billet and at the third ring in from the surface at two different times after the start of the heating cycle. The surface temperatures follow closely the variation in convective coefficients but the temperature differences are fairly small. It is worth noting that the temperature differences at the third ring in are much less than at the surface and thus the method used for subdividing the billet near to its centre (Figure 8.2) would seem to be valid.

TABLE 8.1

Heating Times Calculated from the Two Dimensional Conduction Model

Billet Diameter cm	Heat Input MW/m length	Heating Time min-sec	
		Uniform Coefficients	Varying Coefficients
10.9	0.28	23.22	23.22
10.9	0.466	15.54	15.54
14.5	0.28	38.18	38.20
14.5	0.466	25.54	25.56
18.1	0.28	57.42	57.44
18.1	0.466	38.20	38.22

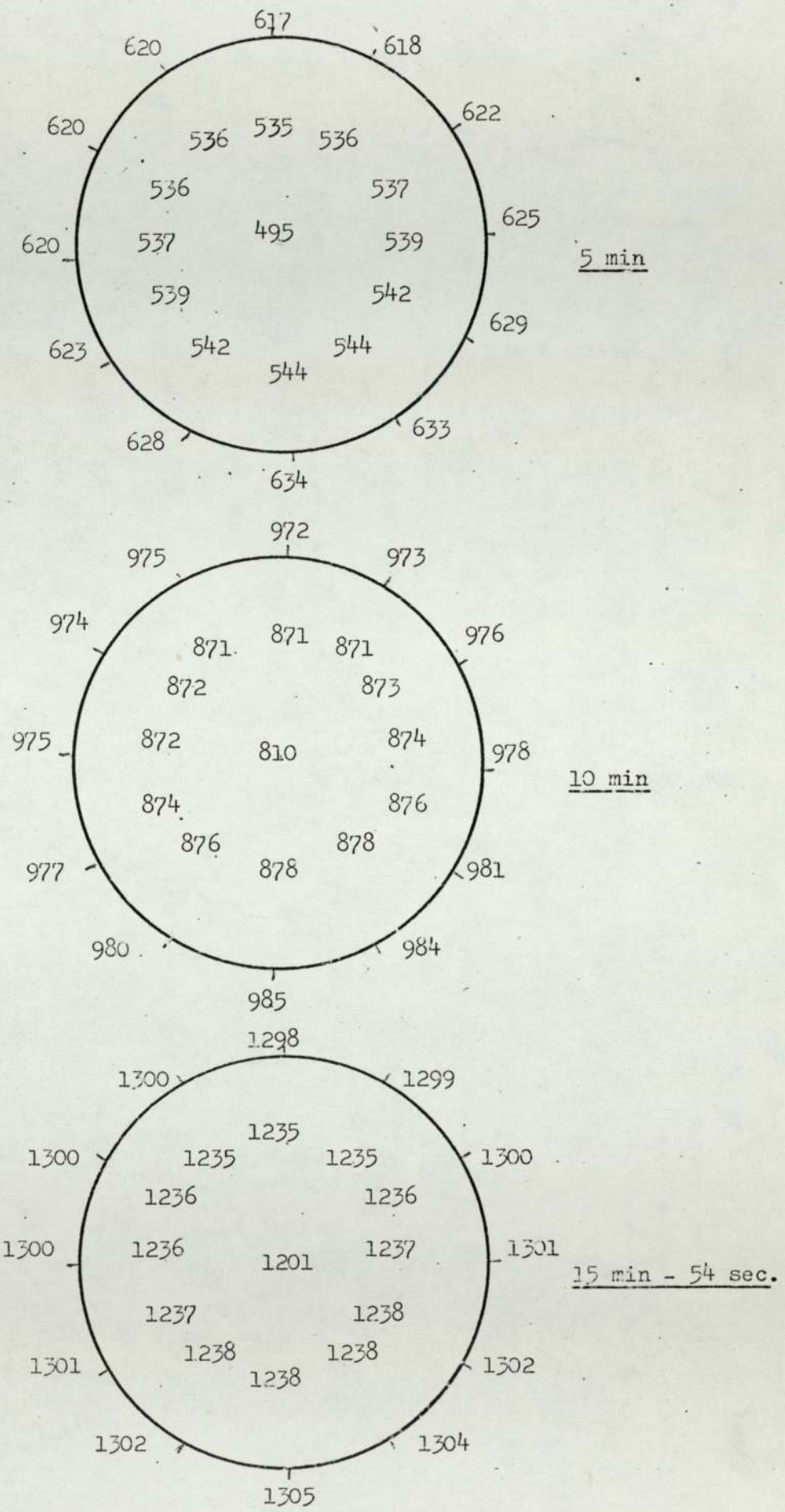

Fig. 8.3 Calculated temperature distributions in a 10.9cm billet. (Heat input to furnace = 0.466 MW/m length)

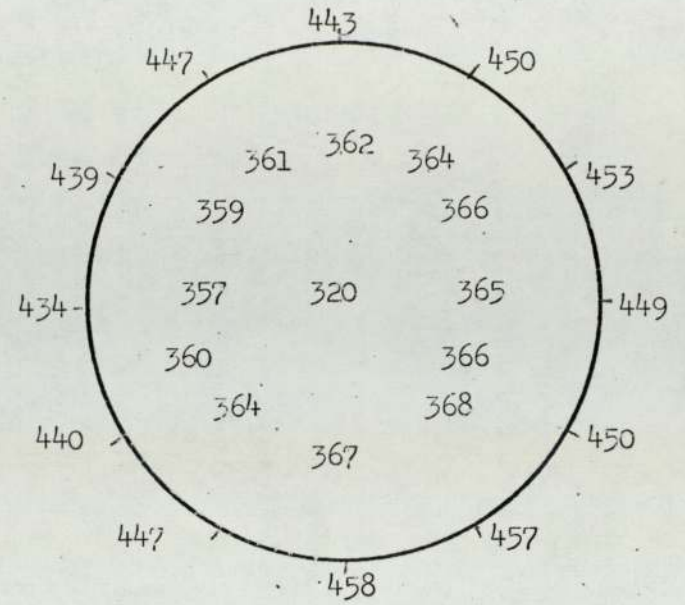

5 min

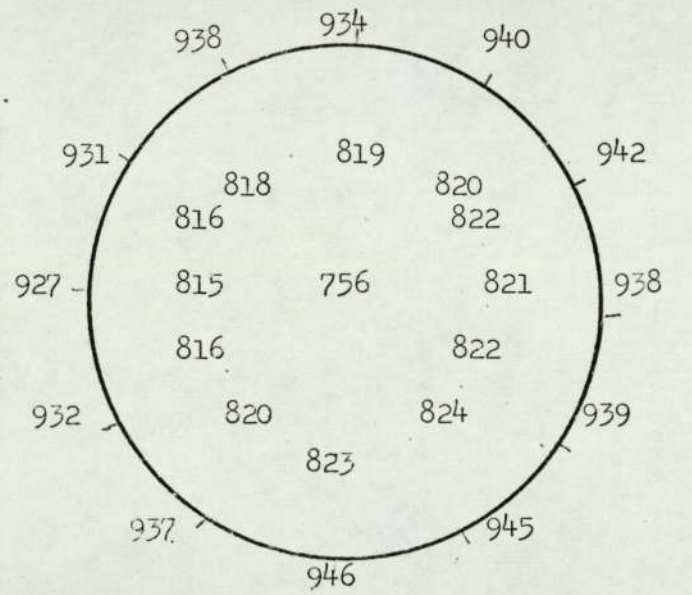

15 min

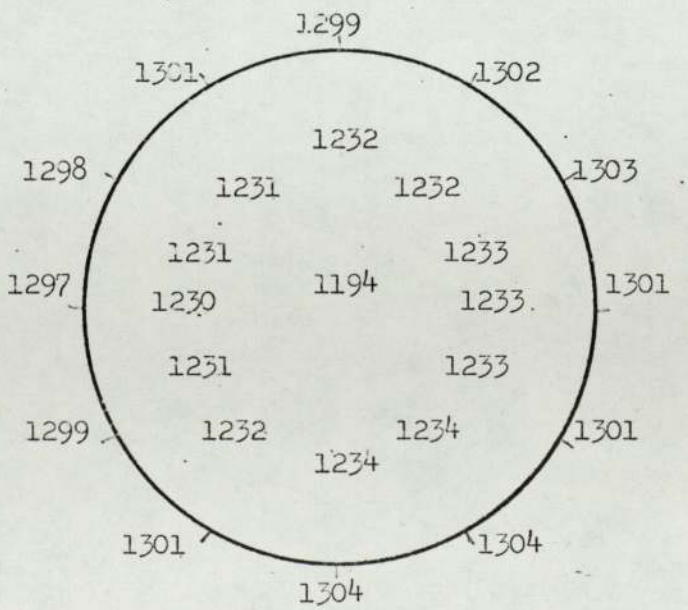

25min - 56s.

Fig. 8.4 Calculated temperature distributions in a 14.5cm billet (Heat input to furnace = 0.466 MW/m length)

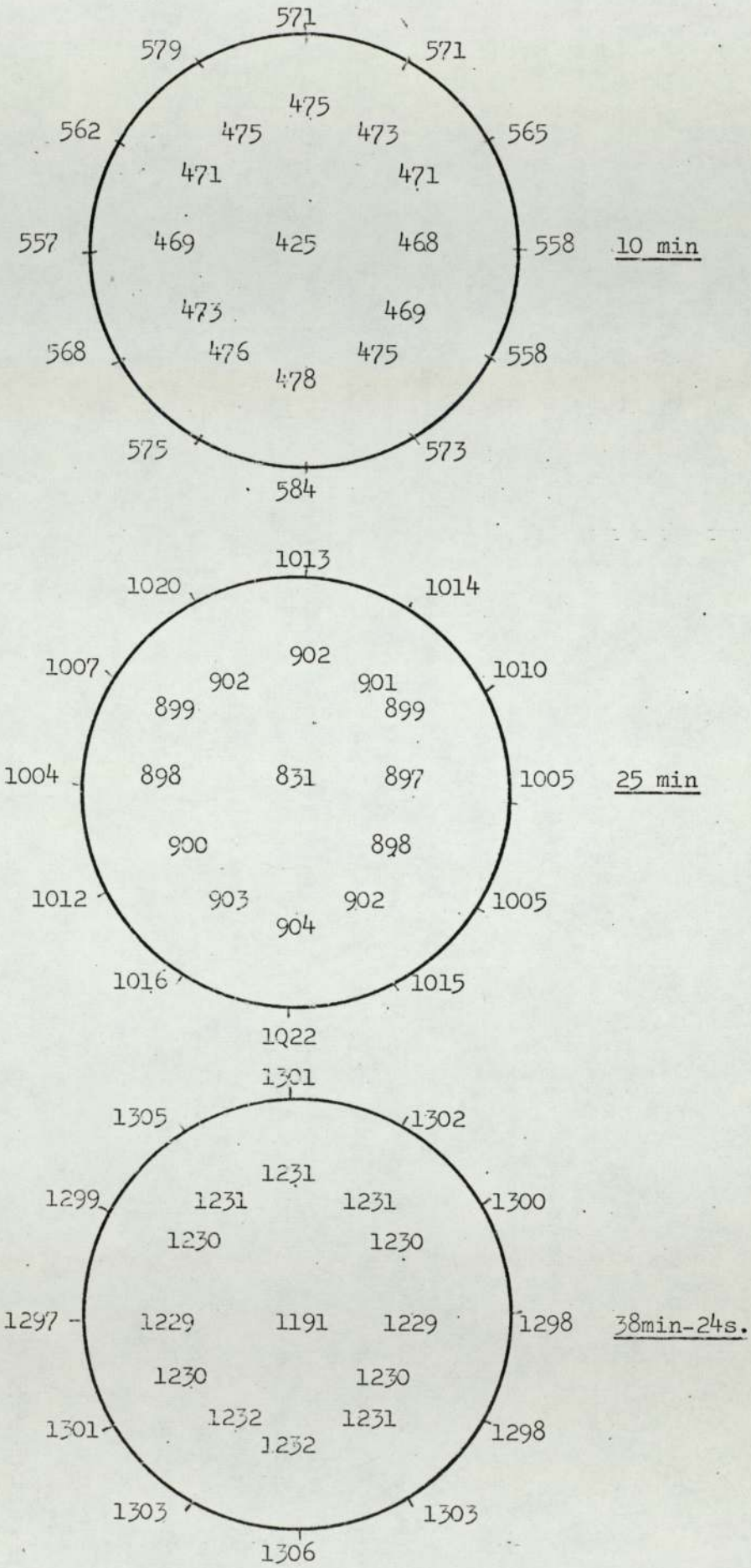

Fig. 8.5 Calculated temperature distributions in a 18.1 cm billet (Heat input to furnace = 0.466 MW/m length)

9. GENERAL DISCUSSION OF MATHEMATICAL MODELS

The development of mathematical models of furnaces, or any other heating processes, serves two main purposes; firstly to allow the thermal performance of new plant or the effect of changes in the operating conditions of existing plant to be predicted, and secondly to obtain a better appreciation of the heat transfer mechanism so that more rational design and operational decisions can be made. Of the three models which have been described in the thesis the simplest is that of Chapter 6 but this nevertheless fulfulls most of the requirements of a predictive model. It is true that it can only be applied once the furnace has been in operation long enough for the structure to become fully warmed but since this state is reached comparatively quickly in rapid heating furnaces this is not a significant limitation to the method. This model has in fact formed the basis of many others which have been applied to a range of gas fired processes.

The method described in Chapter (7) allows the transient response of a furnace to be investigated. Its main use is to analyse in detail the characteristics of one particular furnace or furnace type rather than to serve as a predictive model and the whole of Chapter (7) is concerned with this type of investigation.

The last of the methods is the most complex and requires detailed input information in the form of local convective heat transfer coefficients. Its use is again thus restricted to fairly lengthy investigations of furnace types or heating methods. The main application would be to situations in which there are severe differences in local coefficients, such as are produced when a burner is fired directly at the load surface, and the principal reason for developing the method was that it should subsequently be applied to this type of system.

The basis of all three methods is the assumption of the 'well stirred'

furnace, which for the furnaces and loads dealt with in this thesis has been shown to be adequate. However, in other cases this may not be so due to significant temperature variations in the furnace space. This problem has been considered by many workers and two main approaches have been evolved. The first is that of Hottel et al[3 53] and this involves setting up heat balances on small finite elements of the furnace chamber. This gives a series of simultaneous equations which can in principal be solved to obtain the distribution of both the temperature within the furnace space and the heat flux to the load. The method, however, requires a large amount of input data including the flow patterns within the furnace and the local convective heat transfer coefficients. In some circumstances these data may be available from the literature or from other theoretical work, but usually they must be obtained from detailed experimental measurements made either in the actual furnace or in an isothermal model.

The alternative method for dealing with furnaces that cannot be treated as 'well stirred' is that of Spalding[54] et al. This involves the numerical integration of the basic differential equations describing the transport of mass, momentum and energy. Apart from the computational difficulties the principal disadvantage of the method is that it does not yet contain a mechanistic model for the turbulent properties of the flow. Instead these properties are obtained from fitting simplified models to experimental data. Once, however, this limitation is removed the method would be extremely useful since it could eliminate the need for any experimental measurements and thus provide the required information more quickly and cheaply than can present techniques.

10. CONCLUSIONS

This thesis has shown how a combination of physical and mathematical modelling has been used to predict and analyse the thermal performance of tangentially fired rapid billet heating furnaces. The experimental work has demonstrated that the results from two different mass transfer and one heat transfer experiment can be correlated by the Chilton-Colburn analogy. It has further been shown that when these results are included in a mathematical model of the heat transfer processes in the furnace then the thermal performance can be predicted fairly accurately. The mathematical models have been used to demonstrate that improvements in the performance of the original prototype furnace can be made and they have also illustrated the significantly better transient response of these furnaces compared with more traditional designs. Finally, both the mass transfer measurements and mathematical models have been extended to deal with situations in which there is significant non-uniformity in the heat transfer rate to the surface of the stock.

Although this thesis has been concerned with the prediction of the performance of one particular type of furnace the experimental and theoretical methods can be, and have been, applied to other plant.

APPENDIX 1

Electroplating Nickel onto Perspex

A suitable method of coating the surface was difficult to find since the model walls were quite complex surfaces, including varying concave curvature and two rectangular holes for the flues. Also the nickel coating had to stay adhered when a large flow of a very caustic solution was pumped through the model. The method set out below was found to be satisfactory for these conditions.

Method

(1) Fix a piece of tinned copper wire through the perspex, so that the end is flush with the surface to be plated, to form an electrical contact.

(2) Clean the perspex surface. Silver paste from a previous plating may be removed with ethyl acetate.

(3) Liberally paint the surface with chloroform.

(4) After allowing the surface to soften for 30 to 60 seconds, spray with silver paste to get a thin uniform silver layer completely covering the surface. The silver paste used was JMC air-drying preparation FSP 51 produced by Johnson, Matthey and Co., Limited.

(5) Leave for 1 hour to allow solvents to evaporate off.

(6) Copper plate in a copper sulphate bath at room temperature (70°F) for $\frac{1}{2}$ hour at a current density of between 20 and 50 amps/ft^2. The copper anode must be kept in a filter bag to prevent anode slime reaching the surface being plated. The solution should be agitated by bubbling air through it. The recommended composition of the solution is as follows:-

Copper sulphate. $Cu\ SO_4\ 5H_2O$	225 g/l
Sulphuric Acid	63 g/l
U.B.A.C. No. 1 Additive	3 ml/l

(7) Nickel plate in a nickel sulphate bath at 45 to 55°C for approximately 10 minutes at a current density of between 20 and 40 amps/ft^2. An anode filter bag and air agitation are again required. The recommended composition for this bath is:-

Nickel Sulphate $NiSo_4$ $7H_2O$	300 g/l
Nickel Chloride $NiCl_2$ $6H_2O$	55 g/l
Boric Acid H_3 BO_3	45 g/l
Nickel Gleam N.S.22 Additive	50 ml/l
Nickel Gleam LNW Additive	2.5 ml/l

The two additives are supplied by M.L. Alkan Ltd. The pH of the solution should be controlled at 3.5 to 4.0 by addition of dilute sulphuric acid.

(8) Wash surface with dilute sodium hydroxide and distilled water before use.

The thickness of the copper is about .001" and the nickel a third of this. The electroplating process gives a good uniform nickel surface which is free from impurities. The use of chloroform on the perspex surface results in good adhesion, although for simple surfaces such as cylinders it is not always necessary.

APPENDIX 2

Example of Experimental Measurement for One Billet Size

Billet size = 5.1 cm

Electrolyte concentration : 0.0103 N Potassium Ferricyanide

0.02 N Potassium Ferrocyanide

1 N Sodium Hydroxide

Solution Temperature = 24.5°C

Solution Density = 1049 kg/m^3

Solution Viscosity = 1.1209×10^{-3} Ns/m^2

Ferricyanide Ion Diffusivity = 0.6688×10^{-10} m^2/s

Schmidt Number for Ferricyanide ion = 1598

(a) Current/Voltage Measurements

235 g.p.h.		310 g.p.h.	
V	I(mA)	V	I (mA)
0.006	10	0.014	13
0.025	57.5	0.035	78
0.16	140	0.045	100
0.36	144	0.080	139
0.9	143	0.095	150
1.2	143	0.125	160
1.35	145	0.18	169
1.43	156	0.2	169
1.51	188	0.38	170
1.58	275	0.48	170
		0.56	170

(b) Calculated Mass Transfer Results

Flow Rate (g.p.h.)	Flow Rate (kg/s)	Limiting Current (mA)	h_D μm/s	Re	j_D
20	0.026	30.5	2.52	310	0.0265
30	0.040	34	2.82	464	0.0197
50	0.066	58	4.31	774	0.0181
70	0.093	60	4.96	1085	0.0148
90	0.119	71	5.89	1395	0.0138
110	0.146	78	6.51	1705	0.0125
130	0.172	90	7.47	2010	0.0120
150	0.198	100	8.29	2320	0.0116
180	0.238	113	9.37	2790	0.0109
210	0.278	130	10.80	3250	0.0108
235	0.311	141	11.70	3640	0.0105
260	0.344	150	12.45	4030	0.0101
285	0.377	160	13.25	4410	0.0098
310	0.410	170	14.05	4800	0.0095

APPENDIX 3

Summary of Experimental Measurements for all Billet Sizes

1. Average Coefficients for Billets

(a) Billet diameter = 3.5 cm

Ferricyanide concentration = 0.00984 N

Flow rate g.p.h.	Solution temperature °C	Limiting Current mA	h_D µm/s
20	25.3	15.6	1.99
26	25.3	17.0	2.16
31	25.3	18.3	2.33
36	25.5	20.4	2.59
40	25.5	23.0	2.92
45	25.5	25.0	3.18
51	25.5	28.0	3.56
58.	25.3	30.4	3.87
63	25.3	33.0	4.19
70	25.3	36.5	4.64
81	25.8	40.1	5.11
90	25.8	44.2	5.62
98	25.8	47.5	6.03
115	26.0	54.3	6.90
141	26.0	61.3	7.79
160	26.0	69.8	8.87
179	26.0	72.8	9.25
200	26.0	77.0	9.79
225	26.0	84.4	10.7
251	26.3	96.5	12.3
278	26.3	103	13.1
295	26.3	107	13.6

(b) Billet diameter = 3.8 cm

Ferricyanide concentration = 0.1025 N

Flow rate g.p.h.	Solution temperature °C	Limiting Current mA	h_D µm/s
36	24.5	25	2.79
45	24.5	30	3.36
57	24.5	35	3.92
67	24.5	38	4.26
80	24.5	42	4.69
100	24.5	51.5	5.77
120	24.5	60.5	6.77
140	24.5	66.5	7.43
160	24.5	75.5	8.45
179	24.5	81	9.05
198	24.5	89	9.95
220	24.5	93	10.4
230	24.5	94	10.5
245	24.5	95	10.6
270	24.5	103	11.5
208	24.5	112	12.5
305	24.5	115	12.9

(c) Billet diameter = 5.1 cm

See Appendix 2

(d) Billet diameter = 5.7 cm

Ferricyanide concentration = 0.0100 N

Flow rate g.p.h.	Solution temperature °C	Limiting Current mA	h_D μm/s
20	24.0	30	2.29
30	24.5	43	3.26
40	24.0	50	3.84
55	24.0	61	4.70
67	24.5	71	5.42
77	24.0	76	5.82
99	24.0	90	6.88
121	24.0	102	7.80
153	24.0	120	9.18
166	24.1	127	9.70
182	24.1	133	10.2
198	24.1	139	10.6
223	24.1	151	11.5
245	24.25	162	12.4
265	24.25	171	13.1
281	24.25	177	13.5
309	24.25	187	14.3

(e) Billet diameter = 6.35 cm

Ferricyanide concentration = 0.1074 N

Flow rate g.p.h.	Solution temperature °C	Limiting Current mA	h_D µm/s
18	23.5	39	2.50
26	23.5	45	2.88
35	23.5	53	3.40
43	23.5	60	3.85
50	23.75	67	4.30
59	23.75	72	4.61
66	23.75	79	5.07
76	23.75	85	5.44
83	23.75	91	5.84
92	23.75	97	6.21
100	23.75	101	6.47
115	23.5	110	7.05
132	23.5	119	7.61
152	23.5	131	8.39
170	23.75	140	8.97
190	23.75	151	9.68
204	23.75	155	9.94
217	23.75	163	10.5
237	23.9	175	11.2
253	23.9	189	12.1
266	23.9	196	12.5
283	23.9	203	13.0
296	23.9	210	13.5
308	23.9	216	13.8

2. Average Coefficients for Wall 1

(a) Billet diameter = 3.5 cm

Ferricyanide concentration = 0.00984 N

Flow rate g.p.h.	Solution temperature °C	Limiting Current mA	h_D µm/s
22	26.25	44	4.54
33	26.25	57	5.9
46	26.25	72	7.45
58	26.25	84	8.70
68	26.25	94	9.75
85	26.25	108	11.1
100	26.5	119	12.3
127	26.5	140	14.4
153	26.5	163	16.8
180	26.5	183	16.9
201	26.8	199	20.5
225	26.8	213	21.2
258	26.8	239	24.4
275	26.8	252	25.8
299	26.8	268	27.4

(b) Billet diameter = 3.8 cm

(i) Ferricyanide concentration = 0.100 N

Flow rate g.p.h.	Solution temperature °C	Limiting Current mA	h_D µm/s
210	25.5	172	17.1
225	25.0	179	17.8
240	25.0	184	18.2
253	25.0	190	18.9
270	24.5	197	19.6
285	24.5	206	20.3
300	24.5	217	21.6

(ii) Ferricyanide concentration = 0.01025 N

Flow rate g.p.h.	Solution temperature °C	Limiting Current mA	h_D µm/s
180	24.5	145	15.1
200	24.5	160	16.7
230	24.5	178	18.6
264	24.5	197	20.6
301	24.5	219	22.9

(c) Billet diameter = 5.1 cm

(i) Ferricyanide concentration = 0.0103 N

Flow rate g.p.h.	Solution temperature °C	Limiting Current mA	h_D µm/s
143	24.5	130	13.1
200	24.5	165	16.7
250	24.5	185	18.7
300	24.5	210	21.2

(ii) Ferricyanide concentration = 0.0108 N

Flow rate g.p.h.	Solution temperature °C	Limiting Current mA	h_D µm/s
250	27.0	211	20.1
280	27.0	224	21.3
300	27.25	235	22.4

(d) Billet diameter = 5.7 cm

Ferricyanide concentration = 0.0100 N

Flow rate g.p.h.	Solution temperature °C	Limiting Current mA	h_D µm/s
54	24.9	76	7.66
81	24.9	99	9.97
110	24.9	120	12.1
130	25.0	130	13.1
166	25.0	149	15.0
190	25.0	163	16.5
229	25.0	188	19.0
268	25.0	208	20.9
296	25.0	223	22.5
301	25.0	228	23.0

(e) Billet diameter = 6.35 cm

Ferricyanide concentration = 0.01074 N

Flow rate g.p.h.	Solution temperature °C	Limiting Current mA	h_D µm/s
50	23.75	74	6.98
58	23.75	82	7.23
67	23.9	90	8.43
78	23.9	100	9.38
90	23.9	108	10.1
101	23.9	116	10.9
110	23.9	121	11.4
120	23.9	128	12.0
130	23.9	135	12.7
140	23.9	141	13.3
152	23.9	151	14.2
160	23.9	157	14.8
175	23.9	161	15.1
181	23.9	166	15.6
190	23.9	170	16.0
200	23.9	179	16.8
220	23.9	190	17.9
242	23.9	203	19.1
260	23.9	216	20.3
278	23.9	224	21.1
302	23.9	236	22.2

3. Average Coefficients for Wall 2

(a) Billet diameter = 3.5 cm

Ferricyanide concentration = 0.00984 N

Flow rate g.p.h.	Solution temperature °C	Limiting Current mA	h_D µm/s
23	26.5	51	4.80
33	26.5	66	6.26
45	26.5	81	7.28
61	26.8	100	9.50
71	26.8	109	10.3
85	26.8	120	11.4
104	26.8	133	11.7
124	27.0	149	14.1
150	27.0	171	16.2
175	27.0	192	18.3
203	27.0	217	20.6
229	27.0	232	22.1
253	27.0	250	23.8
283	27.0	272	25.7
305	27.0	285	26.6

(b) Billet diameter = 3.8 cm

(i) Ferricyanide concentration = 0.0100 N

Flow rate g.p.h.	Solution temperature °C	Limiting Current mA	h_D µm/s
210	27.0	172	15.6
225	27.0	178	16.2
240	26.5	181	16.5
255	26.0	188	17.1
270	26.0	193	17.6
285	26.0	200	18.2
300	26.0	213	19.4

(ii) Ferricyanide concentration = 0.01025 N

Flow rate g.p.h.	Solution temperature °C	Limiting Current mA	h_D µm/s
148	24.5	134	12.3
180	24.5	152	14.0
200	24.5	159	14.6
230	24.5	164	15.0
268	24.5	173	15.9
301	24.5	185	17.0

(c) Billet diameter = 5.1 cm

(i) Ferricyanide concentration = 0.0103 N

Flow rate g.p.h.	Solution temperature °C	Limiting Current mA	h_D µm/s
160	24.5	137	12.4
205	24.5	152	13.8
250	24.5	172	15.6
300	24.5	188	17.1

(ii) Ferricyanide concentration = 0.0108 N

Flow rate g.p.h.	Solution temperature °C	Limiting Current mA	h_D µm/s
250	24.75	196	16.7
280	24.75	210	17.9
302	25.0	230	19.6

(d) Billet diameter = 5.7 cm

Ferricyanide concentration = 0.0100 N

Flow rate g.p.h.	Solution temperature °C	Limiting Current mA	h_D µm/s
53	25.0	67	6.26
78	25.0	86	8.04
104	25.0	108	10.1
132	25.0	125	11.7
170	25.1	153	14.3
190	25.1	170	15.9
232	25.1	190	17.8
274	25.1	219	20.5
290	25.1	232	21.6
300	25.1	240	22.5

(e) Billet diameter = 6.35 cm

Ferricyanide concentration = 0.01074 N

Flow rate g.p.h.	Solution temperature °C	Limiting Current mA	h_D µm/s
46	23.9	63	5.50
60	23.9	78	6.80
70	23.9	88	7.66
80	23.9	111	9.67
94	23.9	115	10.0
103	23.9	119	10.3
111	23.9	124	11.2
119	23.9	134	11.7
130	23.9	150	13.0
141	23.9	159	13.8
150	23.9	165	14.4
162	23.9	170	14.8
172	24.0	179	15.6
181	24.0	186	16.2
190	24.0	190	16.5
200	24.0	199	17.3
222	24.0	212	18.4
242	24.1	227	19.8
263	24.1	240	20.9
282	24.1	247	21.5
303	24.1	259	22.5

4. Local Coefficients for Billets

In the results which follow the position of the test electrode is given as the angular displacement (in degrees) measured in a clockwise direction from a position directly under the centre of the flue.

(a) Billet diameter = 3.8 cm

Run number		(i)	(ii)
Flow rate	g.p.h.	90	180
Ferricyanide concentration	N	0.01103	0.01103
Solution temp.	°C	26	26
Average mass transfer coefficient - μm/s		4.74	7.70
Area of test electrode	cm^2	2.08 cm^2	2.08 cm^2

Position	Limiting current mA (i)	(ii)	Position	Limiting current mA (i)	(ii)
0	0.780	1.35	190	1.300	2.075
10	0.785	1.325	200	1.200	2.10
20	0.865	1.325	210	1.075	1.825
30	0.880	1.375	220	1.025	1.70
40	0.915	1.60	230	1.000	1.60
50	1.025	1.625	240	1.000	1.60
60	1.050	1.70	250	0.973	1.60
70	1.050	1.65	260	0.950	1.60
80	1.050	1.70	270	0.925	1.50
90	1.075	1.60	280	0.875	1.475
100	1.050	1.675	290	0.925	1.425
110	1.075	1.75	300	1.000	1.55
120	1.100	1.875	310	1.050	1.60
130	1.250	2.00	320	1.100	1.575
140	1.250	2.10	330	1.100	1.65
150	1.300	2.10	340	1.100	1.65
160	1.400	2.20	350	0.950	1.50
170	1.500	2.35	355	0.825	1.425
180	1.425	2.35	360	0.780	1.35

(b) Billet diameter = 5.1 cm

Run number	(i)	(ii)	(iii)
Flow rate	90	180	270
Ferricyanide concentration N	0.00913	0.00913	0.00991
Solution temperature °C	25.0	25.0	24.5
Average mass transfer coefficient μm/s	5.67	10.32	14.6
Area of test electrode cm^2	2.22	2.22	2.22

Position	Limiting current mA (i)	(ii)	(iii)	Position	Limiting current mA (i)	(ii)	(iii)
0	0.85	1.60	2.05	190	1.55	2.45	3.90
10	0.95	1.70	2.45	200	1.35	2.15	3.55
20	1.35	2.40	3.10	210	1.10	1.90	3.05
30	1.45	2.60	3.25	220	1.075	1.85	3.00
40	1.55	2.60	3.45	230	1.075	1.80	2.95
50	1.65	2.65	3.50	240	1.10	1.70	2.90
60	1.60	2.70	3.45	250	0.95	1.65	2.90
70	1.40	2:50	3.10	260	0.875	1.45	2.45
80	1.20	2.25	3.00	270	0.70	1.15	2.05
90	1.10	1.95	2.85	280	0.60	1.25	1.95
100	1.00	1.95	2.80	290	0.75	1.40	2.20
110	1.025	1.95	2.90	300	1.00	1.95	2.55
120	1.05	2.00	2.95	310	1.15	2.05	2.75
130	1.25	2.20	3.10	320	1.475	2.40	3.50
140	1.35	2.45	3.40	330	1.55	2.65	3.55
150	1.525	2.90	3.90	340	1.50	2.45	3.20
160	1.70	3.25	4.40	350	1.05	1.85	2.25
170	1.70	3.20	4.75	360	0.85	1.60	2.05
180	1.60	3.00	4.35				

(c) Billet diameter = 6.35 cm

Run number	(i)	(ii)	(iii)
Flow rate g.p.h.	90	180	270
Ferricyanide concentration N	0.01035	0.01018	0.01018
Solution temperature ^{o}C	25	25	25
Average mass transfer coefficient μm/s	7.2	9.5	16.5
Area of test electrode cm^2	2.14	2.19	2.19

Position	Limiting current mA (i)	(ii)	(iii)	Position	Limiting current mA (i)	(ii)	(iii)
0	1.325	2.00	3.85	190	2.30	3.25	5.70
10	1.60	2.45	4.20	200	1.925	2.90	4.85
20	1.975	2.90	4.80	210	1.775	2.45	4.30
30	1.90	2.65	4.40	220	1.75	2.35	4.20
40	1.875	2.65	4.25	230	1.75	2.40	4.30
50	1.80	2.40	4.00	240	1.70	2.40	4.45
60	1.75	2.25	3.75	250	1.575	2.40	4.35
70	1.55	2.10	3.45	260	1.40	1.95	3.45
80	1.425	2.00	3.25	270	1.20	1.35	2.15
90	1.325	1.70	2.70	280	0.80	1.25	2.70
100	1.20	1.60	2.55	290	0.90	1.55	3.10
110	1.20	1.60	2.50	300	0.875	1.60	3.70
120	1.15	1.55	2.45	310	1.15	2.20	4.90
130	1.20	1.75	2.80	320	1.75	3.05	4.80
140	1.425	1.90	3.25	330	2.30	3.55	6.45
150	1.75	2.75	4.50	340	2.35	3.70	6.90
160	2.10	3.40	5.70	350	1.40	2.50	4.75
170	2.40	3.60	6.25	360	1.325	2.00	3.85
180	2.425	3.55	6.20				

REFERENCES

Introduction

(1) Lawrence, M.N., and Spittle, J. 'Forced-convection Techniques for Gas-fired Rapid Billet Heating' J.I.G.E. 1965, 5 (7), 515 to 534.

(2) Francis, W.E., and Oeppen, B. 'Developments in Gas-fired Reheating Furnaces for Hot Working'. Reheating for Hot Working Conference I.S.I. 1967.

(3) Hottel, H.C. and Sarofim, A.F. 'Radiative Heat Transfer' McGraw - Hill Book Company. New York. 1967.

(4) Field, M.A., Gill, D.W., Morgan. B.B. and Hawksley, P.G.W. 'Combustion of Pulverised Coal' B.C.U.R.A. Leatherhead, England. 1967.

(5) Sinnott, M.J. and Siebert, C.A. 'Heat Transfer in a Recirculating Furnace' Ind. Eng. Chem., 1948, 40 (6) 1039-1044.

(6) Genna. S.J., Nolan, E.J. and Furczyk, A.A. 'Heat Transfer in a Gas -Fired Furnace' Trans. ASME, 1954, 76 (4) 527-536.

(7) Hulse, C. 'Forced Convective Heat Transfer in Furnace Chambers' Sheffield Univ. Ph.D. Thesis 1953.

(8) Trinks, W. 'Industrial Furnaces' Vol. 1 4th Ed. John Wiley, New York.

(9) Hulse, C. and Sarjant, R.J. 'Thermal Aspects of Furnace Design' J. Inst. Fuel, 1952, 25, 94-102.

(10) Fishenden, M.W. and Saunders, O.A. 'The Calculation of Heat Transmission' H.M.S.O. 1932.

(11) Hottel, H.C. 'Radiation Transfer in Combustion Chambers' J. Inst. Fuel 1961, 34, 220 to 234.

Chapter 1

(15) Beer, J.M. 'The Significance of Modelling'. J. Inst. Fuel, 1966, 39, 466-476.

(16) Kays, W.M. 'Convective Heat and Mass Transfer'. McGraw-Hill Book Company Inc. New York. 1966.

(17) Schlichting, H. 'Boundary Layer Theory' 4th Ed. McGraw-Hill Book Company, New York 1960.

(18) Deissler, R.G. 'Analytical and Experimental Investigation of Adiabatic Turbulent Flow in Smooth Tubes'. N.A.C.A. TN 2138. 1950.

(19) Prandtl, L. 'Uber die ausgabildte Turbulenz' Proc. 2nd Intern Congress Appl. Mech., Zurich 1926. See also reference 17.

(20) Taylor, G.I. 'The Transport of Varticity and Heat Through Fluids in Turbulent Motion' Proc. Roy. Soc. London 1932. A135 685 See also reference 17.

(21) Von Kørman, T. 'Mechaniscke 'A'hnlichkoit und Turbulenz' Proc. 3rd Intern. Congress Appl. Mech., Stockholm, 1930, Pt.1, 85. See also reference 17.

(22) Chilton, T.H. and Colburn. A.P. 'Mass Transfer (Absorption) Coefficients' Ind. Eng. Chem., 1934, 26, 1183-1187.

Chapter 2

(24)

(a) M. Eisenberg, C.W. Tobias and C.R. Wilke
"Ionic Mass Transfer and Concentration Polarization at Rotating Electrodes"
J. Electrochem. Soc. (1954) 101 (16) pp. 306-319

(b) M. Eisenberg, C.W. Tobias and C.R. Wilke
"Mass Transfer at Rotating Cylinders"
Chem. Engng. Prog. Symp. Ser. (1955) 61 (16) pp. 1-16

(c) M.G. Fouad and T. Gouda
"Natural Convection Mass Transfer at Vertical Electrodes"
Electrochim. Acta (1964) 9 pp.979-984

(d) P. Grassman, N. Ibl and J. Trub
"Elektrochemische Messung Von Stoffubergangszahlen"
Chemie-Ingr-Tech. (1961) 33 (8) pp. 529-533

(e) D.W. Hubbard and E.N. Lightfoot
"Correlation of Heat and Mass Transfer Data for High Schmidt and Reynolds Numbers"
Ind. Engng. Chem. Fundamentals (1966) 5 (3) pp.370-379

(f) A. Iribane, A.D. Gosman and D.B. Spalding
"A Theoretical and Experimental Investigation of Diffusion-Controlled Electrolytic Mass Transfer Between a Falling Liquid Film and a Wall"
Int. J. Heat Mass Transfer (1967) 10 pp. 1661-1676

(g) K.R. Jolls and T.J. Hanratty
"Transition to Turbulence for Flow through a Dumped Bed of Spheres"
Chem. Engng. Sci (1966) 21 pp. 1185-1190

(h) K.R. Jolls and T.J. Hanratty
"Use of Electrochemical Techniques to Study Mass Transfer Rates and Local Skin Friction to a Sphere in a Dumped Bed"
A.I. Ch. E. Jl. (1969) 15 (2) pp. 199-205

(i) A.J. Karabelas and T.J. Hanratty
"Determination of the Direction of Surface Velocity Gradients in the Three-Dimensional Boundary Layer"
J. Fluid Mech. (1968) 34 (1) pp. 159-162

(j) D.H. King and J.W. Smith
"Wall Mass Transfer in Liquid-Fluidized Beds"
Can. J. Chem. Engng. (1967) 45 (6) pp.329-333

(k) C.S. Lin, E.B. Denton, H.S. Gaskill and G.L. Putnam
"Diffusion - Controlled Electrode Reactions"
Ind. Engng. Chem (1951) 43 (9) pp.2136-2143

(l) J.E. Michell and T.J. Hanratty
"A study of Turbulence at a Wall using an Electrochemical Wall Shear-Stress Meter"
J. Fluid Mech. (1966) 26 (1) pp. 199-221

(m) P. Noordsij and J.W. Rotte

"Mass Transfer Coefficients to a Rotating and to a Vibrating Sphere"

Chem. Engng. Sci (1967) 22 pp.1475-1481

(n) M.P. Noordsij and J.W. Rotte

"Mass Transfer for a Simultaneously Rotating and Translating Sphere"

Chem. Engng. Sci (1968) 23 pp. 657-660

(o) E. Ravoo, J.W. Rotte and F.W. Sevenstern

"Theoretical and Electrochemical Investigation of Free Convection Mass Transfer at Vertical Cylinders"

Chem. Engng. Sci.(1970) 25 pp. 1637.1652

(p) L.P. Reiss and T.J. Hanratty

"Measurement of Instantaneous Rates of Mass Transfer to a Small Sink on a Wall

A.I. Ch.E. Jl. (1962) 8 (2) pp 245-247

(q) L.P. Reiss and T.J. Hanratty

"An Experimental Study of the Unsteady Nature of the Viscous Sublayer"

A.I.Ch.E. Jl. (1963) 9 (2) pp.154-160

(r) T.K. Ross, D.U. Campbell and A.A. Wragg

"An Electrochemical Investigation of the Hydrodynamics of Liquid Films in Grid Packings"

Trans. Instn. Chem. Engrs. (1967) 45 pp.401-407

(s) J.W. Rotte, G.L.T. Tummers and J.L. Dekker

"Mass Transfer to a Moving Continuous Cylinder"

Chem. Engng. Sci. (1969) 24 pp 1009-1015

(t) P.Van Shaw, L.P. Reiss and T.J. Hanratty

"Rates of Turbulent Transfer to a Pipe Wall in the Mass Transfer Entry Region"

A.I. (1963) 9 pp.362-364

(u) K.K. Sirkar and T.J. Hanratty

"Limiting Behaviour of the Transverse Turbulent Velocity Fluctuations Close to a Wall"

Ind. Engng. Chem. Fundamentals (1969) 8 (2) pp.189-192

(v) A.M. Sutey and J.G. Knudsen

"Mass Transfer at the Solid-Liquid Interface for Climbing Film Flow in an Annular Duct"

A.I. Ch.E. Jl (1969) 15 (5) pp.719-726

(w) P.H. Vogtlander and C.A.P. Bakker

"An Experimental Study of Mass Transfer from a Liquid Flow to Wires and Gauzes"

Chem. Engng. Sci (1963) 18 pp.583-589

(x) J.S. Watson and D.G. Thomas

"Forced Convective Mass Transfer: Part IV"

A.I.Ch.E. Jl. (1967) 13 (4) pp.676-677

(y) A.A. Wragg

"Free Convection Mass Transfer at Mesh Electrodes'.
Int. J. Heat Mass Transfer (1968) 11 pp 979-984

(z) A.A. Wragg, P. Serafimidis and A. Einarsson

"Mass Transfer between a Falling Liquid Film and a Plane Vertical Surface"

Int. J. Heat Mass Transfer (1968) 11 pp.1287-1289

See also 24 (a), (b) and (k)

(25) T. Akehata and K. Sata

"Flow Distribution in Packed Beds"

Chem. Engng, Tokyo (1958) 20 (7) pp. 430-436

(26) A.A. Wragg and T.K. Ross

"Superposed Free and Forced Convective Mass Transfer in an Electrochemical Flow System"

Electrochim. Acta (1967) pp.1421-1428

(27) M. Daguenet

"Etude du Transport de Matiere en Solution,

a l'aide des Electrodes a Disque et a Anneau Tournants"

Int. J. Heat Mass Transfer (1968) 11 pp. 1581-1596

see also 24 (k)

(28) Glasstone, S. 'Elements of Physical Chemistry' Ist. ed.

D. Van Nostrand, New York 1946.

(29) M. Eisenberg, C.W. Tobias and C.R. Wilke

"Selected Physical Properties of Ternary Electrolytes Employed in Ionic Mass Transfer Studies"
J. Electrochem. Soc. (1956) 103 (7) pp.413-416

(30 J.C. Barzan and A.J. Arvia

"The Diffusion of Ferro and Ferricyanide Ions in

Aqueous Solutions of Sodium Hydroxide"

Electrochim. Acta (1965) 10 pp.1025-1032

(31) S. Glasstone, K.J. Laidler and J. Eyring

'Theory of Rate Processes' 1st Edition

McGraw Hill, New York (1941) pp.516-521

(32) Galsworthy, Mrs. R.A. 'Mass Transfer Measurements on Furnace

Models using the Naphthalene Sublimation Technique'. Gas Council,

Midlands Research Station External Report No. ER 134 (1969).

(33) Sherwood, T.K. and Bryant Jr. H.S. 'Mass Transfer Through Compressible

Turbulent Boundary Layers'. Canadian J. Chem. Eng. 1957, 35

51-57

Chapter 3

(35) Francis, W.E. Moppett, Mrs. B.E. and Read, G.P. 'Studies of Flow

Patterns and Convection in Rapid Heating Furnaces'. J.I.G.E.,

1967 7 (5) 335-352

Chapter 6

(38) Foeppl Festschrift, Schmidt, E. Beitrage Zur Techn. Mech. Und. Techn. Phys. 1924. 179. See also 'Conduction of Heat in Solids' 2nd Ed. Carslaw, H.S. and Jaegar, J.C. Clarenden Press, Oxford, 1959.

(39) Liebmann, G. 'The Solution of Transient Heat Flow and Heat Transfer Problems by Relaxation'. Brit. J. Appl. Phys., 1955, 6, 129 to 135.

(40) Crank, J. and Nicolson. P. 'A Practical Method for the Numerical Evaluation of Solutions of Partial Differential Equations of the Heat Conduction Type' Proc. Cam. Phil. Soc., 1947, 43, 466-475.

(41) Francis, W.E. and Toth Mrs. H.E. 'The Physical Properties of Town Gas and its Combustion Products'. Gas Council I.G.D.C. Special Report No. 3.

(42) 'Heat Transmission' 3rd Ed. McAdams, W.H. McGraw-Hill Book Company, Inc, New York 1954.

(43) Francis, W.E. and Toth Mrs H.E. 'Equilibrium Compositions and Heat Contents for Combustion Products of Town Gas and its Constituents'. Gas Council I.G.D.C. Special Report No. 2.

(44) Toth Mrs. H.E. 'Equilibrium Compositions and Physical Properties Of Products of Combustion of Methane and Natural Gases with Air'. Gas Council I.M.C. Special Report No. 6.

(45) 'Technical Data on Fuel' 6th Ed. Spiers, H.M. Brit. Nat. Committee. World Power Conference, London. 1961.

(46) Harrison,W.P., Oeppen, B. and Sourbutts, S. 'The Design of Self Recuperative Burners'. J.I.G.E. 1970, 10 (8) 538-563.

Chapter 7

(48) 'Numerical Solution of Partial Differential Equations', Smith G.D. Oxford University Press, London, 1969.

Chapter 8

(50) Peaceman, D.W. and Rachford Jr. H.H. 'The Numerical Solution

of Parabolic and Elliptic Differential Equations'. J. Soc. Indust. Appl. Math., 1955, 3 (1), 28-41.

Chapter 9

(53) Hottel, H.C. and Sarofirm, A.F. 'The Effect of Gas Flow Patterns on Radiation Transfer in Cylindrical Furnaces'. Int. J. Heat Mass Transfer, 1965, 8, 1153-1169

(54) Spalding D.B. 'Combustion as Applied to Engineering'. J. Inst. F., 1971, 64, 196-203.